CHARLES UNIVERSITY OF PRAGUE
Faculty of Mathematics and Physics

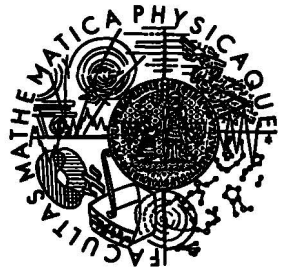

Anharmonic and solvation effects in vibrational spectroscopy

by
Mgr. Petr DANĚČEK

Supervisor:
Doc. RNDr. Petr BOUŘ, CSc.

Consultant:
Doc. RNDr. Vladimír BAUMRUK, DrSc.

Prague 2007

Acknowledgements

It is a pleasure to thank the many people who made this thesis possible. I would like to give thanks namely to my supervisor, Doc. RNDr. Petr Bouř, CSc., for his guidance. Thanks are due also to many others, who helped me one way or another during my work: my consultant Doc. RNDr. Vladimír Baumruk, DrSc.; Melanie Glynn for proof-reading; and all colleagues. Last, but not least, much gratitude is due to my beautiful wife and two daughters for their patience. Their support has been invaluable.

Contents

Acknowledgements 2

Abstract 6

1 Introduction 7

Developments . . . 8

Document structure . . . 9

2 Theory 11

2.1 Basic concepts of quantum mechanics . . . 11

2.2 General techniques . . . 14

2.2.1 The variational principle . . . 14

2.2.2 Perturbation method . . . 15

Time-independent perturbation theory . . . 15

Simplified degeneracy treatment . . . 16

Time-dependent perturbation theory . . . 17

2.3 Approximate methods of quantum chemistry . . . 19

2.3.1 The Hartree-Fock approximation . . . 19

2.3.2 Configuration interaction . . . 21

2.3.3 Coupled cluster . . . 22

2.3.4 Møller-Plesset perturbation theory . . . 23

2.3.5 Density functional theory . . . 23

DFT approximations . . . 25

2.3.6 Semi-empirical methods . . . 26

2.3.7 Basis sets . . . 26

Split-valence basis set . . . 27

Polarization functions . . . 27

Diffuse functions . . . 28

Correlation consistent basis sets . . . 28

2.4 Nuclear motion . . . 29

2.4.1 Harmonic approximation . . . 29

2.4.2 Linear harmonic oscillator . . . 31

2.4.3 Anharmonic potential . . . 32

2.4.4 Vibrational self-consistent field . . . 35
2.4.5 Vibrational perturbation theory . . . 36
2.4.6 Vibrational configuration interaction . . . 37
2.5 Molecules in radiation fields . . . 39
2.5.1 Electromagnetic radiation . . . 39
2.5.2 Optical activity . . . 39
2.5.3 Absorption . . . 40
Absorption observables . . . 42
Selection rules . . . 42
2.5.4 Raman scattering . . . 43
Classical description . . . 43
Quantum-mechanical description . . . 44
Raman observables . . . 45
Selection rules . . . 45
2.5.5 Vibrational circular dichroism . . . 46
2.5.6 Raman optical activity . . . 46
ROA observables . . . 48
2.6 Spectral shapes . . . 50
2.7 Solvation models . . . 50

3 Results **52**
3.1 Performance of anharmonic methods . . . 52
3.1.1 Model potentials . . . 52
3.1.2 Water . . . 53
3.1.3 Formaldehyde . . . 55
3.1.4 Furan . . . 57
3.1.5 N-methyl acetamide . . . 59
3.1.6 α-Pinene . . . 59
3.2 Publications . . . 64
3.2.1 Numerical stability of anharmonic methods (summary) . . . 64
3.2.2 Anharmonic methods applied to solvated systems (summary) . . . 64
3.2.3 Conformational flexibility (preliminary results) . . . 65
3.2.4 Transfer of molecular property tensors (in progress) . . . 68

4 Conclusions **69**

Appendix A **71**
A.1 Simplified degeneracy treatment . . . 71
Non-degenerated states . . . 71
Two-fold degenerated states . . . 72
A.2 Units . . . 73
Frequencies . . . 73

Abstract

The aim of this work is to systematically investigate the role of anharmonic corrections and solvation effects in vibrational spectra and thus try to explore two important sources of errors in spectra simulations of molecules in polar liquids. Several anharmonic methods were implemented in one program package and applied to a number of small and medium-sized systems (up to 26 atoms), which enabled consistent comparison of performance of the methods.

All of the implemented anharmonic methods are based on the expansion of the nuclear potential in the fourth-order Taylor series. While all of the anharmonic methods significantly improved the region of hydrogen stretching vibrations, the agreement with experiment was not significantly improved in mid- and low- frequency region. According to the results, selection of a good electronic model is very important and errors in the *ab initio* potential easily surpass the anharmonic corrections. In agreement with previous results, it has been shown that a high-precision model must be used for evaluation of harmonic frequencies, but it may be sufficient to evaluate the anharmonic corrections at a lower level of electronic theory. Performance of a number of electronic methods and basis sets were compared for selected systems.

One of the issues investigated was numerical stability of the anharmonic methods. Most sensitive to potential variations were the perturbation methods, partly because many near-degenerate energy levels occur in larger systems. Therefore, a modified degeneracy-corrected formula was developed and successfully applied to a number of systems. The solvation effects were accounted for by including the polarizable continuum model into the electronic calculations. Inclusion of anharmonic and solvation corrections improved parts of spectra. However, a detailed peak-to-peak assignment was not possible due to the limited precision of the approximative electronic and vibrational methods used.

Finally, on model zwitterionic dipeptides, the Boltzmann averaging was used for lowest-frequency modes in order to investigate the effect of molecular flexibility on vibrational spectra.

CHAPTER 1

Introduction

Vibrational spectroscopy is one of the main spectroscopic methods employed by molecular biology and biophysics. It comes in many flavors and is an invaluable technique for studying the structure of molecules either in solid, liquid or gas phase. It is particularly useful for determining the structure and dynamics of biological molecules (or even whole living systems), for they can be studied by the Raman technique non-destructively in water, their natural environment. Time-resolved vibrational spectroscopy enables the visualization and tracking of fundamental events such as molecular reaction mechanisms or protein folding. Advanced systems utilizing high-power pulse lasers enable the study of the dynamics of fast processes occurring in the region of picoseconds. Vibrational spectroscopy has found its way from academic laboratories into practical applications across a range of diverse fields including: biomedical, pharmaceutical, agricultural, forensic and many more.

The most commonly used vibrational techniques are infrared absorption (IR) and Raman spectroscopy. While IR spectroscopy measures the decrease in the intensity of incident light due to excitation of vibrational energy levels in a molecule, Raman spectroscopy measures light inelastically scattered from a sample with a frequency different from that of incident light. Both methods have their chiroptical variants, collectively known as vibrational optical activity (VOA). The IR form is known as vibrational circular dichroism (VCD). In an analogy to electronic circular dichroism, VCD is a measurement of differential absorption of left- and right-polarized light. The Raman form, known as Raman optical activity (ROA), measures differential inelastic scattering with respect to left- and right-polarized light. The largest ROA signals are often associated with vibrations of the most rigid chiral parts of molecular structure and therefore ROA is particularly suitable for conformation studies of peptides. Although the first part of the work presented here concerns vibrational spectroscopy in general, the main focus lies in the interpretation and modeling of Raman and ROA spectra.

Raman scattering was first observed in 1928 [1]. Because it is such a weak effect (only one photon from a million scatters inelastically), it was not used widely until the development of laser and multichannel detectors. In the 1970s, the ability of chiral molecules to differentially scatter circularly polarized light was first predicted [2,3] and observed shortly afterward [4]. The number of photons scattered with different circular polarization is of three orders of magnitude weaker than the Raman signal. The ROA experiment therefore requires delicately sensitive instrumentation, which was not commercially available until 2003. Among the few laboratories which developed their own ROA spectrometers is the Institute of Physics of the Charles

University in Prague [5–7].

Vibrational spectra are generally very complex and consist of a large number of peaks. The peak intensity and position are sensitive to molecular structure and conformation, therefore the spectra are highly characteristic for each molecule. The analysis of measured spectra is not straightforward. In some applications it is sufficient to inspect spectra empirically by comparing marker bands with characteristic features of known structural motifs, but for detailed understanding and interpretation accompanying *ab initio* calculations are essential. Although a remarkably good agreement of calculation with experiment can be achieved on model systems [8], theoretical predictions for larger or medium-sized molecules give only qualitative results and differ significantly from experiment, especially in the high-frequency region of the spectra. One of the goals of this work is therefore to provide a theoretical support for interpretation of spectra measured by the high-quality ROA instrument at the Institute of Physics of the Charles University in Prague.

Due to the complexity of the calculations involved it is necessary to use many approximations to simplify the computational problem down to a feasible level. Thus several sources of errors are introduced. The most prominent one is the limited accuracy of electronic methods used for evaluation of the potential energy surface, on which the nuclei vibrate. The inaccurate potential energy surface (PES) is then further simplified to allow calculation of vibrational frequencies using, traditionally, the harmonic approximation. Moreover, unless studying molecules in the gas phase, the molecular vibrations may be strongly affected by interactions with other molecules of the same kind or by interactions with solvent molecules. Developments in these areas will be outlined in the following paragraphs and after that the structure of this document will be given.

Developments

The starting point for prediction of molecular properties is usually the harmonic approximation. Because it generally overestimates observed frequencies (especially the hydrogen stretching vibrations) some kind of correction is applied to account for anharmonic effects. Because the errors in calculations appeared largely systematic, scaling of force field constants by empirical factors had been suggested [9, 10]. The method can be remarkably successful [11], but it may fail when experimental reference data are not available. There has been also considerable effort to account for anharmonic effects directly by including the anharmonic part of the potential into the vibrational Schrödinger equation. However, calculation of the anharmonic potential is computationally demanding task. In the past many applications relied on empirical or semi-empirical force fields with parameters determined by fitting of an analytic function to experimental data, but the accuracy of such models is not very high [12, 13]. For small and medium sized molecules, accurate *ab initio* potential energy surface can be calculated at selected points around the equilibrium geometry and interpolated by use of standard approximation techniques [14]. This approach is particularly useful, when only interactions between a limited number of vibrational modes can be considered and thus only integrals of limited

dimension need to be evaluated [15,16]. Another approach is to represent the potential by the lowest coefficients of Taylor series, determined from analytic second derivatives calculated at geometries displaced from the optimized geometry along nuclear coordinates [17]. Working in the basis of linear harmonic oscillator wave functions, only one-dimensional integrals need to be considered this way at the cost of truncating the higher coefficients of the Taylor expansion. In this work, PES was represented by a Taylor polynomial of the fourth order.

The beauty of the harmonic approximation is that it enables one to split the multidimensional Schrödinger equation into a set of independent one-dimensional problems with a simple analytic solution. For anharmonic potentials this is generally not possible and therefore approximative methods must be employed. The vibrational self-consistent field method (VSCF) developed by Bowman in 1978 [18] became very popular. The method includes anharmonic terms in the potential, yet retains separability of the harmonic approximation. Once the anharmonic potential is known, the method is efficient enough to be applied to large systems with thousands of degrees of freedom, such as was the case of the protein BPTI studied by Roitberg and Gerber [13]. The efficiency of VSCF comes at the price of lower accuracy, because the method neglects correlation of vibrational motions. Several extensions to VSCF have been therefore proposed, in a close parallel to methods applied in the electronic mean-field problem. The most general method is the vibrational configuration interaction (VCI), which looks for a solution expanded in some complete basis set, for instance linear harmonic oscillators (LHOs) or the VSCF solutions [19]. An alternative method is the vibrational perturbation theory (VPT), where the Rayleigh-Schrödinger perturbation method is used to correct either the harmonic [20,21] or the VSCF approximation [22]. Recently, Christiansen formulated vibrational coupled cluster theory (VCC) [23]. In this work, multiple anharmonic methods were implemented: VCI in the basis of LHOs, VSCF, and VPT of the second order for both the VSCF and harmonic approximation.

For biochemical problems it is important that vibrational spectra can be collected in an aqueous environment. Because the conformational changes induced by solvation often have a large effect on the spectra, there is a need for computationally affordable model. Continuum models are very popular, where the solute molecule is placed in a cavity surrounded by a polarizable continuum, whose reaction field modifies the energy and the properties of the solute molecule [24]. Polarizable continuum models are flexible and efficient, but they partially neglect important effects, such as hydrogen bonding and dispersion interactions. More precise but computationally expensive is inclusion of explicit solvent molecules. In this work, the conductor solvent model CPCM was used [25].

Document structure

The document is organized as follows. In the introductory Chapter 1, a brief account on developments in the *ab initio* modeling of vibrational spectra of large molecules in liquid phase is given.

Chapter 2 is devoted to theory. First there is a reminder of basic concepts and notations

of quantum chemistry, then a review of electronic methods used in this study for evaluation of potential energy surface follows. Although PES constitutes mere input data in this work, the choice of proper electronic method for evaluation of PES is of utmost importance for modeling of vibrational spectra. The vibrational problem is then reviewed and the anharmonic methods VCI, VPT and VSCF are discussed. The theory required for understanding how the intensities of IR, VCD, Raman and ROA transitions can be determined, follows. The chapter finishes with a review of the conductor solvent model.

In the concluding Chapter 3, the results of anharmonic calculations performed on a number of systems are presented, starting from the benchmark two-dimensional Henon-Heiles potential up to real molecules containing 26 atoms. The chapter also briefly summarizes two papers published by the author of this work in the Journal of Computational Chemistry and the Journal of Chemical Physics. Some preliminary results for the next paper under preparation are included.

CHAPTER 2

Theory

2.1 Basic concepts of quantum mechanics

In this section will be presented a cursory review of quantum mechanical principles and approximations ubiquitous in quantum chemical calculations.

In the quantum view of the world, a system at a time t is represented by a state vector $|\Psi(t)\rangle$ in a Hilbert space. State vectors can be projected onto a particular basis, e.g. the coordinate basis $\{|\boldsymbol{r}\rangle\}$

$$\Psi(\boldsymbol{r},t) = \langle \boldsymbol{r}|\Psi(t)\rangle. \tag{2.1.1}$$

A system of N spinless particles in three-dimensional space can be described by a *wave function* $\Psi(x_1, y_1, z_1, \ldots, z_N, t)$ of $3N+1$ variables. Physical observables are represented by self-adjoint operators, that is, ones whose matrix is *Hermitian.*[1] A distinct role is played by the *Hamiltonian* operator $\hat{\mathrm{H}}$, which gives the value of energy and also determines time evolution of a system through the *Schrödinger equation*

$$i\hbar\frac{\partial\Psi(\boldsymbol{r},t)}{\partial t} = \hat{\mathrm{H}}\Psi(\boldsymbol{r},t). \tag{2.1.2}$$

When the Hamiltonian does not depend on time, a stationary wave function can be separated into product functions

$$\Psi(\boldsymbol{r},t) = \Psi(\boldsymbol{r})\,\varphi(t), \qquad \varphi(t) = \mathrm{e}^{-iEt/\hbar}, \tag{2.1.3}$$

and the Schrödinger equation can be simplified into

$$\hat{\mathrm{H}}\,\Psi(\boldsymbol{r}) = E\,\Psi(\boldsymbol{r}). \tag{2.1.4}$$

The stationary wave function changes as a function of time only by a complex phase, therefore the probability amplitude

$$\langle\Psi(\boldsymbol{r})\,\varphi(t)|\Psi(\boldsymbol{r})\,\varphi(t)\rangle \equiv \int \Psi^*(\boldsymbol{r})\,\varphi^*(t)\,\Psi(\boldsymbol{r})\,\varphi(t)\,d\boldsymbol{r}\,dt = \langle\Psi(\boldsymbol{r})|\Psi(\boldsymbol{r})\rangle \tag{2.1.5}$$

is constant.[2]

[1] A Hermitian matrix is identical to its transpose with complex conjugate elements. An operator is defined as an entity which, when acting on a vector, converts it into a vector. The operator $\hat{\mathrm{O}}$ is completely determined by its matrix representation O_{ij} in a complete basis $\{|i\rangle\}$ by the expansion $\hat{\mathrm{O}}|j\rangle = \sum_i O_{ij}|i\rangle$. Note that $O_{ij} = \langle i|\hat{\mathrm{O}}|j\rangle$.

[2] The asterisk symbol (*) denotes complex conjugate.

Our system of interest is a molecule which consists of N_n nuclei and N_e electrons. The stationary wave function of a molecule can be found by solving the time-independent Schrödinger equation

$$\left[-\sum_{\alpha_i \in \boldsymbol{R}} \frac{\hbar^2}{2M_i} \frac{\partial^2}{\partial R_{\alpha_i}^2} - \sum_{\alpha_i \in \boldsymbol{r}} \frac{\hbar^2}{2m_e} \frac{\partial^2}{\partial r_{\alpha_i}^2} + V(\boldsymbol{R}, \boldsymbol{r}) \right] \Psi(\boldsymbol{R}, \boldsymbol{r}) = E\, \Psi(\boldsymbol{R}, \boldsymbol{r}), \tag{2.1.6}$$

where $\boldsymbol{R} = \{x_1, y_1, \ldots, z_{N_n}\}$ are the nuclei positions, $\boldsymbol{r} = \{x_1, y_1, \ldots, z_{N_e}\}$ are the positions of electrons, m_e is mas of electron and M_i is mass of i-th nucleus.

In a vacuum without external fields and without relativistic effects, the only forces between the particles are Coulomb interactions. The potential then has the form

$$V(\boldsymbol{R}, \boldsymbol{r}) = \frac{e^2}{4\pi\varepsilon_0} \left[\sum_{i<j} \frac{1}{|\boldsymbol{r}_i - \boldsymbol{r}_j|} + \sum_{i<j} \frac{Z_i Z_j}{|\boldsymbol{R}_i - \boldsymbol{R}_j|} - \sum_{i,j} \frac{Z_i}{|\boldsymbol{R}_i - \boldsymbol{r}_j|} \right], \tag{2.1.7}$$

where the electron i at $\boldsymbol{r}_i$ has charge $-e$ and the nucleus at $\boldsymbol{R}_i$ has charge eZ_i.

An analytic solution to this mathematical problem exists only for the simplest case of atoms with a single electron, such as the hydrogen atom or the He^+ ion. For other systems it must be solved numerically by employing approximative methods. The dimension of the problem grows very quickly and many simplifications must be introduced. Because even the smallest nucleus is much heavier than an electron[3], the motions of electrons and nuclei can be separated and the wave function can be expressed as a product of the electronic and the nuclear part

$$\Psi(\boldsymbol{R}, \boldsymbol{r}) = \Psi_e(\boldsymbol{r}; \boldsymbol{R})\, \Psi_n(\boldsymbol{R}). \tag{2.1.8}$$

The equation is called *adiabatic approximation*, and it is justified by the fact that the electronic charge distribution adjusts almost instantaneously to slow changes in nuclear positions. When the Schrödinger equation is applied to the adiabatic wave function, it is common to neglect nuclear derivatives of the electronic wave function $\nabla_n \psi_e$ in the nuclei kinetic energy term

$$\begin{aligned} \frac{\partial^2}{\partial \boldsymbol{R}^2} \Psi_e(\boldsymbol{r}; \boldsymbol{R})\, \Psi_n(\boldsymbol{R}) &= \Psi_e \nabla_n^2 \Psi_n + \Psi_n \nabla_n^2 \Psi_e + 2\, (\nabla_n \Psi_n)\, (\nabla_n \Psi_e) \\ &\simeq \Psi_e \nabla_n^2 \Psi_n. \end{aligned} \tag{2.1.9}$$

In the *Born-Oppenheimer approximation* (BOA), Eq. 2.1.6 can be then written as

$$\left[-\sum_{\alpha_i \in \boldsymbol{r}} \frac{\hbar^2}{2m_e} \frac{\partial^2}{\partial r_{\alpha_i}^2} + V_{ee} + V_{en} \right] \Psi_e(\boldsymbol{r}; \boldsymbol{R}) = E_e(\boldsymbol{R})\, \Psi_e(\boldsymbol{r}; \boldsymbol{R}) \tag{2.1.10}$$

$$\left[-\sum_{\alpha_i \in \boldsymbol{R}} \frac{\hbar^2}{2M_i} \frac{\partial^2}{\partial R_{\alpha_i}^2} + V_{nn} \right] \Psi_n(\boldsymbol{R}) = E_n\, \Psi_n(\boldsymbol{R}). \tag{2.1.11}$$

[3]The proton-electron mass ratio is 1836.

The electronic part of the wave function now depends on the positions of nuclei only parametrically. If evaluated for different nuclear positions, the electronic energy is obtained as a function of $\boldsymbol{R}$. This function is known as the *potential energy surface.* Thus in the Born-Oppenheimer approximation, the nuclei move on a potential energy surface obtained by solving the electronic problem 2.1.10.

The mathematical separation of nuclear and electronic motions respects experimental observation, because transitions between electronic states are usually energetically well separated from vibrational and rotational transitions: electronic transitions correspond to energies of photons from the visible and ultraviolet region of spectra, but energy differences between vibrational states are measured in the infrared region. Similarly, energy differences between rotational states correspond to photons from the microwave region and are therefore well separated from the infrared region of vibrational transitions. Consequently, nuclear vibrations can be often treated separately from rotational motions. Before proceeding to this problem, approximate electronic methods of quantum chemistry will be outlined.

2.2 General techniques

2.2.1 The variational principle

An important approach for finding solutions to the eigenvalue equation

$$\hat{\mathrm{H}}\,|\Psi\rangle = E\,|\Psi\rangle \tag{2.2.1}$$

is the *variational principle*, which states that the expectation value of the Hamiltonian is larger or equal to the exact ground state energy

$$E_0 \leq \langle\Psi|\hat{\mathrm{H}}|\Psi\rangle, \tag{2.2.2}$$

where $|\Psi\rangle$ is normalized, that is, $\langle\Psi|\Psi\rangle = 1$. The inequality can be easily proved. The function $|\Psi\rangle$ can be expanded into the complete set $\{\Psi_n\}$ of orthonormal eigenfunctions of $\hat{\mathrm{H}}$, so that

$$\langle\Psi|\hat{\mathrm{H}}|\Psi\rangle = \sum_{i,j} c_i^* c_j \langle\Psi_i|\hat{\mathrm{H}}|\Psi_j\rangle = \sum_i |c_i|^2 E_i \geq \sum_i |c_i|^2 E_0 = E_0. \tag{2.2.3}$$

Thus the task of finding the ground state eigenfunction takes on the form of determining the optimum set of coefficients $\{c_i\}$. As will be shown, it can be solved by matrix diagonalization. Since the function $|\Psi\rangle$ is normalized, the coefficients are subject to the constraint

$$\langle\Psi|\Psi\rangle = \sum_i |c_i|^2 = 1. \tag{2.2.4}$$

The problem of minimizing the function $\langle\Psi|\hat{\mathrm{H}}|\Psi\rangle$ can be solved by the method of Lagrange multipliers. The Lagrange function is

$$\begin{aligned} \mathcal{L}(c_1, c_2, \ldots) &= \langle\Psi|\hat{\mathrm{H}}|\Psi\rangle - E\,(\langle\Psi|\Psi\rangle - 1) \\ &= \sum_{i,j} c_i^* c_j \langle\Psi_i|\hat{\mathrm{H}}|\Psi_j\rangle - E\left(\sum_i |c_i|^2 - 1\right). \end{aligned} \tag{2.2.5}$$

Note that the second term in the equation is zero and therefore the minimum of both $\langle\Psi|\hat{\mathrm{H}}|\Psi\rangle$ and $\mathcal{L}$ occurs at the same value of coefficients. The values c_i which minimize $\mathcal{L}$ are then sought by finding the extreme of $\mathcal{L}$

$$0 = \frac{\partial \mathcal{L}}{\partial c_k^*} = \sum_i c_i H_{ik} - c_k E, \qquad k = 1, \ldots \tag{2.2.6}$$

which yields the standard matrix eigenvalue problem

$$\sum_i H_{ij} c_i = E\, c_j. \tag{2.2.7}$$

In general, the basis $\{\Psi_n\}$ is infinitely large, but only a limited number of functions can be included in practice. Within a given finite subspace, the lowest eigenvalue is the best approximation to the ground state energy.

2.2.2 Perturbation method

Perturbation theory (PT) is a tool for finding an approximate solution to a problem which is too complicated to be solved exactly. It starts from an exact solution to a simpler problem and applies a small disturbance to the system. For instance, the harmonic potential describes the vibrational motion of molecules rather well and thus the anharmonic terms in the potential can be regarded as a perturbation. Another example is the interaction of electromagnetic radiation with molecules, inside of which much stronger electrostatic interactions take effect. The anharmonicity of the vibrational potential does not depend on time. In such case we talk about *time-independent perturbation theory*. On the other hand, electromagnetic radiation falls in the category of *time-dependent perturbation*, because the radiation electromagnetic field varies with time.

Time-independent perturbation theory

Assume that the system of interest can be described by a Hamiltonian $\hat{\mathrm{H}}$ which can be split into a part $\hat{\mathrm{H}}^{(0)}$ with known exact solutions and a small perturbation $\hat{\mathrm{W}}$. An arbitrary dimensionless parameter λ is introduced

$$\hat{\mathrm{H}} = \hat{\mathrm{H}}^{(0)} + \lambda\hat{\mathrm{W}}. \tag{2.2.8}$$

Because the Hamiltonian depends on λ, also the energy and wave functions depend on it. It is assumed that for a weak perturbation they can be written in terms of power series

$$\begin{aligned} E &= E^{(0)} + \lambda E^{(1)} + \lambda^2 E^{(2)} + \cdots \\ |\Psi\rangle &= |\psi^{(0)}\rangle + \lambda|\psi^{(1)}\rangle + \lambda^2|\psi^{(2)}\rangle + \cdots, \end{aligned} \tag{2.2.9}$$

where $E^{(0)}$ is the energy of the unperturbed system and $\psi^{(0)}$ is the corresponding wave function. Inserting the power series into the Schrödinger equation 2.1.4 and comparing terms of each power of λ, one obtains an infinite series of simultaneous equations

$$\begin{aligned} \hat{\mathrm{H}}^{(0)}|\psi_i^{(0)}\rangle &= E_i^{(0)}|\psi_i^{(0)}\rangle \\ \hat{\mathrm{H}}^{(0)}|\psi_i^{(1)}\rangle + \hat{\mathrm{W}}|\psi_i^{(0)}\rangle &= E_i^{(0)}|\psi_i^{(1)}\rangle + E_i^{(1)}|\psi_i^{(0)}\rangle \\ \hat{\mathrm{H}}^{(0)}|\psi_i^{(2)}\rangle + \hat{\mathrm{W}}|\psi_i^{(1)}\rangle &= E_i^{(0)}|\psi_i^{(2)}\rangle + E_i^{(1)}|\psi_i^{(1)}\rangle + E_i^{(2)}|\psi_i^{(0)}\rangle \\ &\cdots \end{aligned} \tag{2.2.10}$$

The first-order correction to the i-th solution Ψ_i can be expanded in the basis set of unperturbed solutions $\psi_j^{(0)}$

$$\psi_i^{(1)} = \sum_j c_{ij}\,\psi_j^{(0)}. \tag{2.2.11}$$

When the second equation is multiplied by the bra vector $\langle\psi_i^{(0)}|$, the expression for the first-order energy correction is obtained

$$E_i^{(1)} = \langle\psi_i^{(0)}|\hat{\mathrm{W}}|\psi_i^{(0)}\rangle. \tag{2.2.12}$$

The coefficients can be determined by multiplying the second equation by the vector $\psi_k^{(0)}$

$$c_{ik} = \frac{\langle\psi_k^{(0)}|\hat{\mathrm{W}}|\psi_i^{(0)}\rangle}{E_i^{(0)} - E_k^{(0)}}, \qquad k \neq i. \tag{2.2.13}$$

The second-order correction is obtained in a similar way from the third equation of 2.2.10

$$E_i^{(2)} = \sum_{j\neq i} \frac{|\langle\psi_i^{(0)}|\hat{\mathrm{W}}|\psi_j^{(0)}\rangle|^2}{E_i^{(0)} - E_j^{(0)}}. \tag{2.2.14}$$

Simplified degeneracy treatment

The perturbation expressions fail when two or more *degenerate states* with the same energy occur. The perturbation operator $\hat{\mathrm{W}}$ can split the degenerate energy levels. The set of problematic degenerate states $D = \{\psi_i^{(0)}\}$ is replaced by their linear combination

$$\phi_j = \sum_{i\in D} c_{ji}\,\psi_i^{(0)} \tag{2.2.15}$$

obtained by diagonalization of the perturbation operator $\hat{\mathrm{W}}$ in the basis of the degenerate states, that is, by solving the eigenvalue problem

$$\sum_i c_{ji}\,\langle\psi_k^{(0)}|\hat{\mathrm{W}}|\psi_i^{(0)}\rangle = c_{jk}\,w_j, \qquad i,j,k \in D. \tag{2.2.16}$$

The value of the perturbed energy of the degenerate states is then

$$E_i = E_i^{(0)} + \langle\phi_i|\hat{\mathrm{W}}|\phi_i\rangle. \tag{2.2.17}$$

Because of a large number of near-degenerate and degenerate energy levels in large systems, the following simplified degeneracy-corrected formula [26] was used in practical calculations instead of the formula Eq. 2.2.14

$$E_i^{(2)'} = \sum_{j\neq i} \frac{1}{2}(E_j - E_i) \pm \frac{1}{2}\sqrt{(E_i - E_j)^2 + 4W_{ij}^2}, \qquad E_i = E_i^{(0)} + W_{ii}. \tag{2.2.18}$$

In the formula is used + sign when $E_i > E_j$ and − sign when $E_i < E_j$. As shown in Appendix A.1, for non-degenerate states the formula leads to the standard perturbation formula. In the case of two-fold degeneracy, the formula is exact.

Time-dependent perturbation theory

When the perturbation operator is not stationary and changes with time, the time-dependent Schrödinger equation (Eq. 2.1.2) must be used

$$i\hbar \frac{\partial \Psi}{\partial t} = \left[\hat{\mathrm{H}} + \hat{\mathrm{W}}(t)\right] \Psi(t). \tag{2.2.19}$$

The state of the system at time t can be expressed in terms of the stationary solutions ψ_j to the unperturbed Hamiltonian

$$\Psi(t) = \sum_j c_j(t)\, e^{-iE_j t/\hbar} \psi_j. \tag{2.2.20}$$

Inserting it into Eq. 2.2.19 and multiplying by the stationary bra vector $\langle \psi_k |$, the equation can be reduced to partial differential equations for the amplitudes

$$i\hbar \frac{d}{dt} c_k(t) = \sum_j W_{kj}(t)\, c_j(t)\, e^{-i\omega_{jk} t}, \qquad \omega_{jk} = (E_j - E_k)/\hbar. \tag{2.2.21}$$

Up to this point, the expression is exact. Similarly to the stationary PT, the approximation is introduced that the coefficients c_k can be expanded in terms of the perturbation parameter λ

$$c_k = c_k^{(0)} + \lambda c_k^{(1)} + \lambda^2 c_k^{(2)} + \cdots. \tag{2.2.22}$$

By comparing terms with each power of λ, iterative solutions are obtained. The amplitudes in the first-order approximation can be written as

$$c_k(t) = c_k(0) + \frac{1}{i\hbar} \sum_j \int_0^t W_{kj}(\tau)\, c_j(0)\, e^{-i\omega_{jk}\tau}\, d\tau. \tag{2.2.23}$$

In the particular case of electromagnetic radiation, the perturbation is oscillating with angular frequency ω

$$\hat{\mathrm{W}}(t) = W e^{i\omega t} + W^* e^{-i\omega t} \tag{2.2.24}$$

and the equation can be easily integrated. To simplify the equation, assume that the system was initially in the state ψ_j. Therefore the initial values of amplitudes are $c_k(0) = \delta_{kj}$. Integrating the equation with the perturbation in the harmonic form, one obtains

$$c_k(t) = \frac{1}{\hbar} \left[W_{kj} \frac{e^{-i(\omega_{jk}-\omega)t} - 1}{\omega_{jk} - \omega} + W_{kj}^* \frac{e^{-i(\omega_{jk}+\omega)t} - 1}{\omega_{jk} + \omega} \right]. \tag{2.2.25}$$

When studying resonance effects, such as absorption of photons, the frequency of the incident light ω is close to the frequency ω_{jk}. The first term will be therefore much more significant and

we neglect the other. The probability amplitude is then

$$|c_k(t)|^2 = \frac{4\,|W_{kj}|^2}{\hbar^2}\frac{\sin^2(\omega_{jk}-\omega)t/2}{(\omega_{jk}-\omega)^2}. \tag{2.2.26}$$

This result will become useful later when discussing transition probabilities between vibrational states in Sec. 2.5.

2.3 Approximate methods of quantum chemistry

The quality of predicted vibrational frequencies and intensities undoubtedly rises and falls with the quality of the nuclear potential energy surface. Several electronic structure methods have been used in this study to test the influence of the nuclear potential on calculated spectra.

2.3.1 The Hartree-Fock approximation

The electronic wave function in Eq. 2.1.10 depends only on spatial coordinates. The spin associated with an electron gives an additional two-valued degree of freedom. The one-electron wave function with spin is represented by a product of the spatial part and one of the two *spin functions*, α or β, corresponding to spin-up and spin-down

$$\psi(\boldsymbol{x}) \equiv \psi(\boldsymbol{r})\,\alpha \quad \text{or} \quad \psi(\boldsymbol{x}) \equiv \psi(\boldsymbol{r})\,\beta. \tag{2.3.1}$$

The wave functions $\psi(\boldsymbol{x})$ are called *spin orbitals*, where $\boldsymbol{x}$ is a generalized coordinate which includes spatial and spin coordinate.

Because the electrons obey the Fermi-Dirac statistic, the wave function must change sign upon exchange of any pair of electrons. The antisymmetry of the wave function is in the Hartree-Fock theory (HF) enforced by the use of wave functions in the form of a Slater determinant. Given a set of linearly independent spin orbitals $\{\psi_i(\boldsymbol{x}_i)\}$, the n-electron *Slater determinant* is

$$\Psi_e(\boldsymbol{x}_1,\ldots,\boldsymbol{x}_n) = \frac{1}{\sqrt{n!}}\begin{vmatrix} \psi_1(\boldsymbol{x}_1) & \cdots & \psi_n(\boldsymbol{x}_1) \\ \vdots & \ddots & \vdots \\ \psi_1(\boldsymbol{x}_n) & \cdots & \psi_n(\boldsymbol{x}_n) \end{vmatrix}. \tag{2.3.2}$$

The factor $1/\sqrt{n!}$ is a normalization factor. The mathematical form of the determinant assures that upon switching two rows (i.e. exchanging two electrons), the wave function changes sign. If a single spin-orbital was occupied by two electrons, two identical columns would make the determinant zero.

For a wave function in the form of a Slater determinant, the expectation energy is given as a sum of one-electron kinetic terms

$$\langle i|\hat{\mathrm{h}}|i\rangle = -\frac{\hbar^2}{2m_e}\int \psi_i^*(d\boldsymbol{r})\frac{\partial^2\psi_i(d\boldsymbol{r})}{\partial \boldsymbol{r}_i^2}\,d\boldsymbol{r} \tag{2.3.3}$$

and two-electron potential terms

$$\frac{1}{2}\sum_{i,j}\left[(ij \mid ij) - (ij \mid ji)\right], \tag{2.3.4}$$

where

$$(ij \mid kl) \equiv \frac{e^2}{4\pi\epsilon_0}\iint d\boldsymbol{x}_1\,d\boldsymbol{x}_2\,\psi_i^*(\boldsymbol{x}_1)\psi_j^*(\boldsymbol{x}_2)\frac{1}{|\boldsymbol{x}_1-\boldsymbol{x}_2|}\psi_k(\boldsymbol{x}_1)\psi_l(\boldsymbol{x}_2). \tag{2.3.5}$$

The first two-electron term of the potential corresponds to the classical Coulomb repulsion,

the other is the so called exchange term with no classical analog, which is not zero only for electrons with parallel spins. The integrals are usually expressed using the convenient form of the *Coulomb operator* $\hat{\mathrm{J}}_i$ and the *exchange operator* $\hat{\mathrm{K}}_i$

$$\hat{\mathrm{J}}_i\,\psi_j(\boldsymbol{x}) \equiv \frac{e^2}{4\pi\epsilon_0}\left(\int \frac{|\psi_i(\boldsymbol{x}_1)|^2}{|\boldsymbol{x}-\boldsymbol{x}_1|}\,d\boldsymbol{x}_1\right)\psi_j(\boldsymbol{x}) \tag{2.3.6}$$

$$\hat{\mathrm{K}}_i\,\psi_j(\boldsymbol{x}) \equiv \frac{e^2}{4\pi\epsilon_0}\left(\int \frac{\psi_i(\boldsymbol{x}_1)^*\psi_j(\boldsymbol{x}_1)}{|\boldsymbol{x}-\boldsymbol{x}_1|}\,d\boldsymbol{x}_1\right)\psi_i(\boldsymbol{x}). \tag{2.3.7}$$

The exchange integrals arise because of the antisymmetric nature of the wave function. The operator is non-local, in the sense that when operating on $\psi(\boldsymbol{x}_0)$, it does depend on the value of $\boldsymbol{x}$ throughout all space, not just at $\boldsymbol{x}_0$.

The Hartree-Fock theory is based on the variational principle described in Sec. 2.2.1, but instead of differentiating with respect to the coefficients, the more general technique of functional variation is used. To find the best energy, the functional $E[\Psi_e] = \langle\Psi_e|\hat{\mathrm{H}}|\Psi_e\rangle$ is minimized with respect to the spin orbitals $\{\psi_i(\boldsymbol{x}_i)\}$. Introducing the Lagrange multipliers ϵ_i and assuming orthonormality of the spin orbitals, the functional $\mathcal{L}$ has the form

$$\mathcal{L}[\{\psi_i\}] = \sum_i \langle i|\hat{\mathrm{h}}|i\rangle + \frac{1}{2}\sum_{i,j}[(ij\mid ij) - (ij\mid ji)] - \sum_i \epsilon_i(\langle\psi_i|\psi_i\rangle - 1). \tag{2.3.8}$$

Minimizing the functional $\mathcal{L}$ by setting its first variation to zero, one arrives at the *Hartree-Fock equations*

$$\left[\hat{\mathrm{h}} + \sum_j\left(\hat{\mathrm{J}}_j - \hat{\mathrm{K}}_j\right)\right]|\psi_i\rangle = \epsilon_i\,|\psi_i\rangle \qquad i = 1,\ldots,n. \tag{2.3.9}$$

Note that although the equations formally resemble linear eigenvalue equations, the Coulomb and exchange operators depend on the solutions ψ_i. Therefore the Hartree-Fock equations are usually solved by iterative procedures. Starting from an initial guess of the spin orbitals, the equations are solved to obtain new spin orbitals. The solutions are inserted into the equations again and new orbitals are calculated. The procedure is repeated until self-consistency is reached, i.e. the spin orbitals do not vary.

Only for atoms is it common to calculate the equations numerically. Molecular calculations are performed by expanding the spatial part of spin orbitals (also known as *molecular orbitals*) into a set of k known spatial basis functions (*atomic orbitals*)

$$|\psi_i\rangle = \sum_{\mu=1}^{k} c_{i\mu}\,|\phi_\mu\rangle \qquad i = 1,\ldots,n, \quad n \le k. \tag{2.3.10}$$

The problem leads to the *Roothaan equations*

$$\sum_{\mu=1}^{k} F_{\nu\mu}\,c_{i\mu} = \epsilon_i \sum_{\mu=1}^{k} S_{\nu\mu}\,c_{i\mu} \qquad i = 1,\ldots,n, \quad \nu = 1,\ldots,k, \tag{2.3.11}$$

where

$$F_{\mu\nu} = \langle\phi_\mu|\hat{\mathrm{h}} + \sum_\pi \left(\hat{\mathrm{J}}_\pi - \hat{\mathrm{K}}_\pi\right)|\phi_\nu\rangle \tag{2.3.12}$$

$$S_{\mu\nu} = \langle\phi_\mu|\phi_\nu\rangle. \tag{2.3.13}$$

The equations are solved iteratively with the aid of matrix diagonalization. Because the molecular orbitals ψ_i are in Roothaan equations approximated by a linear combination of a finite number of atomic orbitals ϕ_μ, the quality of the solution depends on the quality and the number of atomic orbitals. The problem of choice of basis set will be discussed in Sec. 2.3.7.

The Hartree-Fock approximation plays an important role in quantum chemistry. By describing the electronic wave function by a product of one-electron functions, it is possible to split the multidimensional Schrödinger equation 2.1.6 into a set of one-dimensional equations 2.3.9 and solve large many-body problems.[4] However, in this description the electrons move independently in a mean field electrostatic potential, which leads to an error in the prediction of the total molecular energy. The energy calculated by Roothaan equations in a finite basis is larger than the exact solution of Hartree-Fock equations, and the Hartree-Fock energy lies higher than the Schödinger energy. The difference between the Hartree-Fock limit and the Schödinger energy is called *correlation energy*. Although the neglect of correlation energy may lead to large deviations from experimental results, Hartree-Fock approximation serves as a starting point for more accurate methods.

2.3.2 Configuration interaction

The main deficiency of the Hartree-Fock method is the neglect of correlation between motions of electrons with different spins. A principal and conceptually simple solution to this problem is to solve the secular equation (Eq. 2.2.7) in the basis of, for example, variously configured Slater determinants, obtained by solving Roothaan's equations. The method is known as *configuration interaction* (CI). With a complete basis, the full CI method yields the exact solution. In practical applications, however, only a finite basis set can be used. A systematic approach to forming the basis set is to take the HF solution and replace a limited number of occupied spin orbitals ψ_i by virtual orbitals[5] ψ_a, to form singly, doubly, etc., excited determinants $\{\Psi_{ijk\ldots}^{abc\cdots}\}$. The number of thus created functions grows exponentially with the size of the system. Even when including only singly and doubly excited determinants, the method is impractical for all but the smallest

[4]The dominant step in Hartree-Fock calculations is the evaluation of all two-electron integrals in the basis of atomic orbitals

$$(ij \mid kl) = \sum_{\mu\nu\lambda\sigma} c_{i\mu}^* c_{j\nu}^* c_{k\lambda} c_{l\sigma} (\mu\nu \mid \lambda\sigma). \tag{2.3.14}$$

The number of the integrals grows as $O(N^4)$ with the number of atomic orbitals. Fortunately, many of the integrals are negligibly small and may be screened out by employing the Schwartz inequality. In modern quantum chemistry programs, the scaling can be reduced below $O(N^3)$ [27].

[5]For k spatial functions ϕ_μ, the eigenvalue problem 2.3.11 yields for each i a set of $2k$ orthonormal spin orbitals. The n spin orbitals with the lowest energies are called *occupied*, while the remaining $2k - n$ are called *virtual* spin orbitals.

systems.[6] Another problem of partial CI is that it is not *size consistent*, that is, a sum of energies calculated for non-interacting subsystems is not equal to the energy calculated for the whole system.

2.3.3 Coupled cluster

The size inconsistency of the CISD method is remedied by another approximate approach to full CI, called *coupled cluster* theory (CC) [28]. The exact wave function in the coupled cluster formalism is expressed in terms of the exponential operator

$$e^{\hat{\mathrm{T}}} = 1 + \hat{\mathrm{T}} + \frac{1}{2}\hat{\mathrm{T}}^2 + \frac{1}{6}\hat{\mathrm{T}}^3 + \cdots, \tag{2.3.15}$$

operating on the ground state Slater determinant. The operator $\hat{\mathrm{T}}$ is a cluster operator

$$\hat{\mathrm{T}} = \hat{\mathrm{T}}_1 + \hat{\mathrm{T}}_2 + \hat{\mathrm{T}}_3 + \cdots, \tag{2.3.16}$$

where the subscribed operators cluster linear combinations of singly, doubly, etc., excitations of the reference wave function. For instance,

$$\hat{\mathrm{T}}_1\Psi_0 = \sum_i t_i^a \Psi_i^a, \qquad \hat{\mathrm{T}}_2\Psi_0 = \sum_{\substack{i>j \\ a>b}} t_{ij}^{ab}\Psi_{ij}^{ab}, \tag{2.3.17}$$

where the expansion coefficients $t_{ij\cdots}^{ab\cdots}$ are to be determined. To better see a link, or rather a difference, between the CC and CI methods, compare the expressions for the exact CC wave function

$$\Psi_{\mathrm{CC}} = \left[1 + (\hat{\mathrm{T}}_1 + \hat{\mathrm{T}}_2 + \cdots) + \frac{1}{2}(\hat{\mathrm{T}}_1 + \hat{\mathrm{T}}_2 + \cdots)(\hat{\mathrm{T}}_1 + \hat{\mathrm{T}}_2 + \cdots) + \cdots\right]\Psi_0. \tag{2.3.18}$$

and the exact CI wave function

$$\Psi_{\mathrm{CI}} = \left[1 + \hat{\mathrm{C}}_1 + \hat{\mathrm{C}}_2 + \cdots\right]\Psi_0. \tag{2.3.19}$$

For example, the four-excitation operator $\hat{\mathrm{C}}_4$ can be decomposed into the terms

$$\hat{\mathrm{C}}_4 = \hat{\mathrm{T}}_4 + \frac{1}{2}\hat{\mathrm{T}}_2^2 + \hat{\mathrm{T}}_1\hat{\mathrm{T}}_3 + \frac{1}{2}\hat{\mathrm{T}}_1^2\hat{\mathrm{T}}_2 + \frac{1}{4!}\hat{\mathrm{T}}_1^4. \tag{2.3.20}$$

The **CCSD** method [29] truncates the operator $\hat{\mathrm{T}}$ after the second term. A rather tedious derivation of CCSD equations starts by inserting the CCSD wave function in the Schrödinger

[6] Such a calculation is referred to as singly (CIS) and doubly (CISD) excited configuration interaction. CISD scales as $O(N^6)$.

equation and projecting onto a set of functions Ψ_0, $\{\Psi_i^a\}$ and $\{\Psi_{ij}^{ab}\}$

$$\begin{aligned}
\langle\Psi_0|\hat{\mathrm{H}} - E|e^{(\hat{\mathrm{T}}_1+\hat{\mathrm{T}}_2)}\,\Psi_0\rangle &= 0, \\
\langle\Psi_i^a|\hat{\mathrm{H}} - E|e^{(\hat{\mathrm{T}}_1+\hat{\mathrm{T}}_2)}\,\Psi_0\rangle &= 0, \\
\langle\Psi_{ij}^{ab}|\hat{\mathrm{H}} - E|e^{(\hat{\mathrm{T}}_1+\hat{\mathrm{T}}_2)}\,\Psi_0\rangle &= 0.
\end{aligned} \tag{2.3.21}$$

Because the Hamiltonian contains at most two-electron operators, only a limited number of expansion terms are non-zero. For example, the first equation evaluates to

$$\langle\Psi_0|\hat{\mathrm{H}} - E|(1 + \hat{\mathrm{T}}_1 + \hat{\mathrm{T}}_2 + \frac{1}{2}\hat{\mathrm{T}}_2^2)\Psi_0\rangle = 0. \tag{2.3.22}$$

The energy E from the first equation is inserted into the two other equations and evaluated in terms of the coefficients t_i^a and t_{ij}^{ab} to obtain nonlinear equations, which have to be solved iteratively.

The CCSD method solves the size consistency problem of CI and effectively includes also some triple and quadruple excitation terms of the CI [29]. CCSD scales as $O(N^6)$.

2.3.4 Møller-Plesset perturbation theory

The correlation effects can be accounted for also by employing the Rayleigh-Schrödinger perturbation theory. The perturbation method where the Hartree-Fock solution appears as the zero-order approximation is known as the *Møller-Plesset perturbation theory* [30]. It is completely analogous to the vibrational perturbation theory given in Sec. 2.4.5. In this work the perturbation theory of the second order (MP2) was used. The method gives often results similar to CCSD, but scales more favorably with the size of the molecule: MP2 scales as $O(N^4)$.

2.3.5 Density functional theory

An alternative approach to the electronic problem is the *density functional theory* (DFT). In the Born-Oppenheimer approximation the electrons move in an "external" static potential of nuclei

$$\hat{\mathrm{V}}_{en} = -\frac{e^2}{4\pi\varepsilon_0}\sum_i \frac{Z_i}{|\boldsymbol{R}_i - \boldsymbol{r}|}. \tag{2.3.23}$$

The rest of the Hamiltonian

$$\hat{\mathrm{F}} = -\sum_{\alpha_i\in\boldsymbol{r}} \frac{\hbar^2}{2m_e}\frac{\partial^2}{\partial r_{\alpha_i}^2} + \frac{e^2}{4\pi\varepsilon_0}\sum_{i<j}\frac{1}{|\boldsymbol{r}_i - \boldsymbol{r}_j|} \tag{2.3.24}$$

is the same for all n-electron systems, therefore the Hamiltonian and hence the ground state $|\Psi_0\rangle$ is completely determined by the external potential $\hat{\mathrm{V}}_{en}$. The ground state wave function gives rise to the ground state *electronic density*

$$\rho_0(\boldsymbol{r}) = \int |\Psi_0(\boldsymbol{r}, \boldsymbol{r}_2, \ldots, \boldsymbol{r}_n)|^2\, d\boldsymbol{r}_2 \ldots d\boldsymbol{r}_n. \tag{2.3.25}$$

The density functional theory is based on the concept of the electronic density as the *fundamental variable.* Formal justification for utilizing the three-dimensional function $\rho(\boldsymbol{r})$ instead of the many-dimensional wave function Ψ_0 comes from the theorems of Hohenberg and Kohn [31]. They presented an elegant proof, that the external potential $\hat{\mathrm{V}}_{en}$ (and therefore the Hamiltonian and also the ground state solution) is uniquely determined by the corresponding ground state electronic density, up to an additive constant. Consequently, the variational principle for the *energy functional*

$$E_V[\rho] = \langle \Psi_\rho | \hat{\mathrm{F}} | \Psi_\rho \rangle + \int V(\boldsymbol{r})\, \rho(\boldsymbol{r})\, d\boldsymbol{r} \tag{2.3.26}$$

can be formulated. Given any electronic density ρ' associated to a n-electron system with an external potential $\hat{\mathrm{V}}'$, the energy will be always higher than or equal to that of the ground state

$$E_V[\rho] \leq E_V[\rho']. \tag{2.3.27}$$

Thus the ground state energy may be determined by minimization with respect to the electronic density alone. The original formulation requires that the ground state is non-degenerate and that densities must be associated with some external potential. These requirements were weakened by Levy [32] in the new *constrained search* formulation, where the only requirement is that the density must be obtainable from some n-electron wave function.

Although the theorems assure the existence of the universal functional $F[\rho] = \langle \Psi_\rho | \hat{\mathrm{F}} | \Psi_\rho \rangle$, which is independent of the external potential, its exact form is not known. In the practical computational method introduced by Kohn and Sham [33], the problem of many interacting electrons is treated as the problem of non-interacting electrons, with the difference accounted for by addition of some extra terms. The electrons are described by one-dimensional functions ψ_i known as *Kohn-Sham orbitals.* The functional is formally split into three parts

$$F[\rho] = T[\rho] + \frac{1}{2} \int \frac{\rho(\boldsymbol{r})\, \rho(\boldsymbol{r}')}{|\boldsymbol{r} - \boldsymbol{r}'|}\, d\boldsymbol{r}\, d\boldsymbol{r}' + E_{xc}[\rho]. \tag{2.3.28}$$

The first term is the kinetic energy of non-interacting electron gas, the second is the classical electrostatic electron-electron interaction and the remaining term is the unknown *exchange-correlation energy*, containing non-classical electron-electron interactions and the difference between the kinetic energy of interacting and non-interacting system. The effective Kohn-Sham potential is defined

$$\hat{\mathrm{V}}_{KS} \equiv \hat{\mathrm{V}}_{en} + \int \frac{\rho(\boldsymbol{r}')}{|\boldsymbol{r} - \boldsymbol{r}'|}\, d\boldsymbol{r}' + \frac{\delta E_{xc}[\rho]}{\delta \rho} \tag{2.3.29}$$

and the *Kohn-Sham equations* are obtained by use of the variational principle

$$\left[-\frac{1}{2} \nabla_i^2 + \hat{\mathrm{V}}_{KS} \right] |\psi_i\rangle = \epsilon_i\, |\psi_i\rangle, \quad i = 1, \ldots, n. \tag{2.3.30}$$

The electronic density is determined from the Kohn-Sham orbitals by

$$\rho(\boldsymbol{r}) = 2\sum_{i=1}^{n} |\psi_i(\boldsymbol{r})|^2. \tag{2.3.31}$$

The factor of 2 is valid for systems with closed shells and comes from a double degeneracy due to the spin of electrons.

Note that HF is in a sense just a special case of DFT, with the correlation part of the energy E_c being zero and the exchange part E_x being equal to the mean value of the exchange operator $\hat{\mathrm{K}}_i$ (Eq. 2.3.7). Because the form of the exchange-correlation energy functional and its derivative is usually too complex to be integrated analytically, the exchange-correlation energy must be evaluated by numerical integration, which adds a source of numerical errors to DFT implementations, in contrast to HF.

DFT approximations

In any practical implementation, the unknown exchange-correlation energy $E_{xc}[\rho]$ must be approximated and a large number of functionals have been proposed. The construction of the functionals is not straightforward and there is no systematic way for improving them. The functionals often incorporate some empirical parameters. For instance, the exchange energy functional of Becke [34] contains one numerical parameter, which was determined by a least squares fit to exact atomic Hartree-Fock exchange energies of noble gas atoms.

The first and simplest approximation to the exchange-correlation energy is the *local density approximation* (LDA) [33]. The exchange-correlation energy is defined as a sum of local contributions $\epsilon_{xc}^{\mathrm{LDA}}$, which are set equal to that of a homogeneous electron gas

$$E_{xc}^{\mathrm{LDA}}[\rho] = \int \rho(\boldsymbol{r})\, \epsilon_{xc}^{\mathrm{LDA}}(\rho)\, d\boldsymbol{r}. \tag{2.3.32}$$

Although the approximation is simple and justified only for slow varying densities, it gives qualitatively accurate results even for systems with rapidly varying charge densities. A straightforward generalization of LDA to include electron spin is the *local spin density approximation* (LSDA), where the exchange-correlation energy per particle becomes a function of two spin densities $\epsilon_{xc}^{\mathrm{LSDA}}(\rho_\alpha, \rho_\beta)$. The local density approximations were known to overestimate bond energies. New exchange correlation functionals were devised, which depend also on density gradients and higher order density derivatives. These methods fall in the category of *generalized gradient approximation* (GGA) methods.

In this work the functionals BPW91 and B3LYP were used. The **BPW91** functional combines the exchange energy functional of Becke [34] and the correlation energy functional of Perdew and Wang [35]. The hybrid **B3LYP** functional [36] includes an empirical mixture of Hartree-Fock exchange energy with the non-local exchange-correlation energy of Lee, Yang and Parr [37].

2.3.6 Semi-empirical methods

The computational cost of quantum mechanical *ab initio* methods restricts their use only for small systems. Many molecules of interest are much larger and therefore computationally less demanding methods have been developed. In this study, the method **PM3** has been used for comparison with quantum mechanical models. It is based on the Hartree-Fock formalism described in Sec. 2.3.1, but it uses a simplified Hamiltonian, avoiding the calculation of computationally expensive two-electron integrals. To compensate for the approximations, empirical parameters are introduced.

In the PM3 method, only the valence electrons are considered. The central simplification is to not permit overlaps of atomic orbitals (ϕ_μ in Eq. 2.3.10) residing on different atomic centers. The two-electron Coulomb and exchange integrals (Eq. 2.3.14) are simplified to ignore all integrals with atomic orbitals residing on different atoms as well as all three- and four-centers integrals. The interactions with core electrons and nuclei are approximated by an average potential in which the valence electrons move.

2.3.7 Basis sets

The accuracy of electronic structure calculations is limited not only by the form of the wave function and the Hamiltonian, but also by the basis set used for the expansion of the wave function. In this section, the basis sets which were used in this study for evaluation of the nuclear potential, will be reviewed.

Any complete basis set may be used in Eq. 2.3.10. However, in practical calculations it is advantageous to use functions which resemble real atomic orbitals. For instance, the Slater type orbitals can be used for their similarity to atomic orbitals of the hydrogen atom. However, because they are not suitable for fast calculation of two-electron integrals (Eq. 2.3.5), *Gaussian type orbitals* were introduced. Atomic orbitals of this type are expressed as a linear combination of Gaussian primitives

$$\theta_{n,m,l}(\alpha, \boldsymbol{r}) = N x^n y^m z^l \, e^{-\alpha r^2}, \tag{2.3.33}$$

where N is a normalization factor. The sum of exponents at Cartesian coordinates $L = n+m+l$ is used to mark functions as s-type (L=0), p-type (L=1), d-type (L=2), f-type (L=3), etc. The Gaussian primitives can be grouped into fixed linear combinations to form *contracted Gaussian functions*

$$\phi_\mu(\boldsymbol{r}) = \sum_p d_{p\mu} \, \theta_p(\alpha_{p\mu}, \boldsymbol{r}). \tag{2.3.34}$$

Coefficients and exponents of the Gaussian functions are chosen from a best fit to some theoretically justified function. For instance the ϕ_{1s} orbital may be chosen to be the best fit to the Slater function $e^{-r}/\sqrt{\pi}$, which is the solution for the $1s$ orbital of the hydrogen atom. In another approach the parameters $\alpha_{p\mu}$ and $d_{p\mu}$ are varied to minimize the total energy.

Even though the contracted Gaussian functions are not optimal,[7] they permit fast calculation

[7] For example, the ϕ_{1s} function has a zero slope at zero, while Slater function has a finite slope. At large values of r the Gaussian function decays more rapidly. See Fig. 2.1.

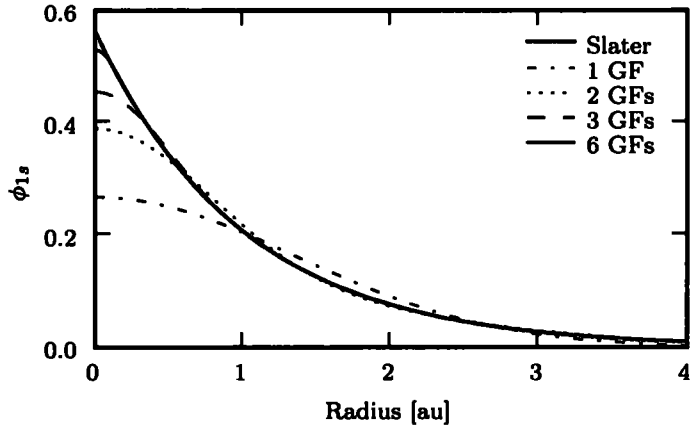

Figure 2.1: Least squares fit of variable number of Gaussian functions to the Slater $1s$ function. Six Gaussian functions provide enough flexibility and fit the Slater function well.

of two-electron integrals. In the simplest type of calculation, the set $\{\phi_\mu\}$ is minimal and consists of one function ($1s$) for hydrogen and helium, five functions ($1s$, $2s$, $2p_{x,y,z}$) for first row atoms Li to Ne, and so on. The minimal basis set may give qualitatively correct results of chemical bonding, but it has a limited flexibility. Extended basis sets are therefore introduced.

Split-valence basis set

The simplest basis set used in this study is the **6-31G** basis set [38]. Inner shells of heavy atoms are represented by single functions, composed of a sum of six Gaussian functions. Each valence shell is split into an inner and an outer part, expanded into three and one Gaussian functions, respectively. For instance, the valence shell of first row atoms will be described by four *sp* orbitals expanded into three Gaussian functions and four *sp* orbitals described by a single Gaussian function. The same set of exponents α may be shared in *sp* shells, which significantly speeds up calculations. If each of the minimal basis functions, not only the valence orbitals, were split into two, such a basis set is known as *double zeta.*

The 6-31G functions do not extend sufficiently far to adequately describe valence regions of oxygen and other atoms. Therefore the triple split basis set, **6-311G**, was introduced, where four additional atomic orbitals are added to the valence shell of the first row atoms [39].

Polarization functions

To create a well balanced basis set, also functions with higher angular quantum numbers must be added. A basis set with *d*-type functions added to first row atoms is usually denoted by a single star * or **(d)**. If in addition to that *p*-type functions are added to hydrogen, such a basis set is indicated by two stars ** or **(d,p)**. These functions are called polarization functions, because they give electrons the potential to respond to an electric field. For instance, the spherical symmetry of the minimal $1s$ orbital for the hydrogen atom must be combined with a *p*-type function to enable charge redistribution in the direction of the electric field.

Diffuse functions

When the electronic density is more spread over the molecule, it is appropriate to include functions with smaller Gaussian exponents α. Diffuse functions are most important in description of anions and weakly bound complexes involving hydrogen bonding or cation-molecule interactions. A basis set with diffuse functions on heavy atoms is indicated by $+$ and a basis set with diffuse functions on heavy atoms and hydrogen is indicated by $++$. The inclusion of diffuse functions can prolong calculations significantly, but it seems to be important for evaluation of tensors responsible for Raman scattering and Raman optical activity.

Correlation consistent basis sets

Basis sets optimized for use with methods which attempt to describe correlation effects require functions with high angular momenta. For instance, the correlation consistent polarized valence triple-zeta set **cc-pVTZ** includes three s, two p and one d function for the hydrogen atom and four s, three p, two d and one f function for first row atoms [40].

2.4 Nuclear motion

The previous sections summarized the approximative methods of quantum chemistry which enable calculation of the molecular energy of a given nuclear configuration. By minimizing the energy with respect to nuclear positions, one obtains the *equilibrium geometry* of the molecule. In practical calculations, it is not easy to find such a configuration, because PES contains for larger systems a wealth of local minima. Chemical intuition and molecular dynamics simulations must be therefore often harnessed. Having found an appropriate nuclear configuration, the investigation of vibrational motions may begin.

2.4.1 Harmonic approximation

The separation of electronic and nuclear motions in Eq. 2.1.11 provided an equation which has a simple form in space-fixed Cartesian coordinates. The equation is, however, in most cases too complicated to be integrated directly. The Hamiltonian is therefore expressed in molecule-fixed coordinates, which leads to a form more complex, but containing terms with clear physical interpretation enabling meaningful simplifications [41,42].

The new coordinate system is positioned in the nuclear center of mass and rotates with the molecule. The nuclear positions are expressed with respect to the molecule-fixed system in *normal mode coordinates* Q_i, which are defined as a linear combination of mass-weighted displacement vectors

$$\sqrt{m_j}\,(r_{\alpha_j} - r^0_{\alpha_j}) = \sum_{i=1}^{n} S_i^{\alpha_j} Q_i, \qquad j = 1, \ldots, n. \tag{2.4.1}$$

The transformation matrix $\mathbf{S}$ is determined by enforcing the (definitional) requirement that the force field matrix is diagonal in normal mode coordinates (see below). The reference nuclear configuration r_i^0 is chosen to minimize the potential energy surface for a given electronic state.

Under the assumption of small amplitudes of vibrations, the nuclear potential may be expanded in power series

$$V(x_1, \ldots, z_n) = V_0 + \sum_{\alpha_i} \frac{\partial V}{\partial r_{\alpha_i}} \Delta r_{\alpha_i} + \frac{1}{2} \sum_{\alpha_i, \beta_j} \frac{\partial^2 V}{\partial r_{\alpha_i} \partial r_{\beta_j}} \Delta r_{\alpha_i} \Delta r_{\beta_j} + \cdots, \tag{2.4.2}$$

where $\Delta r_{\alpha_i} = r_{\alpha_i} - r^0_{\alpha_i}$. The term V_0 can be neglected, as it adds only a constant to the energy. Because the reference geometry r_i^0 was chosen to minimize the potential, the first derivative term is also zero. Truncating the expansion after the third term, the potential can be expressed in terms of the Hessian, known also as the *force field matrix*

$$F_{\alpha_i \beta_j} = \frac{\partial^2 V}{\partial r_{\alpha_i} \partial r_{\beta_j}}. \tag{2.4.3}$$

For consequent simplification of the kinetic operator, it is convenient to introduce the diagonal

matrix of nuclear masses $\mathbf{M}$ and the mass-weighted force field matrix $\mathbf{F}'$

$$\mathbf{F}' = \mathbf{M}^{-1/2}\,\mathbf{F}\,\mathbf{M}^{-1/2}. \tag{2.4.4}$$

Since the mass-weighted force field matrix is obviously symmetric, it can be diagonalized by an orthogonal matrix, which is by definition the transformation matrix $\mathbf{S}$. In the convenient matrix notation, the potential energy can be then written as

$$\begin{aligned} 2V &= \boldsymbol{\Delta}^t F\,\boldsymbol{\Delta} \\ &= \boldsymbol{\Delta}^t \mathbf{M}^{1/2}\,\mathbf{M}^{-1/2}\,\mathbf{F}\,\mathbf{M}^{-1/2}\,\mathbf{M}^{1/2}\,\boldsymbol{\Delta} \\ &= \boldsymbol{Q}^t\,\mathbf{S}^t\,\mathbf{F}'\,\mathbf{S}\,\boldsymbol{Q} \\ &= \sum_i \frac{\partial^2 V}{\partial Q_i^2} Q_i^2, \end{aligned} \tag{2.4.5}$$

where $\boldsymbol{\Delta}$ is the vector of the displacements Δr_{α_i} and a matrix transpose is denoted by the superscript t.

It can be shown from the invariance of V that for nonlinear molecules, six from the total of $3n$ eigenvalues $V_{ii} = \partial^2 V/\partial Q_i^2$ will come out zero, or, due to errors in electronic calculations, close to zero. These modes correspond to translational and rotational movement. There are $3n$ variables in the space-fixed coordinate system, but only $m = 3n - 6$ degrees of freedom in the molecule-fixed system of normal mode coordinates.[8]

While the potential energy operator was significantly simplified, the kinetic operator is complicated by the rotating coordinate system. The vibration-rotation kinetic operator in normal mode coordinates derived by Watson [43] is given by

$$\hat{\mathrm{T}} = \frac{1}{2}\sum_{\alpha,\beta}(\hat{\mathrm{J}}_\alpha - \hat{\pi}_\alpha)\mu_{\alpha\beta}(\hat{\mathrm{J}}_\beta - \hat{\pi}_\beta) - \frac{\hbar^2}{8}\sum_\alpha \mu_{\alpha\alpha} - \frac{\hbar^2}{2}\sum_i \frac{\partial^2}{\partial Q_i^2}, \tag{2.4.6}$$

where $\hat{\mathrm{J}}$ is the total angular momentum operator, $\hat{\pi}$ is the vibrational angular momentum operator and $\mu_{\alpha\beta}$ is inverse of the moment of inertia tensor. It is common to neglect the vibrational angular momentum. The Hamiltonian for a non-rotating molecule is then in the *harmonic approximation* given by

$$\hat{\mathrm{H}} = -\frac{\hbar^2}{2}\sum_i \frac{\partial^2}{\partial Q_i^2} + \frac{1}{2}\sum_i \frac{\partial^2 V}{\partial Q_i^2} Q_i^2. \tag{2.4.7}$$

Thus, vibrational motions have been separated from rotations. Moreover, because of the neglect of higher-order terms in the potential in Eq. 2.4.2, the Hamiltonian does not contain any coupling between normal mode coordinates. The harmonic approximation thus enables splitting of the

[8] For linear molecules $m = 3n - 5$.

m-dimensional vibrational Schrödinger equation into a set of m one-dimensional problems

$$\left[-\frac{\hbar^2}{2}\frac{\partial^2}{\partial Q_i^2}+\frac{1}{2}\frac{\partial^2 V}{\partial Q_i^2}Q_i^2\right]\psi_i(Q_i)=\epsilon_i\,\psi_i(Q_i), \qquad i=1,\ldots,m, \tag{2.4.8}$$

with

$$\Psi_n(Q_1,\ldots,Q_m)=\prod_i \psi_i(Q_i). \tag{2.4.9}$$

The equations are known from the theory of the linear harmonic oscillator and have an analytic solution. The complicated vibrational motion of a molecule can be looked at as a superposition of independent vibrations of linear harmonic oscillators. Perhaps surprisingly, the model of atoms connected to equilibrium positions by tiny springs describes the molecular vibrations rather well. The properties of linear harmonic oscillators will be discussed in more detail in the next section.

2.4.2 Linear harmonic oscillator

The problem of the linear harmonic oscillator (LHO) is given by the equation

$$\left[-\frac{\hbar^2}{2m}\frac{\partial^2}{\partial x^2}+\frac{1}{2}m\omega^2 x^2\right]\psi(x)=E\,\psi(x), \tag{2.4.10}$$

where m is the mass of the oscillating particle and ω is the characteristic frequency of the oscillation. The problem has well known solutions. The eigenvalues take discrete, equidistantly spaced values

$$E_n=(n+\frac{1}{2})\,\hbar\omega, \qquad n=0,1,\ldots \tag{2.4.11}$$

and the corresponding eigenstates are

$$\psi_n(x)=\sqrt[4]{\frac{m\omega}{\pi\hbar}}\frac{1}{\sqrt{2^n\,n!}}\,e^{-\xi^2/2}\,H_n(\xi), \qquad \xi=\sqrt{\frac{m\omega}{\hbar}}x, \tag{2.4.12}$$

where H_n are the *Hermite polynomials*

$$H_n(\xi)=(-1)^n\,e^{\xi^2}\,\frac{d^n}{d\xi^n}e^{-\xi^2}. \tag{2.4.13}$$

The first five Hermite polynomials are

$$\begin{aligned}
H_0(\xi) &= 1,\\
H_1(\xi) &= 2\xi,\\
H_2(\xi) &= 4\xi^2-2,\\
H_3(\xi) &= 8\xi^3-12\xi,\\
H_4(\xi) &= 16\xi^4-48\xi^2+12
\end{aligned}$$

and the corresponding harmonic oscillator wave functions ψ_n are plotted in Fig. 2.2. Because the

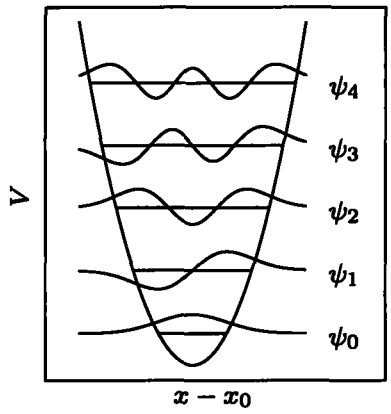

Figure 2.2: Wave functions of the linear harmonic oscillator for $n = 0, \ldots, 4$.

Hermite polynomials are orthogonal, important overlap properties of linear harmonic oscillator wave functions may be formulated, which give rise to many useful approximations and enable derivation of selection rules for spectroscopic transitions. For instance, the following identity can be derived

$$\langle \psi_n | x | \psi_k \rangle = \begin{cases} \sqrt{\frac{\hbar}{m\omega}} \sqrt{\frac{n+1}{2}} & \text{if } k = n+1, \\ \sqrt{\frac{\hbar}{m\omega}} \sqrt{\frac{n}{2}} & \text{if } k = n-1, \\ 0 & \text{otherwise} \end{cases} \tag{2.4.14}$$

and it will be used several times in Sec. 2.5 to show that a transition between two vibrational states cannot occur if their quantum numbers n do not differ by a prescribed value. This and similar identities also enable fast evaluation of multi-dimensional integrals of wave functions expanded in the basis of LHO.

2.4.3 Anharmonic potential

Despite its simplicity, the harmonic approximation gives surprisingly accurate results for energies well below the dissociation limit when the potential is expressible as a second-order polynomial. Obviously, it must fail for strongly anharmonic potentials and for highly excited vibrational states. The mathematical form of the second-order polynomial does not allow for bond breaking – when the distance between two nuclei increases, the energy would grow to infinity, instead of approaching a constant value of the bond dissociation limit. This behavior is demonstrated in Fig. 2.3 showing the plot of a scan along the symmetric C–H stretching vibration mode of formaldehyde calculated at the CCSD/cc-pVTZ level (Fig. 2.4), and the harmonic approximation of the potential. Another problem of the harmonic approximation is that it assumes that the vibrational modes are independent, i.e. can be described by independent one-dimensional Schrödinger equations. While it is sometimes reasonable to assume that the modes oscillate independently in the anharmonic potential, in other cases they are strongly correlated [44].

The most obvious way to extend the harmonic approximation is to include the higher-order terms of the Taylor expansion 2.4.2 into the Hamiltonian. The vibrational Schrödinger equation

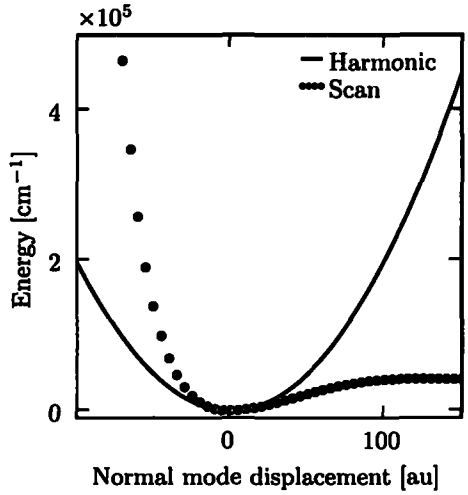

Figure 2.3: Comparison of exact (CCSD/cc-pVTZ scan) and harmonic potential of the symmetric C−H stretching vibration of formaldehyde.

is then no longer separable into a set of independent equations and the problem must be treated in its full dimensionality. Basically, all methods developed for improvement of HF described in Sec. 2.3 are in some form applicable also to the problem of molecular vibrations, as will be shown in the following sections.

Evaluation of the anharmonic potential is computationally a demanding task. In this work an approximate potential was obtained by numerical differentiation of second-order energy derivatives calculated at geometries displaced from an equilibrium geometry along nuclear coordinates. By performing $6n+1$ calculations in Cartesian coordinates (or $2m+1$ calculations for displacements along normal modes), cubic and semidiagonal quartic force field constants can be obtained. Using the shorthand notation for the force field derivatives

$$\begin{aligned} V^0_{\alpha_i\beta_j} &= \left.\frac{\partial^2 V(x_1,\ldots,z_n)}{\partial r_{\alpha_i}\partial r_{\beta_j}}\right|_{(x_1^0,y_1^0,\ldots,z_n^0)} \\ V^{\gamma_k+\Delta}_{\alpha_i\beta_j} &= \left.\frac{\partial^2 V(x_1,\ldots,z_n)}{\partial r_{\alpha_i}\partial r_{\beta_j}}\right|_{(x_1^0,\ldots,r^0_{\gamma_k}+\Delta,\ldots,z_n^0)}, \end{aligned}$$

the cubic constants were obtained from the formula

$$V^0_{\alpha_i\beta_j\gamma_k} = \frac{1}{2\Delta}(V^{\gamma_k+\Delta}_{\alpha_i\beta_j} - V^{\gamma_k-\Delta}_{\alpha_i\beta_j}). \tag{2.4.15}$$

The quartic constants were evaluated as

$$V^0_{\alpha_i\beta_j\gamma_k\gamma_k} = \frac{1}{\Delta^2}(V^{\gamma_k+\Delta}_{\alpha_i\beta_j} + V^{\gamma_k-\Delta}_{\alpha_i\beta_j} - 2V^0_{\alpha_i\beta_j}). \tag{2.4.16}$$

Note that only quartic constants with at most three indices different may be obtained from the $6n+1$ geometries. These constants will be referred to as *semidiagonal quartic constants.*[9]

[9]The precision of constants obtained by numerical differentiation is limited. As shown in Appendix A.4, the errors can be quite large.

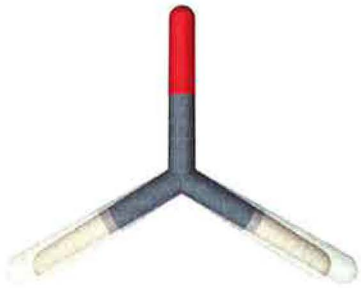

Figure 2.4: The symmetric C−H stretching vibration in formaldehyde.

Potential derivatives with respect to the normal mode coordinates are obtained from Cartesian derivatives by linear transformation. For example, the cubic terms are calculated by the formula

$$V_{ijk} = \frac{\partial V^3}{\partial Q_i \partial Q_j \partial Q_k} = \sum_{\alpha_l,\beta_m,\gamma_n} \frac{S_i^{\alpha_l}}{\sqrt{m_l}} \frac{S_j^{\alpha_m}}{\sqrt{m_m}} \frac{S_k^{\alpha_n}}{\sqrt{m_n}} V_{\alpha_l \beta_m \gamma_n}, \tag{2.4.17}$$

where $\mathbf{S}$ is the transformation matrix (Eq. 2.4.1 and Eq. 2.4.5) and m_i are the nuclear masses. It should be noted that even though the semidiagonal quartic Cartesian derivatives may be used for generating quartic normal-mode derivatives with all indices different, the normal-mode anharmonic potential used in this work was also only semidiagonal, that is, the potential of the form

$$V = \frac{1}{2}\sum_i V_{ii}\, Q_i^2 + \frac{1}{6}\sum_{i,j,k} V_{ijk}\, Q_i Q_j Q_k + \frac{1}{24}\sum_{i,j,k} V_{ijkk}\, Q_i Q_j Q_k^2 \tag{2.4.18}$$

was used. The quartic semidiagonal potential is indeed a more appropriate description of the nuclear potential, as can be seen for example in Fig. 2.5.

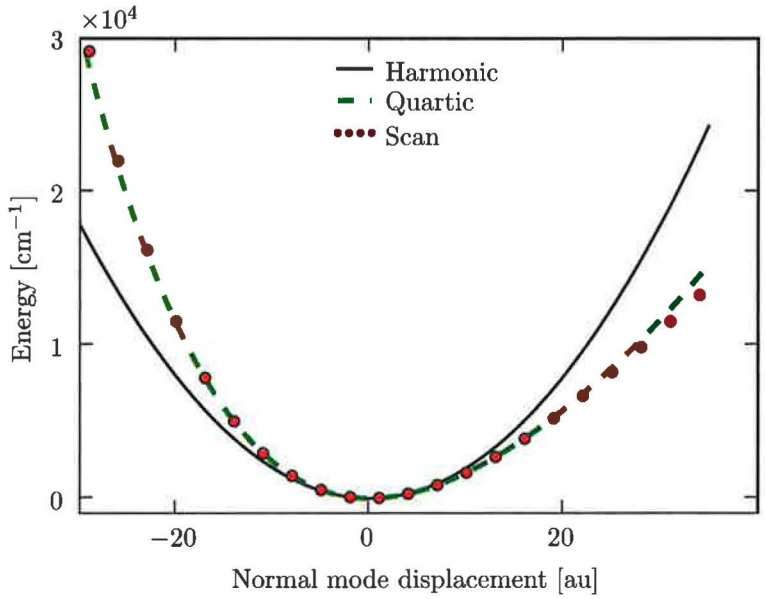

Figure 2.5: Comparison of exact (CCSD/cc-pVTZ scan), semidiagonal quartic and harmonic potential of the symmetric C−H stretching vibration in formaldehyde.

2.4.4 Vibrational self-consistent field

With the introduction of the anharmonic terms into the potential (Eq. 2.4.18), the vibrational Schrödinger equation is no longer separable into independent one-dimensional problems. The VSCF method [18] retains the low dimensionality of the harmonic approximation at the cost of neglect of coupling between vibrational modes. The method approximates the exact potential by an effective mean-field potential, a treatment conceptually identical to the HF method.

The VSCF method assumes that the vibrational wave function can be represented by a product function

$$\Psi^{\mathrm{VSCF}}(Q_1,\ldots,Q_m) = \prod_i \varphi_i(Q_i). \tag{2.4.19}$$

It is reasonable to use normal coordinates in VSCF, where separability is used only as an approximation, because in the limit of negligible coupling the use of normal coordinates will give an exact solution. Application of the variational principle for the function $\varphi_i(Q_i)$ leads to the set of equations

$$\left[-\frac{\hbar^2}{2}\frac{\partial^2}{\partial Q_i^2} + \hat{\mathrm{V}}_i^{\mu}(Q_i)\right]\varphi_i^{\mu}(Q_i) = \epsilon_i^{\mu}\varphi_i^{\mu}(Q_i), \qquad i = 1,\ldots,m. \tag{2.4.20}$$

The subscripts i go over all one-mode functions and the superscripts indicate μ-th solution of the equation, so that $\mu = 0$, for example, is the ground state solution. The effective one-mode potentials are defined by

$$\hat{\mathrm{V}}_i^{\mu}(Q_i) = \langle\prod_{j\neq i}\varphi_j^{\mu_j}(Q_j)|\hat{\mathrm{V}}(Q_1,\ldots,Q_m)|\prod_{j\neq i}\varphi_j^{\mu_j}(Q_j)\rangle \tag{2.4.21}$$

and the total VSCF energy is

$$E^{\mathrm{VSCF}} = \langle\prod_i\varphi_i|\hat{\mathrm{T}}+\hat{\mathrm{V}}|\prod_i\varphi_i\rangle = \sum_i\epsilon_i - (n-1)\langle\prod_i\varphi_i|\hat{\mathrm{V}}|\prod_i\varphi_i\rangle. \tag{2.4.22}$$

Because the potentials V_i^{μ} in Eq. 2.4.20 depend on the unknown solutions which are to be determined, the equations are solved iteratively. First, trial wave functions φ_i are used for evaluation of the averaged potential. The new set of wave functions obtained by solving the equations is then used for evaluation of a new effective potential. The procedure is repeated until self-consistency is reached, that is, until the eigenvalues ϵ_i do not change significantly.

Note that both the ground and excited states may be obtained by inserting φ_i^{μ} into Eq. 2.4.21 with either $\mu = 0$ or $\mu \neq 0$. The notation used for the one-mode functions φ_i is therefore somewhat ambiguous. An excited VSCF function will be a product of variously excited one-mode functions, each of them depending on the excitation of others. Therefore, to explicitly refer to the μ-th solution of Eq. 2.4.20 with the effective potential

$$\hat{\mathrm{V}}_i^{\nu_1,\ldots,\nu_m} = \langle\prod_{j\neq i}\varphi_j^{\nu_j}|\hat{\mathrm{V}}|\prod_{j\neq i}\varphi_j^{\nu_j}\rangle,$$

the following notation will be used

$$\varphi_i^{\mu_i;\nu_1,\ldots,\nu_m}$$

and for the total wave function

$$\Psi_{\mu;\nu} = \prod_i \varphi_i^{\mu_i;\nu_1,\ldots,\nu_m}.$$

This topic was brought to attention to emphasize the fact that although the VSCF method yields self-consistent excited states $\Psi_{\nu;\nu}$, they are generally not orthogonal to each other. If orthogonal states are needed, excited functions $\Psi_{\mu;\nu}$ may be used. However, they are not self-consistent. In this work, two variants of VSCF are distinguished. The standard self-consistent excited states $\Psi_{\nu;\nu}$ are referred to as to **eVSCF**. The orthogonal excited states $\Psi_{\nu;0}$ will be referred to as to **gVSCF**. Whilst in eVSCF the iterative VSCF algorithm is run for each excited state, in gVSCF the iterative procedure is run only once for the ground state.

Fig. 2.6 depicts an example of the effective VSCF potential, the ground state and first excited solution with energy levels, calculated in the harmonic and VSCF approximations. The asymptotic behavior of the VSCF potential is correct (the small embedded graph) and also low-energy states are better described by VSCF than by the harmonic approximation.

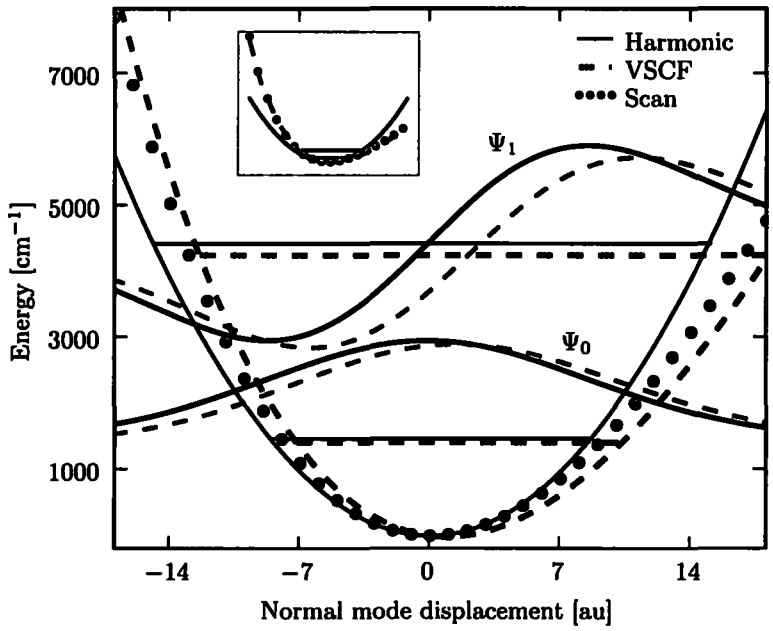

Figure 2.6: Potential of the symmetric C−H stretching vibration in formaldehyde. The black solid line is the harmonic potential with two lowest eigenstates and eigenvalues. The green dashed line is the effective VSCF potential represented by a polynomial of 4-th order and the red dots are results of a scan along the normal mode. The calculations were performed at the CCSD/cc-pVTZ level.

2.4.5 Vibrational perturbation theory

Another approach to account for the anharmonic potential and coupling effects is the perturbation theory developed in Sec. 2.2.2, page 15. Depending on the amount of anharmonicity of the system, either the harmonic approximation or VSCF may be used as starting points for the

perturbation theory. When the potential is only weakly anharmonic, the perturbation operator

$$\hat{\mathrm{W}}^{\mathrm{Harm}} = \frac{1}{6}\sum_{i,j,k} V_{ijk}\, Q_i Q_j Q_k + \frac{1}{24}\sum_{i,j,k} V_{ijkk}\, Q_i Q_j Q_k^2. \tag{2.4.23}$$

is used to correct the harmonic Hamiltonian (Eq. 2.4.7) [20, 21]. In this work, second order perturbation theory was used, and it will be denoted as PT2/Harm.

For larger anharmonicities, it is advantageous to start with VSCF solutions, which are closer to the exact solution, and to use the perturbation operator [22]

$$\hat{\mathrm{W}}^{\mathrm{VSCF}} = \hat{\mathrm{V}}(Q_1, \ldots, Q_m) - \sum_i \hat{\mathrm{V}}_i(Q_i). \tag{2.4.24}$$

The second order perturbation theory used to correct VSCF solutions will be denoted as PT2/VSCF.[10] Note that VSCF solutions are correct within first-order perturbation theory.

A comment should be made about the basis set of unperturbed VSCF solutions. The expansion functions in Eq. 2.2.11 are eigenstates of the unperturbed Hamiltonian and therefore they are orthogonal. Using the notation introduced in the previous section, the index i in the perturbation formula 2.2.14 must be replaced by $\nu_1, \ldots, \nu_m$ and the summation must go over all possible excitation combinations $\mu_1, \ldots, \mu_m$ to yield the second-order perturbation formula for eVSCF

$$E^{(2)}_{\nu;\nu} = \sum_{\mu} \frac{|\langle \Psi_{\nu;\nu} | \hat{\mathrm{W}} | \Psi_{\mu;\nu} \rangle|^2}{E^{(0)}_{\nu;\nu} - E^{(0)}_{\mu;\nu}}. \tag{2.4.25}$$

Similarly, the PT/gVSCF variant is given by

$$E^{(2)}_{\nu;0} = \sum_{\mu} \frac{|\langle \Psi_{\nu;0} | \hat{\mathrm{W}} | \Psi_{\mu;0} \rangle|^2}{E^{(0)}_{\nu;0} - E^{(0)}_{\mu;0}}. \tag{2.4.26}$$

2.4.6 Vibrational configuration interaction

The most general approach to the anharmonic problem is to look for a solution in the form of linear combination of some basis functions and determine the solution by use of the variational principle. It is convenient to use LHO or VSCF product functions as the expansion basis set [20, 46]. For example, the VSCF basis set is generated in a direct analogy to the electronic CI method from the ground state $\Psi_{0;0}(Q_1, \ldots, Q_m)$ by replacing a limited number of one-mode functions $\varphi_i^{0;0}(Q_i)$ by excited solutions $\varphi_i^{\mu_i;0}(Q_i)$. The LHO basis set can be formed analogously.

Because the number of states thus created grows very fast with the number of vibrational modes, it is necessary to formulate a criterion for selection of functions into the basis set. First, the number of total excitations in a basis function $\Psi_{\mu;0}$ must not exceed a prescribed value

[10] The method is in literature known also as the correlation-corrected VSCF (CC-VSCF) [45]. However, as pointed out already by Christiansen [23], this nomenclature is rather unfortunate, because it conflicts with abbreviations widely used for electronic structure methods. The CC abbreviation is recognized as abbreviation for coupled cluster theory.

n_{exc}, that is $\sum_i \mu_i \leq n_{\text{exc}}$. Second, only a certain number of states Ψ_μ with largest ratios

$$\eta = \left| \frac{\langle \Psi_\nu | \hat{\mathrm{W}} | \Psi_\mu \rangle}{E_0^{(0)} - E_\mu^{(0)}} \right| \tag{2.4.27}$$

is included, where functions Ψ_ν are constrained by the condition $\sum_i \nu_i \leq 1$, that is, Ψ_ν is either the ground state or some of the singly excited states.

In this work, the basis of LHOs was used.

2.5 Molecules in radiation fields

2.5.1 Electromagnetic radiation

So far, stationary vibrational states of molecular nuclei have been discussed. Transitions between the states can be mediated through *electromagnetic radiation*, usually represented by a self-propagating planar wave with electric and magnetic field components oscillating at right angles to each other and to the direction of the propagation. The non-quantized electromagnetic radiation can be expressed in terms of the scalar potential $\varphi(\boldsymbol{r}, t)$ and the vector potential $\boldsymbol{A}(\boldsymbol{r}, t)$, which are related to the electric field $\boldsymbol{E}$ and the magnetic field $\boldsymbol{B}$ by

$$\begin{aligned} \boldsymbol{E} &= -\nabla\varphi - \frac{\partial \boldsymbol{A}}{\partial t}, \\ \boldsymbol{B} &= \nabla \times \boldsymbol{A}. \end{aligned} \tag{2.5.1}$$

The definition of the potentials is not unique, but depends on the gauge transformation, which may change the potentials, but preserves the electric and magnetic field vectors. For instance, using the gauge $\nabla \cdot \boldsymbol{A} = 0$ and $\varphi = 0$, the wave equations for the electromagnetic field in a vacuum may be obtained

$$\Delta \boldsymbol{A} - \varepsilon_0 \mu_0 \frac{\partial^2 \boldsymbol{A}}{\partial t^2} = \boldsymbol{0}. \tag{2.5.2}$$

ε_0 is the permittivity and μ_0 the permeability of the vacuum. The radiation vector potential is then given by

$$\boldsymbol{A}(\boldsymbol{r}, t) = \boldsymbol{A}_0 \cos(\omega t + \boldsymbol{k} \cdot \boldsymbol{r}), \tag{2.5.3}$$

where $\boldsymbol{k}$ is the wave vector in the direction of propagation.

An important concept in spectroscopy is the *polarization* of light. In a *linearly polarized* light beam, the tip of the electric field vector in a fixed plane perpendicular to the direction of propagation traces out a line with time. Linearly polarized light can be regarded as a superposition of coherent left and right *circularly polarized* light beams of equal amplitude. In a circularly polarized light beam, the tip of the electric field vector traces out a circle. Circularly polarized light is said to be right handed or left handed depending on whether the electric field vector rotates clockwise or anticlockwise, respectively, when viewed by an observer looking towards the source of light.

2.5.2 Optical activity

A structure is called optically active, if it responds differently to right and left circularly polarized light. In the phenomenon of *optical rotation*, the circularly polarized components propagate through a chiral sample with **different velocities**, which introduces a phase difference, causing a change of the orientation of the plane of polarization. A **difference in absorption** of the two circular components results in ellipticity of the initially linearly polarized light beam. The ellipticity depends on the difference of absorption indices for left and right circularly polarized light, the *circular dichroism* of the medium. In optically active molecular or crystal structures

one can also observe **difference in scattering**, for example, the Rayleigh or Raman scattering.

Optical activity is a property of crystal structures or individual molecules with sufficiently low symmetry so that the system is not superposable on its mirror image. A molecule without symmetry plane or a center of inversion is known as *chiral*. Optical activity may be associated with electronic, vibrational or rotational transitions.

2.5.3 Absorption

A system of particles with charges q_i and masses m_i in an electromagnetic field is described by the Hamiltonian

$$\hat{\mathrm{H}} = \sum_i \frac{(\boldsymbol{p}_i - q_i\boldsymbol{A})^2}{2m_i} + \hat{\mathrm{V}} = \sum_i \frac{\boldsymbol{p}_i^2 - q_i\boldsymbol{p}_i\boldsymbol{A} - q_i\boldsymbol{A}\boldsymbol{p}_i + q_i\boldsymbol{A}^2}{2m_i} + \hat{\mathrm{V}}. \tag{2.5.4}$$

Realizing that the operators $\boldsymbol{p}$ and $\boldsymbol{A}$ commute, and neglecting the second-order term $\boldsymbol{A}^2$, the term linear in $\boldsymbol{A}$ can be regarded as a time-dependent harmonic perturbation. The results of Sec. 2.2.2 may be then applied to the perturbed Hamiltonian

$$\hat{\mathrm{H}} = \hat{\mathrm{H}}_0 - \sum_i \frac{q_i}{m_i}\boldsymbol{A}\cdot\boldsymbol{p}_i. \tag{2.5.5}$$

The probability amplitude of the transition from a state ψ_j to a state ψ_k at time t was shown to be proportional to

$$f(\Delta\omega) = \frac{4\sin^2 \Delta\omega t/2}{\Delta\omega^2}, \qquad \Delta\omega = \omega_{jk} - \omega. \tag{2.5.6}$$

As illustrated in Fig. 2.7, the function has large values only for the limited frequency range $|\Delta\omega| < 2\pi/t$. The transition can therefore occur only if the frequency ω of the light impinging on the molecule is very close to the frequency ω_{jk}. For example, for the value $t = 10\mu$s, the interval $(-\frac{2\pi}{t}, \frac{2\pi}{t})$ is smaller than 1.3 MHz. The laser light is not perfectly monochromatic, but has a finite line width. Having a laser with a very narrow line width of 3 MHz (0.000 1 cm^{-1}),

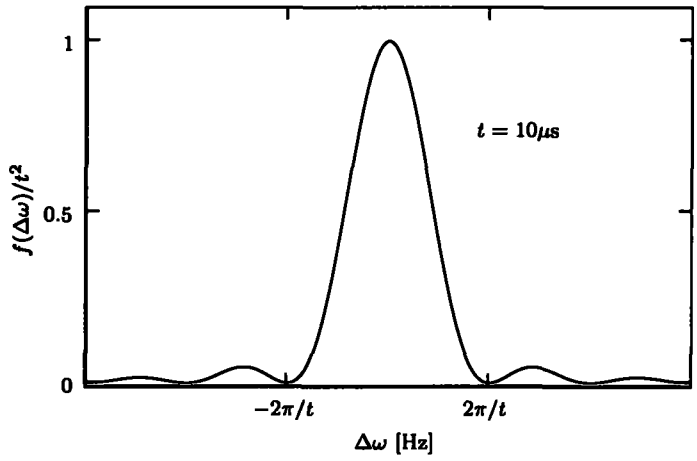

Figure 2.7: Probability amplitude of absorption as a function of frequency of incident light.

the frequency fluctuations of the incident light will greatly exceed the frequency range of the transition's maximal likelihood. Thus in experiments taking longer than, for example, $10\mu s$, the function can be regarded as a δ function centered at ω_{jk}. Because the integral of $f(\Delta\omega)$ evaluates to $\pi t/2$, the function can be written in the form

$$f(\Delta\omega) = \delta(\Delta\omega)\, 2\pi t. \tag{2.5.7}$$

Another simplification can be introduced for molecules much smaller than the wavelength of the incident light. For instance, light of the argon-ion laser has wavelength 514.5 nm, dimension of a small dipeptide is 1 nm and a typical length of the C−H bond is 0.1 nm. The magnitude of the vector potential can be therefore regarded as having a constant value over the spatial extent of the vibrational motion. Expanding the coordinate-dependent part of the vector potential $\boldsymbol{A}_0(\boldsymbol{r})$ in a power series around the molecular center of mass

$$\boldsymbol{A}_0(\boldsymbol{r}) = \boldsymbol{A}_0\, e^{i\boldsymbol{k}\cdot\boldsymbol{r}} = \boldsymbol{A}_0(1 + i\boldsymbol{k}\cdot\boldsymbol{r} + \cdots), \tag{2.5.8}$$

only the first term $\boldsymbol{A}_0(\boldsymbol{r}) \simeq \boldsymbol{A}_0$ can be taken in the first approximation. The assumption of large wavelengths leads to a simplified expression for probability amplitudes of transitions, known as the *dipole approximation*: When the potential in $\hat{\mathrm{H}}_0$ in Eq. 2.5.5 commutes with the coordinate, it can be easily shown that the following relation is valid

$$\langle\psi_k|\boldsymbol{p}|\psi_j\rangle = -\frac{im}{\hbar}\,\langle\psi_k|\boldsymbol{r}|\psi_j\rangle\,(E_j - E_k). \tag{2.5.9}$$

The overlap W_{kj} from Eq. 2.2.26 can be then written as

$$\langle\psi_k|\hat{\mathrm{W}}|\psi_j\rangle = -\sum_i \frac{q_i}{m_i}\boldsymbol{A}_0\cdot\langle\psi_k|\boldsymbol{p}_i|\psi_j\rangle = -i\omega_{jk}\,\boldsymbol{A}_0\cdot\sum_i q_i\langle\psi_k|\boldsymbol{r}_i|\psi_j\rangle. \tag{2.5.10}$$

Introducing the *electric dipole moment*

$$\boldsymbol{\mu} = \sum_i q_i\,\boldsymbol{r}_i, \tag{2.5.11}$$

the probability amplitude of the transition from the state ψ_j to the state ψ_k can be written as[11]

$$\frac{d|c_k|^2}{dt} = \frac{2\pi|\boldsymbol{A}_0|^2\,\omega_{jk}^2}{3\hbar^2}\,|\langle\psi_k|\boldsymbol{\mu}|\psi_j\rangle|^2\,\delta(\omega_{jk} - \omega). \tag{2.5.12}$$

Thus a molecule in the presence of a radiation field may undergo a transition to an excited state, if the frequency of the radiation matches the energy difference between the states. The probability of the transition, and hence the observed absorption intensity, depends on the value of the *dipole strength* D

$$D(j \to k) = \boldsymbol{\mu}^{jk}\cdot\boldsymbol{\mu}^{kj} = \langle\psi_j|\boldsymbol{\mu}|\psi_k\rangle\cdot\langle\psi_k|\boldsymbol{\mu}|\psi_j\rangle. \tag{2.5.13}$$

[11]The factor of three in the denominator comes from averaging for isotropic samples.

Because no assumption was made about the wave functions ψ, the result is valid for the overall wave functions including the electronic, vibrational and spin part. Important relations, such as Franck and Condon principle [47,48] may be derived. However, in this text we are interested in transitions between vibrational states with an unchanged electronic state (usually the ground state).

Absorption observables

The connection between the theory of absorption and experiment is the Lambert-Beer law

$$A = \log_{10} I_0/I = \varepsilon\, c\, L, \tag{2.5.14}$$

which relates the absorbance A to the molecular property of molar extinction coefficient ε and to the experimental conditions, the concentration c, and the path length L of the light through the sample. The molar extinction coefficient ε is usually expressed in $\mathrm{L\,mol^{-1}\,cm^{-1}}$.

Integrated contributions of a molecular transition $\Psi^j \rightarrow \Psi^k$ to ε are proportional to the dipole strength of the transition $D(j \rightarrow k)$.

Selection rules

Because of the separability of the total wave function into the electronic and the nuclear part (Eq. 2.1.8), the *transition dipole moment* $\boldsymbol{\mu}^{kj}$ between the states Ψ^k and Ψ^j may be written as

$$\boldsymbol{\mu}^{kj} = \langle \Psi_n^k(\boldsymbol{R}) | \boldsymbol{\mu}_e^{kj}(\boldsymbol{R}) | \Psi_n^j(\boldsymbol{R}) \rangle, \tag{2.5.15}$$

where

$$\boldsymbol{\mu}_e^{kj}(\boldsymbol{R}) = \langle \Psi_e^k(\boldsymbol{r};\boldsymbol{R}) | e \sum_{i,\alpha} Z_i R_{i\alpha} - e \sum_{i,\alpha} r_{i\alpha} | \Psi_e^j(\boldsymbol{r};\boldsymbol{R}) \rangle. \tag{2.5.16}$$

When the electronic part of the transition dipole moment is expressed in normal coordinates and expanded in Taylor series

$$\boldsymbol{\mu}_e(Q_1,\ldots,Q_m) = \boldsymbol{\mu}_e(\mathbf{0}) + \sum_i \frac{\partial \boldsymbol{\mu}_e}{\partial Q_i} Q_i + \frac{1}{2} \sum_{i,j} \frac{\partial^2 \boldsymbol{\mu}_e}{\partial Q_i \partial Q_j} Q_i Q_j + \cdots, \tag{2.5.17}$$

the overlap properties of LHO wave functions (Eq. 2.4.14) cause only the terms linear in Q_i to evaluate to non-zero in Eq. 2.5.15. Thus in the harmonic approximation, only transitions between vibrational states $\Psi^j \rightarrow \Psi^k$ for which $k = j \pm 1$ are permitted. Moreover, only transitions of those modes are allowed which change the magnitude of the electric dipole moment in the course of the vibration. Closer inspection of the wave functions and the transition dipole moment operator leads to symmetry-based selection rules for molecules with high symmetry. For example, for molecules with a center of inversion, bands that are active in IR spectra are not active in Raman spectra, and *vice versa*. For general systems no such rule can be applied, but the value of the transition dipole moment can be evaluated numerically.

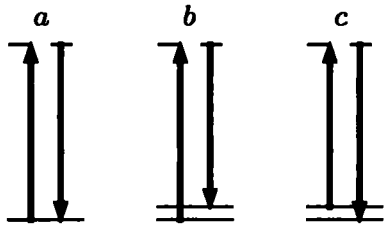

Figure 2.8: Energy-level diagram illustrating Rayleigh (a), Stokes (b) and anti-Stokes (c) Raman scattering.

The tensor of first order derivatives of the electronic part of the transition dipole moment with respect to nuclear positions is called *atomic polar tensor* (APT). For anharmonic vibrational wave functions, also higher-order terms of the Taylor expansion Eq. 2.5.17 may evaluate to non-zero.

2.5.4 Raman scattering

In absorption spectroscopy, a beam of light is passed through a sample and its attenuation is monitored as a function of wavelength, that is, weakening of photon flow with frequencies already present in the incident light is detected. On the other hand, in Raman spectroscopy the sample is illuminated by monochromatic light and the intensity of photon flow with frequencies originally absent from incident light is monitored.

Raman scattering is a two-photon process, where the impinging photon is annihilated and a new photon is scattered. Most of the light is scattered elastically with unchanged frequency, when the initial and the final states have the same energy (*Rayleigh scattering*, Fig. 2.8*a*). A small fraction of photons may end up in a state with higher (2.8*b*) or lower (2.8*c*) energy. In the case *b*, the scattered light has lower frequency and is known as *Stokes scattering*. It is a distinct phenomenon from fluorescence, because Raman scattering is observed for any frequency of the incident light, not only for a particular resonant frequency. The process depicted in Fig. 2.8*c* is *anti-Stokes scattering*, which yields photons with higher frequency than the frequency of the incident light. It occurs much less frequently, because higher-energy levels are less populated, as dictated by Boltzmann's law. Raman spectra are usually recorded in the visible or near-UV region of the electromagnetic radiation, but are plotted as differences from the wavelength of incident light. The frequency differences correspond to frequencies measured by IR spectroscopy. Clearly, for any Stokes transition there is a corresponding anti-Stokes transition with the same frequency difference from the central peak of the elastic Rayleigh scattering.

Classical description

In a classical treatment, scattered light is generated by oscillations of electric and magnetic multipoles which are induced in a molecule by the incident light wave. The most significant contribution to light scattering comes from the induced electric dipole moment

$$\boldsymbol{\mu}^{\text{ind}} = \boldsymbol{\alpha} \cdot \boldsymbol{E}, \tag{2.5.18}$$

where $\boldsymbol{\alpha}$ is the *electric dipole-electric dipole polarizability tensor* and $\boldsymbol{E}$ is the electric field vector. An oscillating electric field will result in an oscillating induced dipole moment, which in turn will produce an electromagnetic field oscillating at the frequency of the incident light, modulated by intrinsic frequencies of molecular vibrations. The polarizability can be expanded into a power series with respect to nuclear displacements along vibrational modes Q_i and the expansion truncated after the second term

$$\boldsymbol{\alpha} \simeq \boldsymbol{\alpha}_0 + \sum_i \frac{\partial \boldsymbol{\alpha}}{\partial Q_i} Q_i. \tag{2.5.19}$$

Denoting the frequency of the electric field oscillations by ω, the intrinsic frequencies of nuclear vibrations by ω_i,

$$\begin{aligned} \boldsymbol{E} &= \boldsymbol{E}_0 \cos \omega t, \\ Q_i &= Q_i^0 \cos \omega_i t, \end{aligned}$$

and inserting in Eq. 2.5.18, one obtains the expression

$$\boldsymbol{\mu}^{\text{ind}} = \boldsymbol{E}_0 \cdot \boldsymbol{\alpha}_0 \cos \omega t + \frac{1}{2} \boldsymbol{E}_0 \cdot \sum_i Q_i \frac{\partial \boldsymbol{\alpha}}{\partial Q_i} \left[\cos(\omega - \omega_i)t + \cos(\omega + \omega_i)t \right]. \tag{2.5.20}$$

The induced electric dipole thus oscillates at multiple frequencies. The first harmonic term with the frequency of the incident light corresponds to Rayleigh scattering. Additionally, for each vibrational mode Q_i there are two terms that correspond to Stokes and anti-Stokes scattering.

Quantum-mechanical description

Although the classical description provides a valuable insight into the origin of Raman scattering, it does not explain quantization of energy levels and does not give a quantitatively correct recipe for evaluation of transition probabilities. Quantum-mechanical expressions for transition probabilities of Raman scattering can be found from time-dependent perturbation theory of the second order. Similarly to Eq. 2.5.15 and Eq. 2.5.16, the polarizability transition element between states $\Psi^i \rightarrow \Psi^j$ may be then written in terms of electronic polarizability. In so-called Placzek approximation [49], an adiabatic wave function is used. Assuming that the electronic part of the state $\Psi^j = \Psi_e^i \Psi_n^j$ does not change during the transition, the components of the electronic polarizability tensor are then given by

$$(\alpha_e)_{\alpha\beta}^{ii} = \frac{2}{\hbar} \sum_{k \neq i} \frac{\omega_{ki}}{\omega_{ki}^2 - \omega^2} \operatorname{Re} \left[\langle \Psi_e^i | \mu_\alpha | \Psi_e^k \rangle \langle \Psi_e^k | \mu_\beta | \Psi_e^i \rangle \right], \qquad \alpha, \beta = x, y, z. \tag{2.5.21}$$

The summation goes over all excited electronic states Ψ_e^k of the molecule and $\omega_{ki} = \omega_k - \omega_i$ is the difference between angular frequency of the initial state Ψ_e^i and the state Ψ_e^k. The vibrational

transition polarizability between the vibrational states Ψ_n^i and Ψ_n^j is then

$$\boldsymbol{\alpha}^{ij} = \langle \Psi_n^i(\boldsymbol{R}) | \boldsymbol{\alpha}_e | \Psi_n^j(\boldsymbol{R}) \rangle. \tag{2.5.22}$$

Raman observables

The transition polarizability is a second rank tensor. Therefore the electric dipole moment $\boldsymbol{\mu}^{\text{ind}} = \boldsymbol{\alpha} \cdot \boldsymbol{E}$, and hence the probability of a transition, depends on the orientation of a molecule with respect to the incident light. The intensity of light scattered by a sample of randomly oriented molecules may be expressed in terms of tensor invariants, which are independent of the coordinate system rotations. The resultant expressions are dependent only on the scattering geometry, that is, on the angle between the direction of the incident and the scattered light. In particular, the Raman and ROA instrument at the Institute of Physics collects light scattered backwards. The total intensity of the back-scattering experimental setup is given by

$$I(180°) = 45\alpha^2 + 7\beta(\alpha)^2. \tag{2.5.23}$$

Here α is the isotropic invariant of the polarizability tensor

$$\alpha = \frac{1}{3}(\alpha_{xx} + \alpha_{yy} + \alpha_{zz}), \tag{2.5.24}$$

and $\beta(\alpha)^2$ is the symmetric anisotropic invariant of the polarizability tensor

$$\beta(\alpha)^2 = \frac{1}{2} \sum_{\alpha,\beta=x,y,z} 3\alpha_{\alpha\beta}^2 - \alpha_{\alpha\alpha}\alpha_{\beta\beta}, \tag{2.5.25}$$

where $\alpha_{\alpha\beta}$ are components of the transition polarizability 2.5.22.

Selection rules

When the electronic polarizability 2.5.22 is expanded in Taylor series with respect to nuclear positions and expressed in normal mode coordinates

$$\boldsymbol{\alpha}_e(Q_1, \ldots, Q_m) = \boldsymbol{\alpha}_e(\mathbf{0}) + \sum_i \frac{\partial \boldsymbol{\alpha}_e}{\partial Q_i} Q_i + \frac{1}{2} \sum_{i,j} \frac{\partial^2 \boldsymbol{\alpha}_e}{\partial Q_i \partial Q_j} Q_i Q_j + \cdots, \tag{2.5.26}$$

the overlap properties of LHO wave functions may be used again to formulate selection rules for Raman transitions. Taking terms of polarizability linear in Q_i, only transitions between vibrational states $\Psi^i \to \Psi^j$ such that $i = j \pm 1$ are allowed within the harmonic approximation. The polarizability must change in course of the vibration so that $\partial \boldsymbol{\alpha}_e / \partial Q_i$ is non-zero. For anharmonic wave functions, also higher-order terms may become significant.

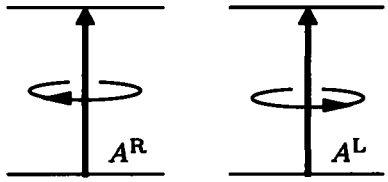

Figure 2.9: Energy-level diagram illustrating VCD.

2.5.5 Vibrational circular dichroism

Vibrational circular dichroism detects differences in attenuation of left and right circularly polarized light passing through a sample (Fig. 2.9). The fundamental quantity associated with the infrared absorption was the dipole strength (Eq. 2.5.13), a quantity which depends on the transition electric dipole moment. When the next term of the vector potential expansion (Eq. 2.5.8) is included in the perturbation operator, the transition probability for absorption of circularly polarized light can be found to be proportional not only to the dipole strength, but also to the quantity of the *rotational strength*. The differential absorption $\Delta A = A^L - A^R$ is therefore proportional to the rotational strength R which depends on both the electric and magnetic dipole transition moments

$$R(j \to k) = \boldsymbol{\mu}^{jk} \cdot \boldsymbol{m}^{kj} = \mathrm{Im}\left[\langle\psi_j|\boldsymbol{\mu}|\psi_k\rangle \cdot \langle\psi_k|\boldsymbol{m}|\psi_j\rangle\right]. \tag{2.5.27}$$

The magnetic dipole moment is defined as

$$\boldsymbol{m} = \sum_i \frac{q_i}{2m_i}(\boldsymbol{r}_i \times \boldsymbol{p}_i), \tag{2.5.28}$$

where particle i at $\boldsymbol{r}_i$ has charge q_i, mass m_i and linear momentum $\boldsymbol{p}_i$. Sensitivity of the handedness of a molecule toward circularly polarized light results from the form of the rotational strength (Fig. 2.10).

The magnetic transition dipole moment $\boldsymbol{m}^{kj}$ can be expanded in Taylor series with respect to nuclear momenta.[12] The tensor of first derivatives with respect to nuclear momenta is called *atomic axial tensor* (AAT). It should be noted that the appearance of the magnetic dipole moment in the transition probability expression brings a difficulty to practical calculations of VCD intensities, because the AAT tensor generally depends on the choice of coordinate system origin.

2.5.6 Raman optical activity

Light scattered from chiral samples carries a small degree of circular polarization, and the scattered intensity is slightly different in right and left circularly polarized light. ROA can be

[12]Derivatives with respect to nuclear positions vanish in the Born-Oppenheimer approximation.

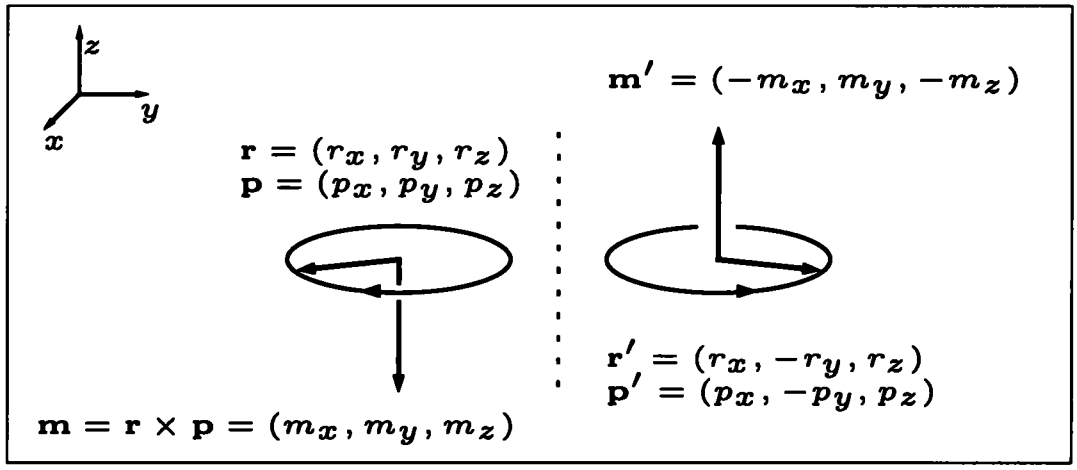

Figure 2.10: The mirror plane on the picture contains the axes x and z. Electric dipole moments of two enantiomers differ in sign of the y component ($\mu = (\mu_x, \mu_y, \mu_z)$ and $\mu' = (\mu_x, -\mu_y, \mu_z)$), while magnetic dipole moments differ in sign of the x and z components. Therefore, the rotational strength must have opposite sign for two enantiomers.

observed in a number of forms, depending on the polarization of the incident and the scattered light. For instance, in the scattered circular polarization (SCP) experiment, the incident light is linearly polarized and differences in circular polarization of the scattered light are measured. In the dual circular polarization (DCP), both the incident and the scattered light are circularly polarized, either in phase ($\mathrm{DCP_I}$) or out of phase ($\mathrm{DCP_{II}}$). The calculations in this work were performed for the incident circular polarization (ICP) form, where the sample is illuminated by a circularly polarized light and the total scattered intensity is measured.

Similarly to Raman scattering, the theory of ROA intensities may be derived by employing time-dependent perturbation method of second order. Analogously to VCD, the term linear in $\boldsymbol{r}$ of the vector potential expansion 2.5.8 must be included in the perturbation operator to describe Raman optical activity. The multipoles associated with ROA are then the electric dipole moment $\boldsymbol{\mu}$ (Eq. 2.5.11), the magnetic dipole moment $\boldsymbol{m}$ (Eq. 2.5.28), and the traceless electric quadrupole moment $\boldsymbol{\Theta}$,

$$\Theta_{\alpha\beta} = \frac{1}{2}\sum_i q_i(3r_{i_\alpha}r_{i_\beta} - r_i^2\delta_{\alpha\beta}), \qquad \alpha,\beta = x,y,z, \tag{2.5.29}$$

where particle i at $\boldsymbol{r}_i$ has charge q_i. In the weak-field approximation, it turns out that the multipoles induced in a molecule by electromagnetic radiation are given as

$$\mu_\alpha^{\mathrm{ind}} = \sum_\beta \alpha_{\alpha\beta}E_\beta + \frac{1}{\omega}\sum_\beta G'_{\alpha\beta}\frac{\partial B_\beta}{\partial t} + \frac{1}{3}\sum_{\beta,\gamma} A_{\alpha\beta\gamma}\frac{\partial E_\gamma}{\partial R_\beta} + \cdots, \tag{2.5.30}$$

$$m_\alpha^{\mathrm{ind}} = -\frac{1}{\omega}\sum_\beta G'_{\beta\alpha}\frac{\partial E_\beta}{\partial t} + \cdots, \tag{2.5.31}$$

$$\Theta_{\alpha\beta}^{\mathrm{ind}} = \sum_{\beta,\gamma} A_{\alpha\beta\gamma}E_\gamma + \cdots, \qquad \alpha,\beta,\gamma = x,y,z, \tag{2.5.32}$$

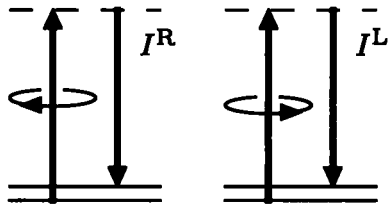

Figure 2.11: Energy-level diagram illustrating ICP ROA experiment.

where $\boldsymbol{E}$ is the electric field vector and $\boldsymbol{B}$ is the magnetic field vector. The tensor $\boldsymbol{\alpha}$ is the linear polarization of the electric dipole moment by an electric field (the electric dipole-electric dipole polarizability, see Eq. 2.5.21), $\boldsymbol{G'}$ determines the linear polarization of the electric dipole moment by the magnetic field component of the incident light (the *electric dipole-magnetic dipole polarizability*) and $\boldsymbol{A}$ determines the linear polarization of the electric dipole moment by the electric field gradient of the incident light (the *electric dipole-electric quadrupole polarizability*). In Placzek approximation, the tensors are given by the formulae

$$G'_{\alpha\beta} = -\frac{2}{\hbar} \sum_{k \neq i} \frac{\omega}{\omega_{ki}^2 - \omega^2} \operatorname{Im} \left[\langle \Psi_e^i | \mu_\alpha | \Psi_e^k \rangle \langle \Psi_e^k | m_\beta | \Psi_e^i \rangle \right], \tag{2.5.33}$$

$$A_{\alpha\beta\gamma} = \frac{2}{\hbar} \sum_{k \neq i} \frac{\omega_{ki}}{\omega_{ki}^2 - \omega^2} \operatorname{Re} \left[\langle \Psi_e^i | \mu_\alpha | \Psi_e^k \rangle \langle \Psi_e^k | \Theta_{\beta\gamma} | \Psi_e^i \rangle \right]. \tag{2.5.34}$$

Analogously to the transition dipole moment (Eq. 2.5.17) and electric dipole-electric dipole polarizability (Eq. 2.5.26), also the tensors $\boldsymbol{G'}$ and $\boldsymbol{A}$ can be expanded in Taylor series with respect to nuclear positions and transformed into normal modes. Thus obtained derivatives are then used in practical calculations of ROA intensities.

ROA observables

For a sample of randomly oriented molecules, the difference in scattering of circularly polarized light for the back-scattering geometry is proportional to

$$I^{\mathrm{R}} - I^{\mathrm{L}} = \frac{48}{c} \left[\beta(G')^2 + (1/3)\beta(A)^2 \right], \tag{2.5.35}$$

where c is the speed of light, I^{R} and I^{L} are the intensities scattered in right and left circularly polarized incident light. The invariants $\beta(G')^2$ and $\beta(A)^2$ are defined as

$$\beta(G')^2 = \frac{1}{2} \sum_{\alpha,\beta} \left(3\alpha_{\alpha\beta} G'_{\alpha\beta} - \alpha_{\alpha\alpha} G'_{\beta\beta} \right), \tag{2.5.36}$$

$$\beta(A)^2 = \frac{1}{2} \omega \sum_{\alpha,\beta,\gamma,\delta} \alpha_{\alpha\beta} \varepsilon_{\alpha\gamma\delta} A_{\gamma\delta\beta}, \tag{2.5.37}$$

where ω is the frequency of the incident light, $\alpha, \beta, \gamma, \delta = x, y, z$ and ε is the permutation symbol.

2.6 Spectral shapes

Spectra were simulated using Lorentz band shapes, so that a peak centered at $\tilde{\nu}_i$ with intensity I_i contributes to a spectrum by

$$S_i(\tilde{\nu}) = \frac{I_i}{4(\tilde{\nu} - \tilde{\nu}_i)^2/\Delta^2 + 1}, \tag{2.6.1}$$

where Δ is a full width at half-maximum height (FWHM). For absorption spectra, I_i was calculated using Eq. A.2.8. Raman spectra were evaluated using Eq. 2.5.23 and ROA spectra using Eq. 2.5.35. When contributions from multiple conformers were averaged in Raman and ROA spectra (see Sec. 3.2.2), the curve S_i was multiplied by the Boltzmann factor

$$B_j = \left[1 - e^{-\Delta E_j/kT}\right]^{-1}, \tag{2.6.2}$$

where ΔE_j is the relative energy of j-th conformer.

2.7 Solvation models

Vibrational spectra may be strongly affected by interactions with molecules of the same kind or by interactions with molecules of a solvent. In biochemical applications, solvent effects are particularly important because hydration is often responsible for three-dimensional structure and conformational flexibility of many biologically active molecules. There are two major types of methods for evaluating solvent effects: those treating the solvent as a continuous medium and those that include individual solvent molecules.

Inclusion of explicit solvent molecules in *ab initio* calculations is computationally very demanding. For example, quantum mechanical dynamics simulations of hydration shells of alanine zwitterion revealed that there are on average six water molecules in the first hydration shell in the vicinity of the charged CO_2^- and NH_3^+ alanine sites [50]. Therefore 18 atoms of water molecules must be included in calculations in addition to the 13 atoms of the alanine molecule.

In continuum models, the solute molecule (possibly supplemented by some solvent molecules from the first solvation shell) is placed in a cavity surrounded by a continuum medium. The *polarizable continuum model* (PCM) [24] represents the solvent by an infinite polarizable medium characterized mainly by its dielectric constant. The cavity is formed by spheres centered on each atom and the surface of the cavity is divided into small regions (called tesserae) on which are evaluated charges induced by the solute. The *conductor-like screening model* (COSMO) which is based on the assumption that the solvent may be represented by a conducting cavity, became extremely popular [51]. COSMO uses a scaled conductor boundary condition instead of the much more complicated dielectric boundary condition. The most important practical aspect is that the procedure replaces the normal component of the electric field on the cavity tesserae with the electrostatic potential, arriving at a noticeable reduction in computational costs. The *conductor-like PCM* (CPCM) [25] used in this work is an implementation of COSMO in the

PCM framework, where a correction for dielectric behavior is included. Some practical aspects of CPCM calculations are discussed in Appendix A.4.

CHAPTER 3

Results

3.1 Performance of anharmonic methods

3.1.1 Model potentials

The anharmonic methods reviewed in Sec. 2.4 were implemented in the GVIB software package [52] and applied to a number of systems. The correctness of the program was verified on simple potentials studied previously, for example, by Bowman, Christoffel and Norris [18, 22, 46].

The two-dimensional Henon-Heiles potential is defined as

$$V = \frac{1}{2}\left(\omega_1^2 Q_1^2 + \omega_2^2 Q_2^2\right) + \lambda\left(Q_1 Q_2^2 + \eta Q_1^3\right), \tag{3.1.1}$$

the parameters were set to $\omega_1^2 = 0.29375$, $\omega_2^2 = 2.12581$, $\lambda = -0.1116$ and $\eta = 0.08414$. The three-dimensional Christoffel potential

$$V = \frac{1}{2}(\omega_1^2 Q_1^2 + \omega_2^2 Q_2^2 + \omega_3^2 Q_3^2) + \lambda\eta Q_1^3 + \mu\zeta Q_2^3 + \lambda Q_1 Q_2^2 + \mu Q_2 Q_3^2 \tag{3.1.2}$$

was used with the values $\omega_1^2 = 0.49$, $\omega_2^2 = 1.69$, $\omega_3^2 = 1.00$, $\lambda = \mu = -0.10$ and $\eta = \zeta = 0.10$.

The vibrational Schrödinger equation was solved for these potentials using the harmonic approximation, VSCF, VCI and perturbation methods. The calculated energies are shown in Tables 3.1 and 3.2 as differences from the VCI results. All methods improve harmonic approximation. Both VSCF variants give similar results, but eVSCF gives consistently smaller errors. The differences can be for some modes exceptionally large. For example, the energy of the $|01\rangle$ state (Table 3.1) is predicted by gVSCF with an error five times larger than by eVSCF. On the other hand, the value obtained from the eVSCF calculation is comparable to PT2/Harm. The perturbation theory improves results of both the harmonic and the VSCF approximation.

The best results are given by the PT2/eVSCF method. The results of the PT2/Harm approach indicate that the harmonic approximation is a poor starting point for perturbation calculations, at least in the case of the model potentials. However, the results of all perturbation methods are comparable for real molecules and none of them gives clearly better energies than any of the others.

$E - E$(VCI)	$\|00\rangle$	$\|10\rangle$	$\|20\rangle$	$\|01\rangle$
Harmonic	0.00837	0.02604	0.05313	0.03911
gVSCF	0.00084	0.00307	0.00564	0.01404
eVSCF	0.00084	0.00303	0.00546	0.00277
PT2/Harm	0.00031	0.00162	0.00469	0.00276
PT2/gVSCF	0.00001	0.00013	0.00045	0.00075
PT2/eVSCF	0.00001	0.00003	0.00008	0.00006
E(VCI)	0.99163	1.51595	2.03085	2.41891

Table 3.1: State energies obtained for the Henon-Heiles potential by various methods, shown as differences from the values obtained by VCI. (Dimensionless numbers.)

$E - E$(VCI)	$\|000\rangle$	$\|001\rangle$	$\|010\rangle$	$\|100\rangle$	$\|101\rangle$	$\|200\rangle$
Harmonic	0.00625	0.01433	0.02814	0.01485	0.02328	0.02689
gVSCF	0.00128	0.00564	0.01259	0.00323	0.00793	0.00532
eVSCF	0.00128	0.00258	0.00618	0.00322	0.00478	0.00528
PT2/Harm	0.00013	0.00045	0.00103	0.00049	0.00116	0.00117
PT2/gVSCF	0.00002	0.00015	0.00036	0.00009	0.00053	0.00028
PT2/eVSCF	0.00002	0.00004	0.00012	0.00004	0.00009	0.00011
E(VCI)	1.49375	2.48567	2.77186	2.18515	3.17672	2.87311

Table 3.2: State energies obtained for the Christoffel potential by various methods, shown as differences from the values obtained by VCI. (Dimensionless numbers.)

3.1.2 Water

One of the smallest real-world systems available for modeling of vibrational spectra is a molecule of water. Biomolecules are preferably studied in their natural environment, that is, dissolved in water, and therefore vibrational transitions of water often interfere in the spectra of molecules of interest. Although the water molecule with only three fundamental vibrational modes may look deceptively simple for calculations, in fact it is not. Being very light and polar, water molecules in the liquid phase form non-covalently bonded clusters. Some of the vibrational motions in these clusters are strongly anharmonic and correlated, therefore the applicability of the potential expansion into a fourth-order polynomial is questionable [12]. The large number of possible configurations of water molecules in the clusters results in broad peaks, which can be simulated *ab initio* possibly only by calculating spectra for each orientation and consequent Boltzmann averaging.

Table 3.3 compares experimental frequencies of water vapor [53] with anharmonic calculations performed at four different levels of electronic theory: CCSD, MP2, B3LYP, and BPW91, all with the large cc-pVTZ basis set. In the harmonic approximation, all internuclear potentials behave similarly: Best is described the bending mode δ, while the strongly anharmonic O−H stretching modes ν_s and ν_{as} show much larger deviation. This is particularly true for CCSD, MP2 and B3LYP, but to a lesser extent also for BPW91. This behavior is quite general and can be observed also for other molecules. All anharmonic methods significantly improve harmonic frequencies calculated at the CCSD, MP2 and B3LYP levels. The internuclear potential calculated by BPW91 strongly underestimates both the angle and bonds stiffness, which results in

	Methods	$\omega_{calc} - \omega_{exp}$			$\omega_{calc} - \omega_{harm}$		
		δ	ν_s	ν_{as}	δ	ν_s	ν_{as}
CCSD/cc-pVTZ	Harmonic	84	224	223			
	gVSCF	29	134	176	-54	-89	-47
	eVSCF	26	134	66	-57	-90	-157
	PT2/Harm	21	86	35	-63	-138	-187
	PT2/gVSCF	19	91	39	-65	-132	-184
	PT2/eVSCF	17	92	37	-66	-131	-186
	VCI	17	91	39	-67	-132	-183
MP2/cc-pVTZ	Harmonic	57	204	220			
	gVSCF	2	116	174	-55	-88	-47
	eVSCF	-1	115	65	-58	-89	-156
	PT2/Harm	-6	68	34	-63	-136	-186
	PT2/gVSCF	-8	74	39	-65	-130	-182
	PT2/eVSCF	-10	75	36	-67	-129	-184
	VCI	-10	74	39	-67	-130	-182
B3LYP/cc-pVTZ	Harmonic	44	152	148			
	gVSCF	-11	68	107	-55	-83	-41
	eVSCF	-14	67	-2	-58	-84	-149
	PT2/Harm	-20	19	-34	-64	-133	-182
	PT2/gVSCF	-22	27	-28	-66	-125	-176
	PT2/eVSCF	-23	27	-30	-67	-124	-178
	VCI	-24	27	-28	-68	-125	-175
BPW91/cc-pVTZ	Harmonic	18	54	52			
	gVSCF	-38	-36	4	-56	-90	-48
	eVSCF	-41	-37	-107	-59	-91	-159
	PT2/Harm	-47	-84	-136	-64	-138	-188
	PT2/gVSCF	-49	-79	-133	-67	-133	-185
	PT2/eVSCF	-50	-78	-136	-68	-133	-188
	VCI	-51	-79	-133	-68	-133	-185
	Expt. (ω_{exp})	1595	3652	3756			

Table 3.3: Calculated and measured [53] frequencies of water vapor. Frequencies of three fundamental vibrations (bending δ, symmetric stretch ν_s, and antisymmetric stretch ν_{as}) are shown as differences from experimental values (the middle columns). In the columns on the right the magnitudes of anharmonic corrections are shown. The vibrational potential was evaluated at the CCSD/cc-pVTZ, MP2/cc-pVTZ, B3LYP/cc-pVTZ and BPW91/cc-pVTZ levels. All frequencies and frequency differences in cm^{-1}. The maximal deviations are emphasized by different color, as explained in the text.

too low anharmonic frequencies.

Somewhat surprising may be the exceptionally good overall agreement in the magnitude of the anharmonic corrections calculated using different electronic methods, as listed in the right part of Table 3.3. In particular, the maximal difference in anharmonic contributions for a given anharmonic method is only 10 cm^{-1} (the asymmetric stretch ν_{as} calculated at the B3LYP and BPW91 level using PT2/eVSCF, the numbers are printed in green color), while the maximal difference in the harmonic frequencies is 171 cm^{-1} (the asymmetric stretch ν_{as} calculated at CCSD and BPW91 levels, the numbers are printed in red color). This result is in accordance with the well known fact that anharmonic contributions are usually smaller than 10% of harmonic values.

Electronic calculations with the cc-pVTZ basis set are computationally very demanding and are feasible only for small molecules. To evaluate the vibrational potential of medium-sized and large systems, it is necessary to reduce the size of the basis set and employ electronic methods with favorable scaling. Table 3.4 shows the results from using several electronic methods

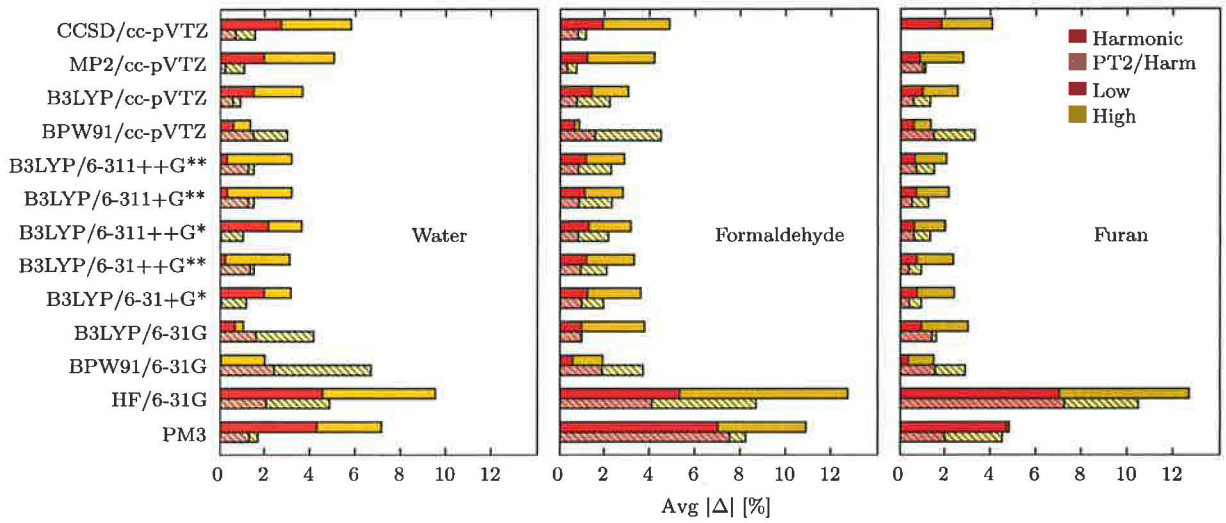

Figure 3.1: Average absolute deviations of fundamental frequencies of water, formaldehyde and furan from experimental frequencies observed in the gas phase, as calculated at various levels of the electronic theory using the harmonic approximation and the PT2/Harm method. The deviations of hydrogen stretching modes are printed in a color different (yellow) from low- and mid-frequency modes (red).

(B3LYP, BPW91, HF and PM3) and basis sets (6-311++G**, 6-31+G*, 6-31G). Similarly to the calculations performed using the cc-pVTZ basis set, the difference in harmonic frequencies greatly exceeds the differences in anharmonic corrections. The largest difference in the harmonic frequencies of 477 cm^{-1} (the symmetric stretch ν_s calculated with BPW91/6-31G and HF/6-31G) greatly exceeds the maximal difference 39 cm^{-1} in the anharmonic contributions (the asymmetric stretch ν_{as} calculated at BPW91/6-31G and B3LYP/6-31+G* using PT2/eVSCF).[1]

3.1.3 Formaldehyde

The results of calculations on formaldehyde follow the general pattern observed for water and, as will be seen later, also for other molecules. Usually, the hydrogen stretching vibrations come out too large from the harmonic approximation and all anharmonic methods tend to improve the agreement with the experiment in this region. The low- and mid-frequency modes, however, are often quite close to the experimental values already within the harmonic approximation. Anharmonic methods shift the harmonic frequencies toward the red end of the spectrum and occasionally change the order of modes.

As shown in Fig. 3.1, very good agreement with experiment can be observed for anharmonic frequencies calculated at the CCSD/cc-pVTZ and MP2/cc-pVTZ levels. With the exception of the asymmetric C−H stretching vibration ν_{as} (Table 3.5), both VSCF methods as well as the perturbation methods give consistently similar results and do not exhibit dramatic differences observed for model potentials in Sec. 3.1.1. The largest deviation of anharmonic frequencies from experimental values in the CCSD/cc-pVTZ calculation is observed for the symmetric C=O

[1]The semi-empirical method PM3 was not included in the comparison.

	Methods	$\omega_{calc} - \omega_{exp}$			$\omega_{calc} - \omega_{harm}$		
		δ	ν_s	ν_{as}	δ	ν_s	ν_{as}
B3LYP 6-311++G**	Harmonic	8	166	166			
	gVSCF	-42	76	121	-49	-90	-46
	eVSCF	-45	75	10	-53	-90	-156
	PT2/Harm	-51	28	-19	-59	-138	-185
	PT2/gVSCF	-53	33	-15	-61	-132	-182
	PT2/eVSCF	-54	34	-19	-62	-132	-185
	VCI	-55	33	-16	-63	-132	-183
B3LYP/6-31+G*	Harmonic	68	85	105			
	gVSCF	9	2	64	-58	-83	-41
	eVSCF	7	1	-43	-61	-84	-148
	PT2/Harm	2	-49	-76	-66	-134	-181
	PT2/gVSCF	-1	-41	-70	-68	-125	-175
	PT2/eVSCF	-2	-40	-71	-69	-124	-176
	VCI	-2	-40	-69	-70	-125	-174
B3LYP/6-31G	Harmonic	23	-33	29			
	gVSCF	-37	-122	-21	-60	-89	-50
	eVSCF	-40	-124	-138	-62	-91	-167
	PT2/Harm	-47	-174	-175	-70	-142	-203
	PT2/gVSCF	-49	-163	-166	-72	-131	-195
	PT2/eVSCF	-51	-163	-168	-74	-130	-197
	VCI	-51	-163	-165	-74	-130	-193
BPW91/6-31G	Harmonic	1	-140	-76			
	gVSCF	-59	-241	-138	-60	-101	-63
	eVSCF	-62	-243	-259	-63	-103	-183
	PT2/Harm	-69	-289	-289	-70	-149	-213
	PT2/gVSCF	-72	-283	-286	-73	-143	-210
	PT2/eVSCF	-73	-283	-290	-74	-143	-215
	VCI	-74	-283	-286	-75	-143	-210
HF/6-31G	Harmonic	142	337	389			
	gVSCF	71	248	348	-71	-88	-42
	eVSCF	68	247	233	-74	-90	-156
	PT2/Harm	61	196	198	-81	-141	-191
	PT2/gVSCF	59	204	205	-83	-132	-184
	PT2/eVSCF	58	205	204	-84	-131	-186
	VCI	57	205	206	-85	-132	-183
PM3	Harmonic	146	217	234			
	gVSCF	70	99	65	-76	-119	-169
	eVSCF	62	13	59	-84	-204	-175
	PT2/Harm	50	16	53	-96	-202	-180
	PT2/gVSCF	50	-9	40	-97	-226	-194
	PT2/eVSCF	47	-18	38	-99	-235	-196
	VCI	47	-13	37	-99	-231	-197
	Expt. (ω_{exp})	1595	3652	3756			

Table 3.4: Calculated and measured [53] frequencies of water vapor. Comparison of frequencies calculated with different electronic methods and lower-quality basis sets. See also Table 3.3. All frequencies and frequency differences are in cm^{-1}. The maximal deviations are emphasized by different color, as explained in the text.

stretching mode ν_{s_1}. The anharmonicity of the mode is weak (1% of the harmonic frequency) and therefore all anharmonic methods yield essentially the same value. The large difference from experiment must be therefore attributed to an inadequate description of the C=O bond strength by the CCSD/cc-pVTZ method. The same mode is described exceptionally well by the MP2 and BPW91 methods. However, the behavior of the electronic methods is too complex to draw straightforward conclusions. For example, it is interesting to notice that the frequency

	Methods	$\omega_{calc} - \omega_{exp}$						$\omega_{calc} - \omega_{harm}$					
		δ_{oop}	δ_{as}	δ_s	ν_{s_1}	ν_{s_2}	ν_{as}	δ_{oop}	δ_{as}	δ_s	ν_{s_1}	ν_{s_2}	ν_{as}
CCSD/cc-pVTZ	Harmonic	48	41	61	85	175	182						
	gVSCF	5	-5	25	70	52	94	-43	-46	-36	-15	-123	-88
	eVSCF	2	-7	24	69	50	15	-45	-48	-37	-16	-125	-167
	PT2/Harm	3	-5	19	64	4	31	-45	-45	-41	-21	-171	-151
	PT2/gVSCF	0	-9	19	63	7	-13	-47	-50	-42	-21	-169	-195
	PT2/eVSCF	-1	-10	19	63	7	6	-48	-51	-42	-22	-169	-176
	VCI	0	-10	19	63	8	-3	-48	-51	-42	-21	-167	-185
MP2/cc-pVTZ	Harmonic	41	31	54	28	189	201						
	gVSCF	-1	-14	22	9	68	115	-42	-45	-32	-18	-121	-86
	eVSCF	-4	-16	20	8	66	36	-45	-47	-33	-20	-123	-165
	PT2/Harm	-4	-14	14	5	15	35	-45	-44	-40	-23	-174	-166
	PT2/gVSCF	-6	-18	15	3	23	-5	-47	-48	-39	-24	-166	-205
	PT2/eVSCF	-7	-19	15	3	23	16	-48	-50	-39	-25	-166	-185
	VCI	-7	-18	15	3	24	13	-48	-49	-39	-24	-165	-187
B3LYP/cc-pVTZ	Harmonic	36	20	36	78	97	90						
	gVSCF	-8	-26	0	66	-38	-8	-44	-46	-36	-12	-134	-98
	eVSCF	-11	-28	-1	65	-40	-92	-47	-48	-37	-13	-136	-182
	PT2/Harm	-11	-26	-4	58	-78	-107	-46	-45	-41	-19	-174	-197
	PT2/gVSCF	-14	-30	-5	59	-85	-116	-49	-50	-41	-19	-182	-206
	PT2/eVSCF	-15	-32	-6	58	-85	-125	-50	-51	-42	-19	-182	-215
	VCI	-14	-31	-5	58	-84	-140	-50	-51	-41	-19	-180	-230
BPW91/cc-pVTZ	Harmonic	-11	-20	-8	23	14	-6						
	gVSCF	-55	-67	-45	11	-119	-101	-45	-47	-37	-11	-133	-95
	eVSCF	-59	-69	-46	10	-121	-187	-48	-49	-38	-13	-135	-181
	PT2/Harm	-57	-66	-50	4	-162	-204	-47	-46	-42	-19	-176	-198
	PT2/gVSCF	-61	-71	-51	4	-168	-210	-50	-51	-42	-19	-181	-204
	PT2/eVSCF	-62	-72	-51	4	-168	-220	-51	-52	-43	-19	-181	-214
	VCI	-61	-72	-51	4	-166	-232	-51	-52	-43	-19	-180	-226
	Expt. (ω_{exp})	1167	1249	1500	1746	2782	2843						

Table 3.5: Calculated and measured [54] frequencies of formaldehyde in the gas phase. All frequencies and frequency differences in cm^{-1}.

of the C=O stretching mode ν_{s_1} is predicted with similar deviation by the CCSD and B3LYP methods ($\approx$ 80 cm^{-1}) and by the MP2 and BPW91 methods ($\approx$ 25 cm^{-1}). On the other hand, the C−H stretching vibrations ν_{s_2} and ν_{as} are predicted similarly by the CCSD and MP2 methods, while the B3LYP and BPW91 methods predict the frequencies far too low.

Similarly to the behavior observed for water, the magnitudes of the anharmonic contributions differ much less than the harmonic frequencies (Tables 3.5 and 3.6). The maximal difference in anharmonic contributions for a given anharmonic method is 68 cm^{-1} (the asymmetric stretching mode ν_{as} calculated at the CCSD/cc-pVTZ and B3LYP/6-31+G* levels using PT2/Harm), while the maximal difference in harmonic frequencies is 462 cm^{-1} (ν_{as} calculated at the BPW91/cc-pVTZ and HF/6-31G levels).

3.1.4 Furan

Furan is a rigid planar molecule made of an aromatic cycle containing oxygen. Consisting of nine atoms, furan has 21 vibrational modes. As mentioned in Sec. 2.4.6, the size of the basis set used in VCI calculations grows very fast with the number of normal modes and only a fraction of the states can be included in a practical computation. In particular, the value of

	Methods	$\omega_{calc} - \omega_{exp}$						$\omega_{calc} - \omega_{harm}$					
		δ_{oop}	δ_{as}	δ_s	ν_{s_1}	ν_{s_2}	ν_{as}	δ_{oop}	δ_{as}	δ_s	ν_{s_1}	ν_{s_2}	ν_{as}
B3LYP 6-311++G**	Harmonic	35	11	31	68	104	101						
	gVSCF	-11	-33	-4	56	-36	-1	-47	-44	-34	-11	-140	-102
	eVSCF	-15	-36	-5	55	-38	-86	-50	-46	-36	-12	-142	-187
	PT2/Harm	-14	-33	-8	49	-76	-104	-49	-44	-39	-19	-180	-205
	PT2/gVSCF	-17	-38	-9	49	-84	-111	-52	-49	-40	-19	-188	-212
	PT2/eVSCF	-18	-39	-10	49	-85	-122	-53	-50	-40	-19	-189	-223
	VCI	-17	-39	-9	49	-83	-93	-53	-49	-40	-19	-187	-194
B3LYP/6-31+G*	Harmonic	24	18	44	77	149	147						
	gVSCF	-20	-28	9	65	7	45	-43	-46	-36	-12	-142	-103
	eVSCF	-23	-31	8	64	5	-41	-47	-49	-37	-13	-144	-189
	PT2/Harm	-22	-28	4	57	-38	-71	-46	-46	-41	-20	-187	-219
	PT2/gVSCF	-25	-33	3	58	-42	-69	-49	-51	-41	-20	-191	-217
	PT2/eVSCF	-26	-34	3	57	-42	-81	-50	-52	-42	-20	-191	-229
	VCI	-26	-34	3	57	-41	-57	-50	-52	-42	-20	-189	-204
B3LYP/6-31G	Harmonic	36	25	60	2	181	192						
	gVSCF	-11	-25	33	-19	35	86	-47	-49	-27	-21	-147	-106
	eVSCF	-14	-27	31	-21	33	-2	-49	-51	-29	-23	-149	-194
	PT2/Harm	-12	-23	22	-23	-2	1	-48	-48	-38	-25	-184	-191
	PT2/gVSCF	-15	-29	24	-25	-15	-50	-51	-53	-36	-27	-196	-242
	PT2/eVSCF	-17	-30	25	-26	-16	-42	-53	-55	-35	-28	-197	-234
	VCI	-16	-29	25	-26	-14	-28	-52	-54	-35	-28	-195	-220
BPW91/6-31G	Harmonic	-4	-10	20	-49	87	84						
	gVSCF	-52	-61	-7	-72	-59	-21	-48	-51	-26	-23	-147	-106
	eVSCF	-55	-63	-9	-74	-62	-111	-51	-53	-29	-25	-149	-196
	PT2/Harm	-53	-59	-19	-74	-96	-108	-49	-49	-39	-26	-183	-192
	PT2/gVSCF	-57	-65	-16	-78	-110	-154	-53	-55	-36	-29	-197	-239
	PT2/eVSCF	-58	-66	-16	-79	-111	-145	-54	-57	-35	-30	-198	-230
	VCI	-57	-66	-16	-78	-108	-131	-53	-56	-36	-29	-195	-215
HF/6-31G	Harmonic	162	125	173	164	425	456						
	gVSCF	117	78	143	144	294	364	-45	-46	-30	-20	-131	-93
	eVSCF	114	76	141	142	292	282	-48	-48	-32	-21	-133	-174
	PT2/Harm	115	79	135	140	247	280	-47	-46	-38	-24	-179	-176
	PT2/gVSCF	113	74	136	138	247	232	-49	-50	-37	-26	-178	-224
	PT2/eVSCF	112	73	136	137	247	255	-50	-51	-37	-26	-178	-201
	VCI	112	73	136	138	248	254	-50	-51	-37	-26	-177	-203
PM3	Harmonic	-119	-159	-212	242	216	184						
	gVSCF	-87	-160	-210	240	19	38	32	-2	2	-1	-197	-145
	eVSCF	-92	-166	-211	240	13	-49	27	-8	1	-2	-203	-232
	PT2/Harm	-94	-167	-215	195	5	-57	25	-8	-3	-47	-211	-241
	PT2/gVSCF	-97	-170	-216	203	-34	-81	22	-11	-3	-38	-250	-265
	PT2/eVSCF	-99	-171	-216	204	-38	-83	20	-13	-4	-38	-254	-267
	VCI	-98	-170	-216	203	-34	-78	21	-12	-3	-39	-249	-262
	Expt. (ω_{exp})	1167	1249	1500	1746	2782	2843						

Table 3.6: Calculated and measured [54] frequencies of formaldehyde in the gas phase. All frequencies and frequency differences in cm^{-1}.

1000 states, used by default in this work, constitutes only 1.5% of the 65780 possible states with at most 5 excitations. The VCI calculation was therefore repeated for the MP2/cc-pVTZ potential also with 4000, 5000 and 6000 basis functions to check the convergence behavior of VCI. The calculation in the smallest basis set yielded absolute average error of 26 cm^{-1}, which is nearly half of the error of the harmonic approximation (49 cm^{-1}). With 4000 states (6% of the possible states), the error is reduced below 20 cm^{-1}. With 5000 (7.6%) and 6000 (9.1%) functions, the VCI results do not differ significantly and can be thus regarded as converged (see

Table 3.8, page 60, and also Ref. 26).

The best agreement with the experiment give the perturbation methods with the potential calculated at the MP2/cc-pVTZ level: the absolute average error was only 10 cm^{-1}.

3.1.5 N-methyl acetamide

N-methyl acetamide (NMA) serves as a model system for understanding spectroscopic properties of the peptide bond. In Table 3.7 are shown calculated frequencies of selected vibrational transitions (amide A, I, II, III, IV, and a collective stretching vibration ν) in comparison to experimental values. As discussed in Appendix A.3, five lowest-energy modes had to be left out from the calculations to avoid numerical instabilities. Although the 6000 functions included in the basis set for the VCI diagonalization constitute only 4% of the total states, the VCI frequencies changed no more than few cm^{-1} from the values calculated in the basis of 5000 functions. (Data not shown.) The best agreement of anharmonic frequencies with experiment was achieved by the B3LYP potential using the perturbation methods.

3.1.6 α-Pinene

α-Pinene is an organic compound of the terpene class (Fig. 3.2) which is routinely used as a standard for measurements of vibrational optical activity. The molecule is rigid and non-polar.

	Methods	$\omega_{calc} - \omega_{exp}$						$\omega_{calc} - \omega_{harm}$					
		IV	ν	III	II	I	A	IV	ν	III	II	I	A
MP2/cc-pVTZ	Harmonic	12	35	33	63	41	203						
	gVSCF	-4	30	15	32	25	32	-16	-5	-18	-31	-16	-171
	eVSCF	-5	26	11	27	21	31	-17	-8	-21	-35	-21	-172
	PT2/Harm	-12	15	-4	20	17	48	-24	-19	-37	-43	-24	-155
	PT2/gVSCF	-13	15	-1	16	18	50	-25	-20	-34	-47	-23	-153
	PT2/eVSCF	-14	14	-2	14	14	51	-26	-21	-34	-48	-27	-152
	VCI (6000)	6	32	12	41	43	85	-6	-2	-21	-22	1	-119
B3LYP/cc-pVTZ	Harmonic	4	14	21	44	29	152						
	gVSCF	-13	5	4	16	10	-21	-17	-8	-16	-28	-18	-172
	eVSCF	-15	2	0	11	6	-22	-19	-12	-20	-33	-23	-173
	PT2/Harm	-21	-8	-14	2	2	-2	-25	-22	-35	-42	-27	-154
	PT2/gVSCF	-22	-10	-10	-1	3	-2	-26	-23	-30	-45	-25	-153
	PT2/eVSCF	-23	-10	-10	-2	1	-1	-27	-24	-30	-47	-28	-153
	VCI (6000)	-2	13	4	26	29	35	-6	-0	-17	-18	1	-116
BPW91/cc-pVTZ	Harmonic	-15	-14	-23	-5	-25	68						
	gVSCF	-33	-21	-39	-35	-43	-119	-18	-7	-16	-30	-18	-187
	eVSCF	-34	-25	-43	-39	-48	-120	-19	-11	-20	-34	-22	-188
	PT2/Harm	-41	-35	-59	-47	-53	-100	-26	-22	-35	-41	-27	-167
	PT2/gVSCF	-43	-36	-54	-50	-51	-102	-28	-23	-31	-45	-26	-169
	PT2/eVSCF	-44	-37	-54	-52	-55	-101	-29	-24	-31	-47	-30	-169
	VCI (6000)	-21	-15	-39	-23	-24	-63	-7	-1	-16	-18	2	-131
	Expt. (ω_{exp})	[b]626	[a]1089	[b]1259	[b]1500	[b]1728	[a]3498						

[a] Exp. values from Ref. 55.
[b] Exp. values from Ref. 56.

Table 3.7: Calculated and experimental frequencies of selected vibrational transitions of N-methyl acetamide in the gas phase. The experimental values were obtained by infrared measurements in low-temperature nitrogen matrix (*a*) and by resonance Raman spectroscopy (*b*). All frequencies and frequency differences are in cm^{-1}.

	Methods	$\omega_{calc} - \omega_{exp}$																					
		ν_{11}	ν_{14}	ν_{10}	ν_{13}	ν_{12}	ν_9	ν_8	ν_{21}	ν_7	ν_{20}	ν_6	ν_5	ν_{19}	ν_{18}	ν_4	ν_3	ν_{17}	ν_{16}	ν_2	ν_{15}	ν_1
[a]	Harmonic	16	19	39	36	41	28	22	23	32	39	37	40	61	44	57	67	74	152	153	152	151
MP2/cc-pVTZ	Harmonic	14	29	5	17	1	4	7	11	31	24	47	25	68	26	37	19	21	160	161	158	156
	gVSCF	46	45	58	73	42	50	0	7	33	25	34	22	53	12	20	4	2	51	41	45	16
	eVSCF	46	44	50	61	37	38	-0	7	29	23	33	20	44	11	15	-0	-5	-6	10	-13	13
	PT2/Harm	33	29	3	-3	1	-8	-8	4	9	2	21	6	31	1	-11	-14	-13	-3	-5	-7	-3
	PT2/gVSCF	33	28	14	12	6	3	-8	3	10	3	22	5	32	-1	-8	-9	-9	-13	-21	-20	-3
	PT2/eVSCF	34	29	16	12	9	3	-9	3	9	1	21	4	31	-2	-7	-9	-4	5	-13	-9	-0
	VCI (1000)	53	48	34	21	18	14	9	20	30	20	42	28	54	21	23	-4	-6	55	31	9	8
	VCI (4000)	45	42	29	21	19	11	-1	12	17	9	31	13	44	7	10	-18	-13	52	6	-8	8
	VCI (5000)	44	41	28	21	19	10	-2	12	17	9	31	12	45	6	9	-20	-13	45	2	-12	9
	VCI (6000)	44	41	28	21	18	9	-2	11	17	9	30	13	43	6	9	-21	-14	41	1	-18	7
B3LYP/cc-pVTZ	Harmonic	19	22	15	16	19	23	21	21	20	19	20	26	18	27	31	22	37	113	114	116	113
	gVSCF	51	41	59	68	53	17	55	17	22	17	7	24	3	13	16	7	21	7	-17	-6	-41
	eVSCF	50	41	53	57	48	16	45	16	18	15	6	23	-4	12	12	3	14	-57	-37	-72	-46
	PT2/Harm	36	23	10	-0	15	9	2	13	-0	-5	-5	7	-19	2	-12	-10	6	-51	-51	-53	-45
	PT2/gVSCF	35	22	18	12	18	9	11	12	0	-5	-5	7	-18	1	-10	-6	10	-56	-61	-66	-75
	PT2/eVSCF	36	23	20	11	21	8	10	12	-1	-6	-5	6	-18	0	-10	-6	15	-16	-55	-96	-89
	VCI (6000)	46	35	30	18	30	15	16	20	6	2	5	14	-8	8	2	13	3	15	-40	-56	-108
BPW91/cc-pVTZ	Harmonic	1	7	-25	-15	-26	-12	-11	-8	-6	-14	-0	-5	-17	-19	-7	-22	-12	51	51	51	49
	gVSCF	33	25	28	46	13	22	-18	-13	-4	-15	-13	-8	-33	-33	-22	-37	-28	-66	-83	-73	-105
	eVSCF	32	24	21	33	8	11	-18	-14	-8	-17	-14	-9	-40	-34	-27	-41	-36	-130	-110	-137	-110
	PT2/Harm	15	6	-27	-31	-27	-33	-26	-17	-28	-39	-26	-25	-55	-45	-52	-55	-45	-122	-125	-122	-118
	PT2/gVSCF	15	6	-16	-15	-23	-23	-26	-18	-27	-38	-25	-26	-55	-45	-49	-50	-42	-132	-145	-136	-109
	PT2/eVSCF	16	7	-13	-15	-20	-24	-27	-18	-29	-40	-26	-27	-54	-47	-49	-50	-38	-102	-131	-175	-149
	VCI (6000)	28	20	-1	-6	-10	-17	-20	-9	-20	-30	-15	-18	-43	-38	-36	-67	-46	-65	-112	-113	-112
[b]	Harmonic	10	16	9	10	12	16	17	20	17	14	16	22	14	17	25	16	30	111	113	118	115
	gVSCF	53	36	60	65	56	79	10	16	20	14	4	21	0	5	11	1	15	7	-22	-6	-44
	eVSCF	52	35	53	54	51	69	10	15	17	12	3	19	-7	5	7	-2	8	-58	-38	-75	-50
	PT2/Harm	42	17	9	-5	17	23	2	12	-2	-9	-8	3	-22	-6	-15	-15	4	-48	-51	-58	-46
	PT2/gVSCF	42	17	19	10	22	35	2	11	-2	-8	-7	3	-21	-6	-14	-11	8	-55	-61	-67	-79
	PT2/eVSCF	43	18	21	8	24	35	2	11	-3	-10	-8	2	-20	-7	-14	-11	15	-16	-59	-94	-93
	VCI (6000)	49	30	32	15	33	42	8	19	5	-1	2	10	-10	0	-4	-3	-0	11	-41	-53	-54
	Expt. (ω_{exp})	600	603	722	745	838	864	870	873	995	1043	1067	1140	1181	1267	1385	1491	1558	3130	3140	3161	3169

[a] CCSD/cc-pVTZ (The evaluation of the anharmonic potential was not possible at this level.)
[b] B3LYP/6-311++G**

Table 3.8: Calculated and measured frequencies of fundamental vibrational transitions of furan in the gas phase. The mode numbering and experimental values were taken from Ref. 57. All frequencies and frequency differences are in cm^{-1}. The number of states included in VCI calculations is indicated by the numbers in brackets.

Figure 3.2: (+)-α-Pinene

Although α-pinene exists in the liquid form, calculations performed for a single molecule in the vacuum yield agreeable results. The size of the molecule (26 atoms) restricts the level of electronic *ab initio* calculations to HF or DFT methods and smaller basis sets. Fig. 3.3 (page 62) shows Raman spectra calculated using different anharmonic methods at the B3LYP/6-31G** level. By visual inspection of dominant peaks in calculated and measured [5] spectra, it is obvious that the VCI method gives in this region the worst agreement with the experiment. This fact is not surprising, because the diagonalization was performed in the basis of 6000 functions, which is only 0.04% of the total of almost 14 million states. The best agreement was attained by the perturbation methods, as indicated by the red dotted lines. Fig. 3.4 shows calculated and measured ROA spectra of (-)-α-pinene.

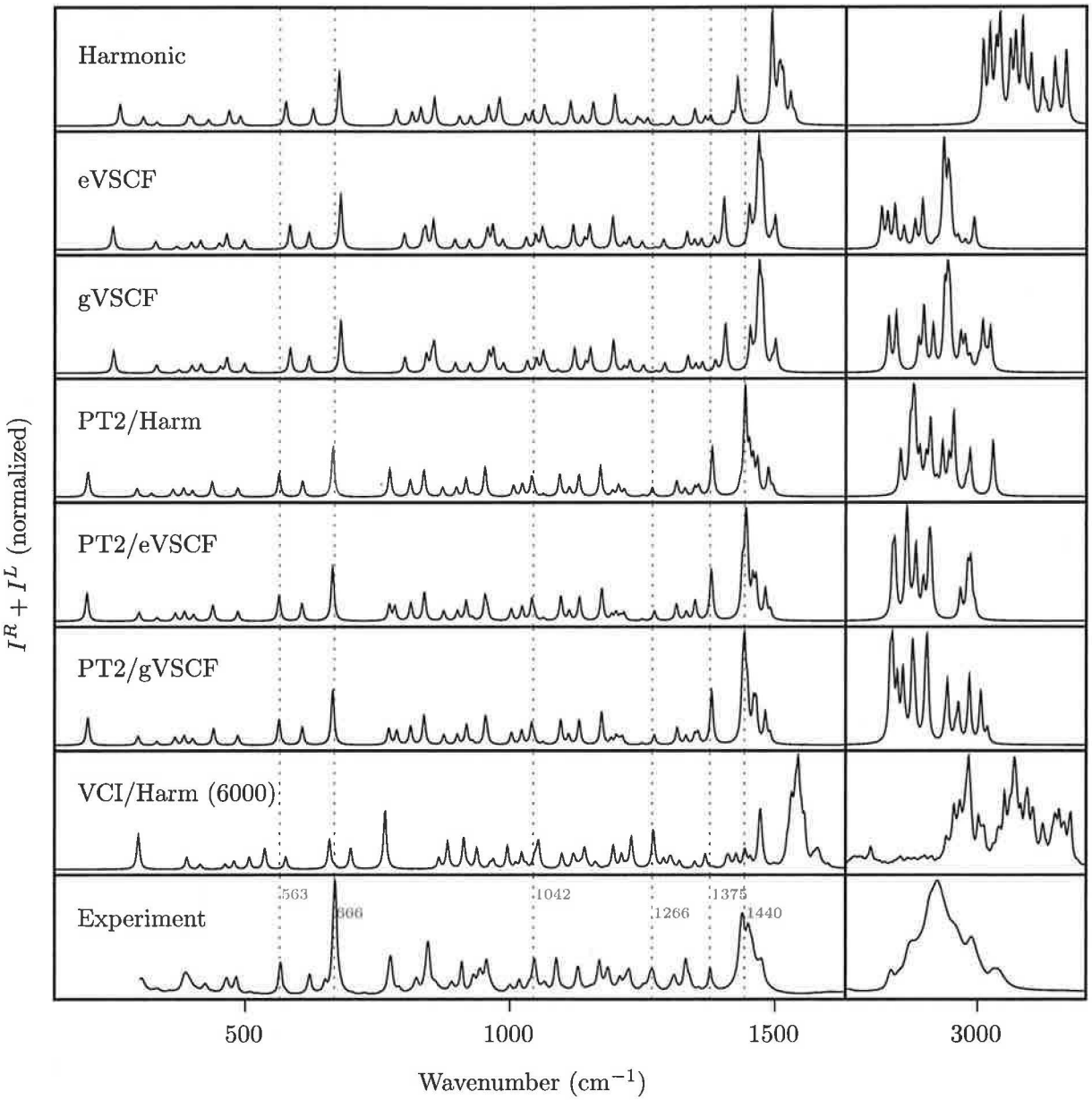

Figure 3.3: Calculated and measured Raman spectra of α-Pinene (neat liquid). The vibrational potential was calculated using the B3LYP/6-31G** method. Five of the lowest-energy modes were left out from the calculations to avoid numerical instabilities. Only first derivatives of intensity tensors were considered. The VCI calculation was performed in the basis of 6000 functions.

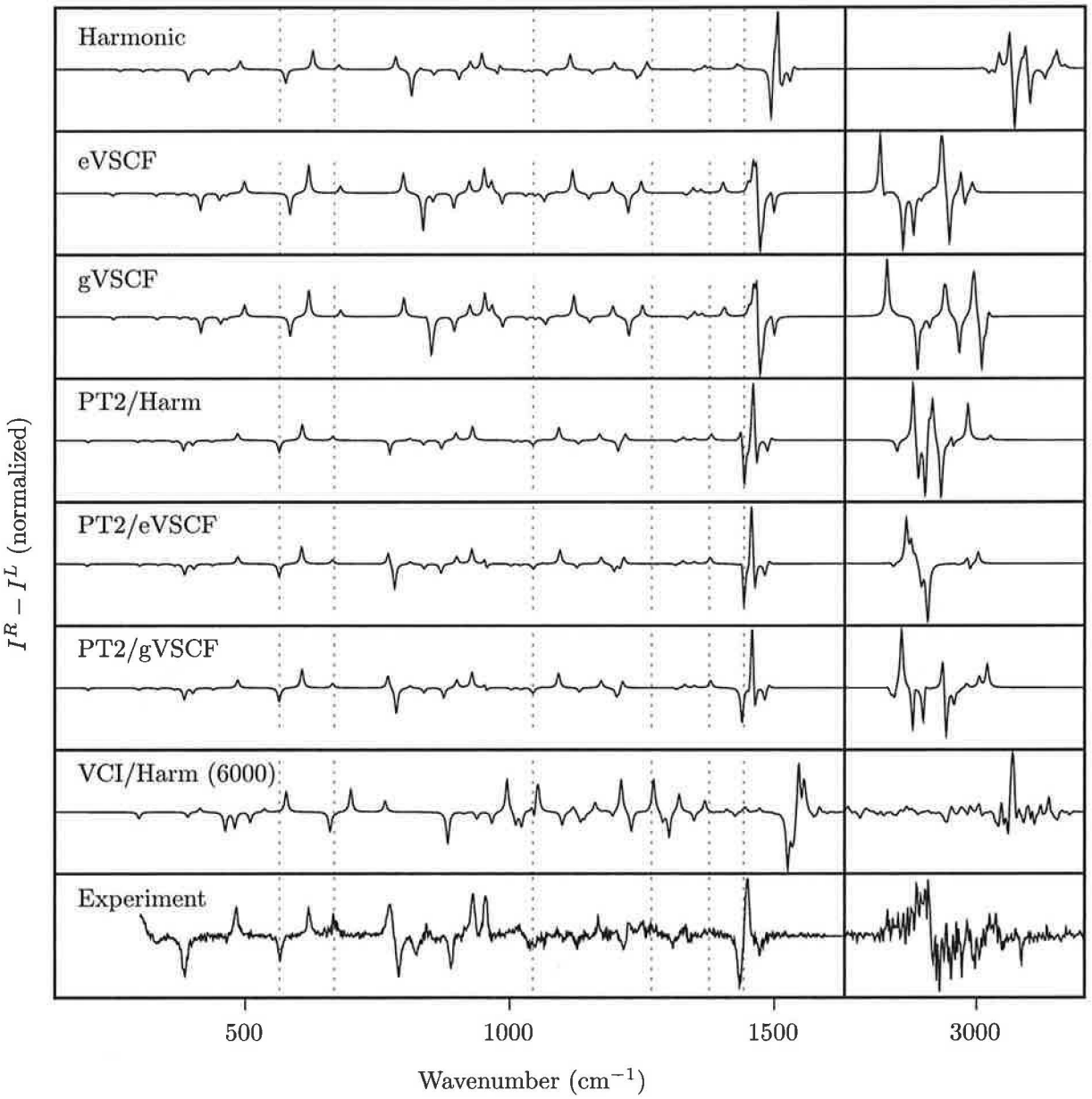

Figure 3.4: Calculated and measured ROA spectra of (-)-α-Pinene (neat liquid). The vibrational potential was calculated using the B3LYP/6-31G** method. Five of the lowest-energy modes were left out from the calculations to avoid numerical instabilities. Only first derivatives of intensity tensors were considered. The VCI calculation was performed in the basis of 6000 functions. The red dotted lines correspond to peaks emphasized in Fig. 3.3.

3.2 Publications

3.2.1 Numerical stability of anharmonic methods (summary)

The accuracy of calculated vibrational energies depends on the quality of input data (the potential energy surface), involved vibrational approximation (harmonic, VSCF, etc.) and numerical stability of the method under consideration.

Because the accuracy of electronic calculations is limited, the cubic and semi-diagonal quartic constants obtained by numerical differentiation from second derivatives can differ significantly not only for different levels of the electronic theory, but also for different options and parameters used in the potential evaluation. For example, harmonic frequencies of alanine evaluated at the B3LYP/6-31G**/CPCM level can occasionally differ as much as 136 cm^{-1} when calculated by GAUSSIAN with the default grid (75,302)[2] or with the "UltraFine" grid (99,590). The maximal difference in frequencies corrected by anharmonic methods is magnified to almost 400 cm^{-1} by some methods. It is expected that different anharmonic methods will respond differently to small potential variations. For example, in the mathematical formalism of the perturbation method of the second order there is a term which contains summation over many terms with the same sign (Eq. 2.2.14). One may expect that the perturbation methods will amplify the differences in the anharmonic potential to a different level than, for example, VSCF.

In Ref. 26 (see Appendix B) we focused on the numerical stability of anharmonic vibrational methods with respect to random variations of anharmonic constants of furan. While VSCF proved to be the most resistant to potential variations, the second-order perturbation methods turned out to be very sensitive to random degeneracies and provided the least stable results. However, the stability could be significantly improved by a simple modification of perturbation formula (Eq. 2.2.18).

Performance of the anharmonic methods was investigated also for other molecules.

3.2.2 Anharmonic methods applied to solvated systems (summary)

In an aqueous environment, many amino acids occur in the zwitterionic form.[3] Zwitterions interact strongly with water, which makes them ideal model systems for studying properties of molecules strongly interacting with polar solvents.

In Ref. 58 (see Appendix B) we analyzed anharmonic contributions to IR, Raman and ROA spectra of alanine and proline zwitterions (Fig. 3.5), studied previously also in [59, 60]. It was found that anharmonic effects dominate in the region of C−H and N−H stretching vibrations. All of the anharmonic methods significantly improved harmonic results in this region. Due to inaccuracies of the vibrational potential and involved approximations, none of the methods enabled peak-to-peak agreement with experiment though. The lower-frequency vibrations (less

[2]The default grid has 75 radial shells and 302 angular points per shell.

[3]A *zwitterion* contains positively and negatively charged groups, but its total charge is zero. In amino acids, a hydrogen ion from the carboxyl group is removed leaving the carboxyl group negatively charged, while the amino group is protonated and positively charged.

L-Alanine L-Proline A L-Proline B

Figure 3.5: L-alanine and L-proline zwitterions. The A and B proline conformers have approximately the same energy and equal populations in aqueous solutions at room temperature [60].

than 2000 cm^{-1}) are in general well described by the harmonic potential. The anharmonic methods improved the agreement only occasionally for some C−H and N−H bending modes.

Conformational flexibility of the molecules contributes to the broadening of peaks, as was demonstrated by the Boltzmann averaging of the spectra calculated for different conformers.

3.2.3 Conformational flexibility (preliminary results)

Raman and ROA spectra are sensitive to molecular conformation. If a molecule can exist in multiple conformations under the given experimental conditions, each of the conformers will contribute to the spectra. For flexible molecules, it is expected that some of the spectral bands will change their relative intensity and will become broader with increased temperature, as more conformers will become energetically accessible. Experimental evidence suggested that more flexible molecules have less complex spectral features than the rigid ones. For example, experimental Raman and ROA spectra of some small dipeptides (Gly-Pro and Ala-Pro) seem to have sharper bands than others (Pro-Gly and Pro-Ala) within 200–750 cm^{-1} [59].

In the paper under preparation, we try to verify that the decreased complexity of the Pro-Gly and Pro-Ala spectra is due to larger conformational flexibility of these molecules: in the "rigid" molecules (Gly-Pro and Ala-Pro), the torsion angle φ is fixed by the covalent bond in the proline ring and only the torsion angle ψ is allowed to move. In the "flexible" molecules (Pro-Gly and Pro-Ala) both torsion angles ψ and φ are allowed to move (Fig. 3.6). To identify possible conformers, systematic scanning of the conformation space was performed: one-dimensional scans along the angle ψ for the rigid molecules and two-dimensional scans along the angles ψ and φ for the flexible molecules.

Four local minima have been found for Gly-Pro and Ala-Pro, differing in the puckering phase[4] or in the *cis* and *trans* form (Table 3.9). For Ala-Pro, both *cis* conformers have significantly lower energy, but their geometries appear unrealistic: according to the calculation, one of the hydrogens from the NH_3 group forms a hydrogen bond with one of the oxygens from the CO_2 group. The calculation shows the vibrational transition associated with this hypothetical

[4]The puckering phase is a characterization of the five-membered ring in proline and it is defined in terms of torsion angles [61]. There are two proline conformers differing in the puckering phase. They have approximately the same energy in aqueous solutions at room temperature (Fig. 3.5).

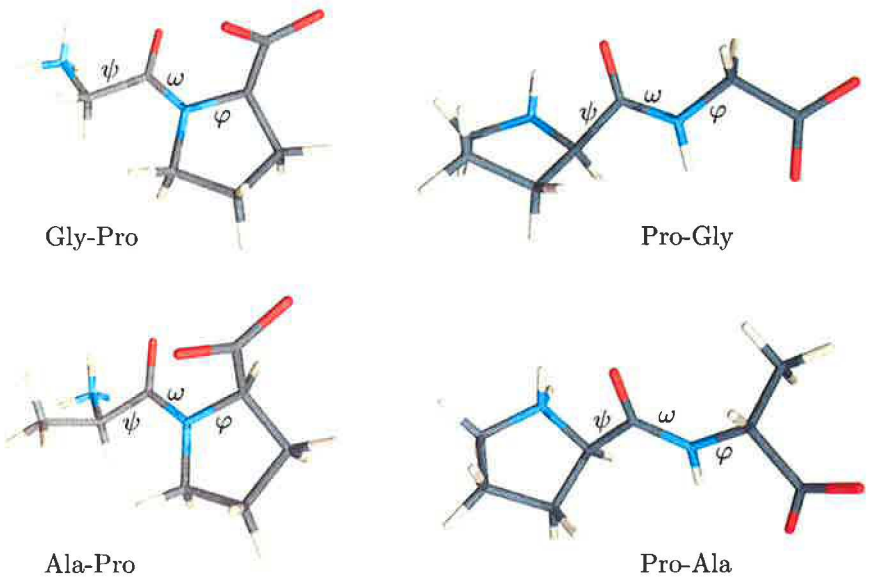

Figure 3.6: *Trans* conformers of Gly-Pro, Pro-Gly, Ala-Pro and Pro-Ala zwitterions. The angle φ is fixed in Gly-Pro and Ala-Pro, but is allowed to move in Pro-Gly and Pro-Ala.

bond as an isolated peak near 2400 cm^{-1}, but there is no such peak present in experimental spectra. For Gly-Pro, the two *cis* conformers also have lower energies, but both appear realistic. Each of the conformers was then used to generate another two geometries by rotating the angle ψ and optimizing with ψ held constant. Ideally, the rotation should be large enough to estimate the effect on the vibrational spectra, but still allowing decent Boltzmann population of the rotamers at room temperature. In Fig. 3.7 the results of the preliminary calculations ale plotted for Gly-Pro. Although the limited number of conformers does not exactly reproduce the smooth experimental bands, broadening of the peaks is clearly visible.

The flexible dipeptides Pro-Gly and Pro-Ala were treated in a similar way. Four local minima differing in the puckering phase and in the *cis* and *trans* form of the amide bond can exist for both molecules. The *cis* form is known to be energetically much less favorable and therefore only the *trans* form was investigated. For both molecules, two-dimensional PES were generated by interpolation between 100 scan points calculated at the B3LYP/6-31G*/CPCM level with φ and ψ ranging from 0° to 360°. Raman spectra were then calculated for 26 conformers and averaged according to Boltzmann populations at room temperature. Because the evaluation of the optical activity tensors is very demanding, the ROA tensors were calculated only for the equilibrium geometries. For other conformers, the algorithm described in Ref. 62 was used to

Gly-Pro	*cis*	*trans*
P_1	0	0.75
P_2	0.17	0.89

Ala-Pro	*cis*	*trans*
P_1	0	4.8
P_2	<1.1	5.0

Table 3.9: Relative energies of Gly-Pro and Ala-Pro conformers calculated at the B3LYP/6-31++G**/CPCM level. They differ in the puckering phase (P_1 and P_2) or in the *cis* and *trans* form. The P_2/*cis* conformer reached a local minimum. The global minimum was not pursued, because the geometry seemed unrealistic, as described in the text. [kcal/mol]

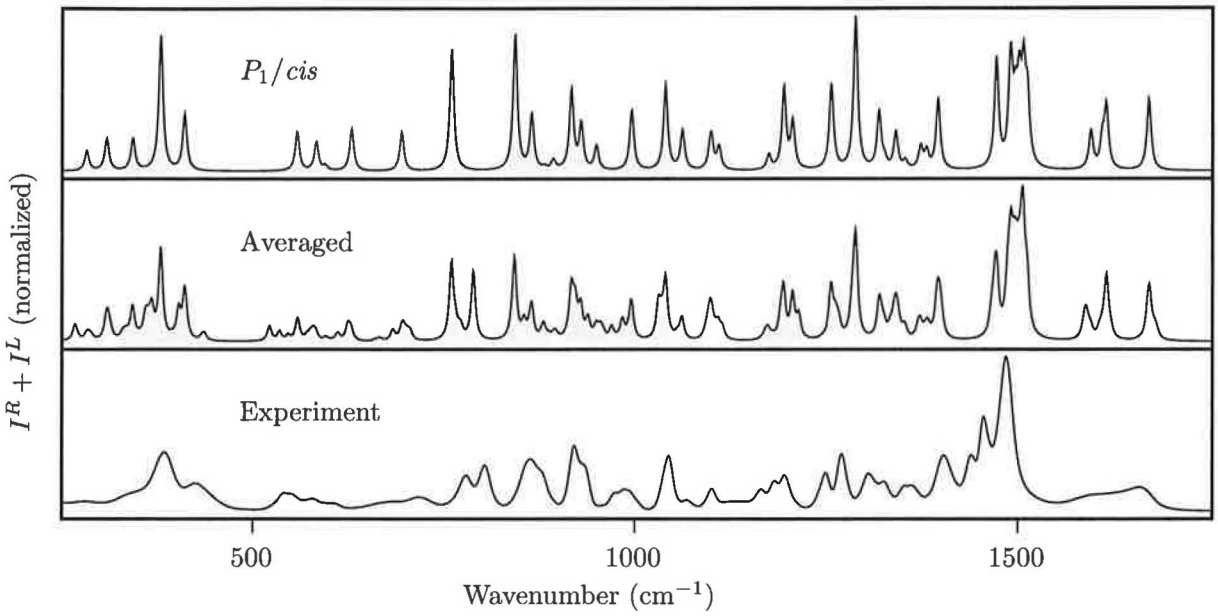

Figure 3.7: Calculated and experimental Raman spectra of Gly-Pro (preliminary results). The top panel shows Raman spectra calculated for the equilibrium geometry P_1/cis, the middle panel shows Boltzmann-averaged spectra of 11 conformers, and in the bottom panel is plotted the measured spectrum. The parts of the spectra susceptible to improvement by Boltzmann averaging are emphasized by gray color. All calculations were performed at the B3LYP/6-31++G**/CPCM level using the harmonic approximation.

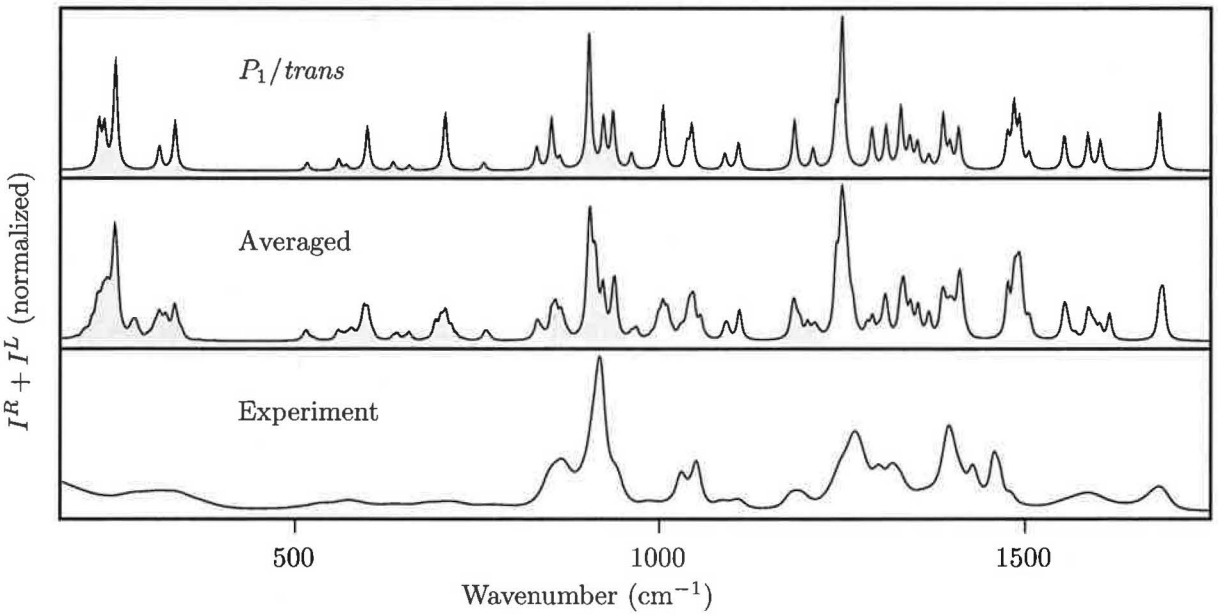

Figure 3.8: Calculated and experimental Raman spectra of Pro-Gly (preliminary results). The top panel shows Raman spectra calculated for the equilibrium geometry $P_1/trans$, the middle panel shows Boltzmann-averaged spectra of 26 conformers, and in the bottom panel is plotted the measured spectrum. The parts of the spectra susceptible to improvement by Boltzmann averaging are emphasized by gray color. All calculations were performed at the B3LYP/6-31++G**/CPCM level using the harmonic approximation.

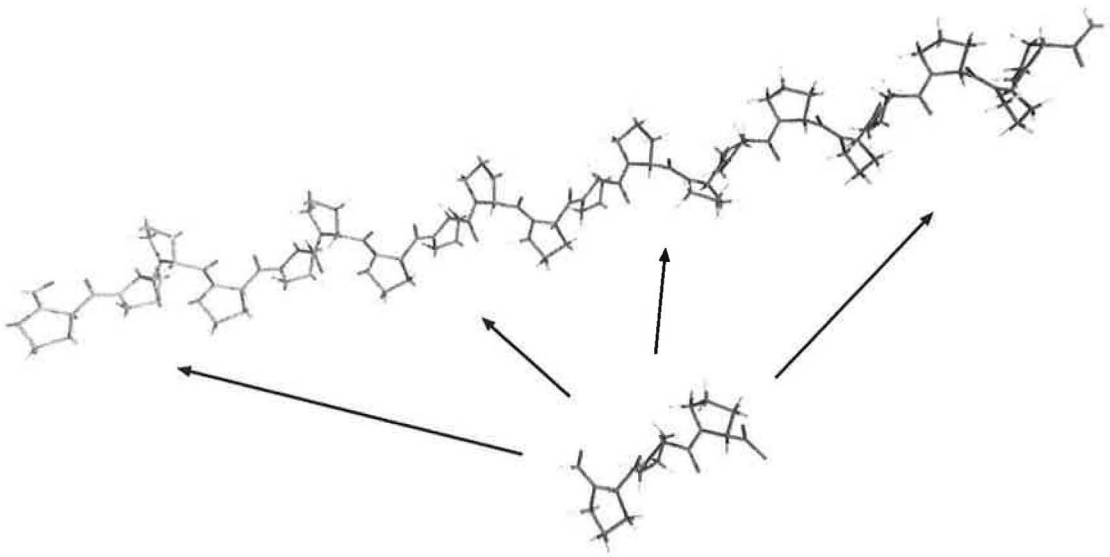

Figure 3.9: Transfer of molecular property tensors from a tripeptide to poly-proline II.

transfer the tensors to the desired geometries.

In Fig. 3.8 the results of the preliminary calculations are plotted. The results obtained so far for Gly-Pro and Pro-Gly do not seem to confirm the hypothesis that the lesser complexity of the Raman and ROA spectra of Pro-Gly and Pro-Ala origin in larger number of conformers. The averaging seems to play a role equally important for all of the studied dipeptides.

3.2.4 Transfer of molecular property tensors (in progress)

The evaluation of *ab initio* force fields and molecular property tensors is feasible only for small molecules. Large systems can be treated only approximately, for example, by dividing them into smaller pieces, then evaluating the properties on a decent electronic level, and transferring the properties to the large molecule (Fig. 3.9). Because the evaluation of the anharmonic potential requires a large amount of computer-time, the algorithm described in Ref. 62 was implemented also for anharmonic force constants. The method will be used for anharmonic frequencies of poly-proline II, the calculations are already in progress.

CHAPTER 4

Conclusions

The aim of this work was to investigate anharmonic and solvation effects in vibrational spectra. Several vibrational anharmonic methods were coded in two implementations using two different programming languages (Fortran and C) to verify the correctness of the software, and thoroughly tested on model potentials studied previously by other authors. The anharmonic methods were then applied to a number of systems, both small and large (water and α-pinene), rigid and flexible (furan and NMA).

For small molecules, several calculations were performed with potentials obtained at various levels of the electronic theory. The most computer-time demanding method CCSD/cc-pVTZ could be used only for water and formaldehyde. In both cases, the anharmonic frequencies based on the CCSD potential deviated from experiment more than the frequencies obtained with the MP2/cc-pVTZ potential. The MP2 method gave the best agreement with experiment in calculations performed for formaldehyde and furan, while for water and NMA the MP2 method was outperformed by the B3LYP/cc-pVTZ calculation. The BPW91/cc-pVTZ method seems to be biased toward the harmonic approximation, so that the harmonic frequencies often give the best results, but anharmonic corrections shift the frequencies far too low.

For larger molecules, the evaluation of the anharmonic potential is restricted to less accurate electronic methods and smaller basis sets. The B3LYP method was tested with several basis sets, but the small number of tested molecules (water, formaldehyde and furan) did not allow generalization. For furan and formaldehyde, the calculations performed with the cc-pVTZ basis set yielded results similar to the results obtained with the 6-311++G** set. Whereas for water, a significant difference between the two was observed. Diffuse functions on hydrogens (++) seemed not to be crucial for water and formaldehyde, but were found important for furan. The double split set (6-31++G**) gave identical results for water as for the triple split basis set (6-311++G**), but very different for furan. Perhaps expectedly, the polarization functions on hydrogen (**) are important for water, but not so much for formaldehyde and furan. Clearly, the basis set must be selected on an individual basis to respect the nature of the studied system.

As expected, the anharmonic effects dominate in the region of C-H and N-H stretching vibrations. All of the anharmonic methods investigated in this work significantly improved harmonic results in this region. Due to inaccuracies of the vibrational potential and involved approximations, none of the methods enabled peak-to-peak agreement with experiment though. The low- and mid-frequency vibrations are in general described well by the harmonic potential and anharmonic corrections do not inevitably improve the agreement with experiment in this

region.

The solvent interactions were accounted for by means of the conductor solvent model CPCM. The model correctly stabilized the zwitterionic peptides and provided reasonable vibrational frequencies. However, due to numerical instabilities, the conductor model sometimes yields inconsistent results and therefore it requires tighter geometry optimization and a higher-density integration grid with DFT calculations. Although the treatment of solvation prolongs the computation time, the effects of solvation often cannot be neglected.

Some of the bands in experimental spectra are less intensive and broader, probably because of direct interactions with solvent molecules and larger molecular flexibility. To reproduce these spectral shapes, full energy scans and the Boltzmann averaging were used successfully. The averaging allowed to partially include the anharmonicity of the low-frequency vibrations which could not be properly treated by the anharmonic methods.

Appendix A

A.1 Simplified degeneracy treatment

This Appendix justifies usage of the degeneracy-corrected perturbation formula. It is shown that for non-degenerate states the formula reduces to the standard second-order perturbation treatment.

Non-degenerated states

The second term in Eq. 2.2.18 may written as

$$\sqrt{(E_i - E_j)^2 + 4W_{ij}^2} = |E_i - E_j|\sqrt{1+\epsilon}, \qquad \epsilon = \frac{4W_{ij}^2}{(E_i - E_j)^2}, \tag{A.1.1}$$

where ϵ is proportional to second power of the perturbation parameter λ from Eq. 2.2.8. Using first two terms of the expansion

$$\sqrt{x+\epsilon} = \sqrt{x} + \frac{1}{2}x^{-1/2}\epsilon - \frac{1}{8}x^{-3/2}\epsilon^2 + \cdots, \tag{A.1.2}$$

the expression may be then approximated by

$$|E_i - E_j|\left[1 + \frac{2W_{ij}^2}{(E_i - E_j)^2}\right]. \tag{A.1.3}$$

Respecting the $\pm$ convention introduced on page 16, it is easy to show that Eq. 2.2.18 then evaluates to

$$\sum_{j\neq i}\frac{1}{2}(E_j - E_i) \pm \frac{1}{2}\sqrt{(E_i - E_j)^2 + 4W_{ij}^2} = \sum_{j\neq i}\frac{W_{ij}^2}{E_i - E_j}. \tag{A.1.4}$$

By use of the expansion

$$\frac{1}{x+\epsilon} = \frac{1}{x} - \frac{\epsilon}{x^2} + \cdots, \tag{A.1.5}$$

the formula may be modified as

$$\sum_{j\neq i}\frac{W_{ij}^2}{E_i - E_j} = \sum_{j\neq i}\frac{W_{ij}^2}{E_i^{(0)} - E_j^{(0)}} - \frac{W_{ij}^2(W_{ii} - W_{jj})}{(E_i^{(0)} - E_j^{(0)})^2} + \cdots. \tag{A.1.6}$$

The terms which are proportional to higher powers of the perturbation coefficient λ are neglected. Thus taking only the first term, one arrives to the standard perturbation formula.

Two-fold degenerated states

When two or more states occur with the same energy, the second-order perturbation formula fails. If there are only two degenerate states, it is straightforward to show that the eigenvalues from Eq. 2.2.16 are

$$w_{\pm} = \frac{1}{2}(W_{11} + W_{22}) \pm \frac{1}{2}\sqrt{(W_{11} - W_{22})^2 + 4W_{12}^2}. \tag{A.1.7}$$

Therefore Eq. 2.2.17 evaluates to

$$E_{\pm} = E_1^{(0)} + \frac{1}{2}(W_{11} + W_{22}) \pm \frac{1}{2}\sqrt{(W_{11} - W_{22})^2 + 4W_{12}^2}. \tag{A.1.8}$$

When also interactions with other states are included, an expression identical to

$$E_1^0 + W_{11} + E_1^{(2)'} \tag{A.1.9}$$

is obtained.

A.2 Units

Frequencies

In vibrational spectroscopy frequencies are traditionally expressed as wave numbers $\tilde{\nu}$ in the cm^{-1} units. The wave number is defined as

$$\tilde{\nu} = 1/\lambda, \tag{A.2.1}$$

where λ is the wave length of the radiation in a vacuum.

Experimental absorption intensities

Absorption spectra in this work were plotted as the molar extinction coefficient ε, with peaks simulated by Lorentz curves of a fixed width Δ. A peak of height h centered at $\tilde{\nu}_i$ is given as

$$L_i(\tilde{\nu}) = \frac{h}{4(\tilde{\nu} - \tilde{\nu}_i)^2/\Delta^2 + 1}. \tag{A.2.2}$$

Calculated absorption intensities I are usually given in km/mol [63]. These units are related to the experimental quantity ε ($L\,mol^{-1}cm^{-1}$) by [64]

$$I_i = 9.184 \times 10^{-3}\, \tilde{\nu}_i \sqrt{2\pi} \int \frac{\varepsilon}{\tilde{\nu}}\, d\tilde{\nu}. \tag{A.2.3}$$

Using the approximation that

$$\int \frac{\varepsilon}{\tilde{\nu}}\, d\tilde{\nu} \simeq \frac{1}{\tilde{\nu}_i} \int \varepsilon\, d\tilde{\nu}, \tag{A.2.4}$$

the unknown height h of the Lorentz curve is determined from the requirement that the area under the curve L has to be equal to the area under ε

$$\int_{-\infty}^{\infty} \varepsilon\, d\tilde{\nu} = \int_{-\infty}^{\infty} \frac{h}{4(\tilde{\nu} - \tilde{\nu}_i)^2/\Delta^2 + 1}\, d\tilde{\nu} \tag{A.2.5}$$

$$= -\frac{1}{2} h \Delta \tan^{-1} \left[\frac{2(\tilde{\nu}_i - \tilde{\nu})}{\Delta} \right]_{-\infty}^{+\infty} \tag{A.2.6}$$

$$= \frac{\pi}{2} h \Delta. \tag{A.2.7}$$

Inserting this result in Eq. A.2.3, the height of the Lorentz curve is found to be

$$h = \frac{1}{9.184 \times 10^{-3}} \frac{I}{\Delta} \sqrt{\frac{2}{\pi^3}}. \tag{A.2.8}$$

A.3 Computation details

The force fields and molecular properties were calculated using the GAUSSIAN software [63]. The results of anharmonic methods presented in this work were calculated using the GVIB program package implemented by the author of this work. The code is freely available for download [52].

Unless explicitly stated otherwise, all calculations were performed using the following default parameters:

Force field constants

- The anharmonic constants were calculated by numerical differentiation with a displacement step of 0.025Å.

VSCF parameters

- VSCF functions were represented by a linear combination of 15 LHOs.
- The convergence criterion for VSCF energy was set to 10^{-6} cm^{-1}. Typically, the energy converged after less than 50 iterations.

VCI and perturbation methods

- The maximal number of allowed excitations in product functions used in VCI and the perturbation calculus was set to $n_{\mathrm{exc}} = 5$.
- Unless stated otherwise, the VCI calculations were performed in the basis of 1000 functions.

Spectra simulations

- The default width (FWHM) of Lorentzian peaks was 6.5 cm^{-1}.
- The evaluation of second-order derivatives of tensors required for anharmonic Raman and ROA intensities is very computer-time demanding. Therefore, the computation may be performed using first-order derivatives only.
- For perturbation methods, the calculation of intensities was not implemented. Instead, intensities are taken from the unperturbed solutions.

For some molecules, the anharmonic methods exhibit convergence problems. The most sensitive is the eVSCF method, which often fails to converge unless the lowest-energy modes are left out from the calculations. Their coupling to higher-frequency modes is believed to be negligible and was in some cases partially accounted for by Boltzmann averaging.

A.4 Numerical differentiation and CPCM

As discussed in Sec. 2.4.3, the vibrational potential can be near a minimum approximated by a Taylor expansion. Cubic and semidiagonal quartic derivatives can be calculated by numerical differentiation of second order derivatives evaluated at geometries displaced from the equilibrium geometry along nuclear coordinates. Some of the constants can be obtained multiple times. For instance, the quartic constant $V^0_{\alpha_i\alpha_i\beta_j\beta_j}$ can be obtained twice

$$V^0_{\alpha_i\alpha_i\beta_j\beta_j} = \frac{1}{\Delta^2}(V^{\beta_j+\Delta}_{\alpha_i\alpha_i} + V^{\beta_j-\Delta}_{\alpha_i\alpha_i} - 2V^0_{\alpha_i\alpha_i}) = \frac{1}{\Delta^2}(V^{\alpha_i+\Delta}_{\beta_j\beta_j} + V^{\alpha_i-\Delta}_{\beta_j\beta_j} - 2V^0_{\beta_j\beta_j}). \qquad \text{(A.4.1)}$$

If the second order derivatives were exact, both formulae would yield exactly the same values. However, due to numerical errors of electronic calculations, the values differ in practice. For example, calculations performed for alanine at the B3LYP/6-31G**/CPCM level with the dif-

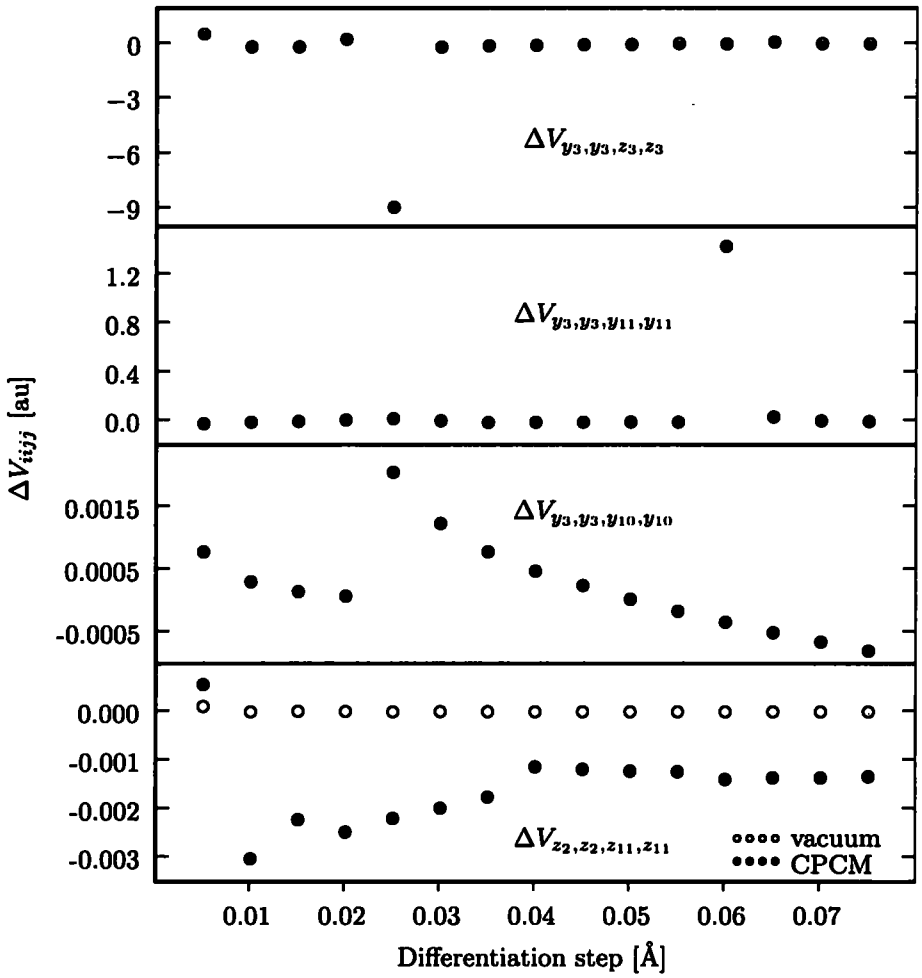

Figure 4.1: Deviations from expected symmetry of semidiagonal quartic constants calculated at the B3LYP/6-31G**/CPCM (red) and the B3LYP/6-31G** (yellow) levels. The two pictures at the top illustrate that there is no best differentiation step: the error of the constant V_{y_3,y_3,z_3,z_3} is minimal for the step of 0.06 Å. Using this step size will, however, magnify the error of the constant $V_{y_3,y_3,y_{11},y_{11}}$. The third picture shows a well-behaved constant. On the last picture are compared errors of CPCM and vacuum calculations.

ferentiation step $\Delta = 0.025$ Å give an alarmingly large error: the maximal error is almost 95% of the value of the largest quartic constant! The magnitude of the error depends on the size of the differentiation step. For example, if the step size is increased to 0.06 Å, the maximal error is reduced below 24%. However, the most significant improvement is achieved when the calculations are performed without the CPCM model or when the CPCM cavities are held fixed at the equilibrium positions and are not allowed to move along with the displaced atoms.[1]

Fig. 4.1 shows deviations of selected symmetric quartic constants, calculated for particular steps. As shown, a randomly chosen quartic constant is much less stable when calculated using the CPCM model (the bottom picture). For most constants, the error changes gradually with the step size (the third picture from the top), but it can be significantly larger for some particular step (the top picture). Choosing a different step size does not help, because different constants have largest deviations for different steps (the second picture from the top).

The results in this Appendix were obtained by the GAUSSIAN 03 software, rev. C.02. Obviously, the results are dependent on a number of the program's options, parameters and optimization criteria. Calculations performed by the same version of the software at a different level of theory (HF/6-31G) or for slightly different starting geometry either did not reproduce these dramatic errors or gave different error curves. In contrast to the suggestion of Barone [21, 65], practical tests (with the CPCM model) favored larger differentiation steps of about 0.05 Å. It was not investigated whether larger steps may contaminate the constants by higher order force constants or if the constants can be affected by coupling between modes for larger steps.

[1]The results of CPCM calculations presented throughout this work were obtained with cavities following the displaced atoms.

References

[1] C. V. Raman and R. S. Krishnan, *A new type of secondary radiation*, Nature **121** (1928), 501.

[2] P. W. Atkins and L. D. Barron, *Rayleigh scattering of polarized photons by molecules*, Mol. Phys. **16** (1969), 453–466.

[3] L. D. Barron and A. D. Buckingham, *Rayleigh and Raman scattering from optically active molecules*, Mol. Phys. **20** (1971), 1111–1119.

[4] W. Hug, S. Kint, G. F. Bailey, and J. R. Scherer, *Raman. circular intensity differential spectroscopy.*, J. Am. Chem. Soc. **97** (1975), 5589–5590.

[5] P. Bouř, V. Baumruk, and J. Hanzlíková, *Measurement and calculation of the Raman optical activity of α-pinene and* trans*-pinane*, Collect. Czech. Chem. Commun. **62** (1997), 1384–1395.

[6] J. Hanzlíková, P. Praus, and V. Baumruk, *Raman optical activity spectrometer for peptide studies*, J. Mol. Struct. **480–481** (1999), 431–435.

[7] J. Kapitán, *Teoretický a experimentální rozvoj Ramanovy optické aktivity jako metody studia biomolekul ve vodném prostředí*, Ph.D. thesis, MFF UK, 2006.

[8] T. Hrenar, H. J. Werner, and G. Rauhut, *Accurate calculation of anharmonic vibrational frequencies of medium sized molecules using local coupled cluster methods*, J. Chem. Phys. **126** (2007), 134108–1–134108–9.

[9] P. Pulay and W. Meyer, *Comparison of the ab initio force constants of ethane, ethylene and acetylene*, Mol. Phys. **27** (1974), 473–490.

[10] C. E. Blom and C. Altona, *Scale factor method for the calculation of vibrational frequencies from ab initio force constants*, Mol. Phys. **31** (1976), 1377–1391.

[11] J. Haesler, I. Schindelholz, E. Riguet, C. G. Bochet, and W Hug, *Absolute configuration of chirally deuterated neopentane*, Nature **446** (2007), 526–529.

[12] J. O. Jung and R. B. Gerber, *SCF for $(H_2O)_n$ wave functions*, J. Chem. Phys. **105** (1996), 10332–10348.

[13] A. E. Roitberg and R. B. Gerber, *A vibrational eigenfunction of BPTI*, J. Phys. Chem. B **101** (1997), 1700–1706.

[14] G. Rauhut, *Efficient calculation of potential energy surfaces for the generation of vibrational wave functions*, J. Chem. Phys. **121** (2004), 9313–9322.

[15] S. Carter, J. M. Bowman, and L. B. Harding, *Ab initio calculations of force fields for H_2CN and ClHCN and vibrational energies of H_2CN*, Spec. Chim. Acta A **53** (1997), 1179–1188.

[16] S. Carter, S. J. Culik, and J. M. Bowman, *Vibrational self-consistent field method for many-mode systems*, J. Chem. Phys. **107** (1997), 10458–10469.

[17] W. Schneider and W. Thiel, *Anharmonic force fields from analytic second derivatives: Method and application to methyl bromide*, Chem. Phys. Lett. **157** (1989), 367–373.

[18] J. M. Bowman, *Self-consistent field energies nad wavefunctions for coupled oscillators*, J. Chem. Phys. **68** (1978), 608–610.

[19] J. M. Bowman, K. Christoffel, and F. Tobid, *Application of SCF-SI theory to vibrational motion in polyatomic molecules*, J. Phys. Chem. **83** (1979), 905–912.

[20] P. Bouř and L. Bednárová, *Anharmonic force field of formamide. a computational study.*, J. Phys. Chem. **99** (1995), 5961–5966.

[21] V. Barone, *Anharmonic vibrational properties by a fully automated second-order perturbative approach*, J. Chem. Phys. **122** (2005), 014108.

[22] L. S. Norris, M. A. Ratner, A. E. Roitberg, and R. B. Gerber, *Møller Plesset perturbation theory applied to vibrational problems*, J. Chem. Phys. **105** (1996), 11261–11267.

[23] O. Christiansen, *Vibrational coupled cluster theory*, J. Chem. Phys. **120** (2004), 2149–2159.

[24] S. Miertus, E. Scrocco, and J. Tomasi, *Electrostatic interaction of a solute with a continuum*, Chem. Phys. **55** (1981), 117–129.

[25] V. Barone and M. Cossi, *Quantum calculation of molecular energies and energy gradients in solution by a conductor solvent model*, J. Phys. Chem. A **102** (1998), 1995–2001.

[26] P. Daněček and P. Bouř, *Comparison of the numerical stability of methods for anharmonic calculations of vibrational molecular energies*, J. Comp. Chem. **28** (2007), 1617–1624.

[27] D. L. Strout and G. E. Scuseria, *A quantitative study of the scaling properties of the Hartree-Fock method*, J. Chem. Phys. **102** (1995), 8448–8452.

[28] J. Čížek, *On the correlation problem in atomic and molecular systems*, J. Chem. Phys. **45** (1966), 4256–4266.

[29] G. D. Purvis and R. J. Bartlett, *Coupled-clusters singles and doubles model*, J. Chem. Phys. **76** (1982), 1910–1918.

[30] C. Møller and M. S. Plesset, *Note on an approximation treatment for many-electron systems*, Phys. Rev. **46** (1934), 618–622.

[31] P. Hohenberg and W. Kohn, *Inhomogeneous electron gas*, Phys. Rev. **136** (1964), B864–B871.

[32] M. Levy, *Universal variational functionals of electron densities, first-order density matrices, and natural spin-orbitals and solution of the v-representability problem*, Proc. Natl. Acad. Sci. **76** (1979), 6062–6065.

[33] W. Kohn and L. J. Sham, *Self-consistent equations including exchange and correlation effects*, Phys. Rev. **140** (1965), A1133–A1138.

[34] A. D. Becke, *Density-functional exchange-energy approximation with correct asymptotic behavior*, Phys. Rev. A **38** (1988), 3098–3100.

[35] J. P. Perdew, in *Electronic structure of solids '91*, P. Ziesche and H. Eschrig (eds.), p. 11, Akademie Verlag, Berlin, 1991.

[36] A. D. Becke, *Density-functional thermochemistry. The role of exact exchange*, J. Chem. Phys. **98** (1993), 5648–5652.

[37] C. Lee, W. Yang, and R. G. Parr, *Development of the Colle-Salvetti correlation-energy formula into a functional of the electron density*, Phys. Rev. B **37** (1988), 785–789.

[38] W. J. Hehre, R. Ditchfield, and J. A. Pople, *Further extensions of gaussian-type basis sets for use in molecular orbital studies of organic molecules*, J. Chem. Phys. **56** (1971), 2257–2261.

[39] R. Krishnan, J. S. Binkley, R. Seeger, and J. A. Pople, *A basis set for correlated wave functions*, J. Chem. Phys. **72** (1980), 650–654.

[40] T. H. Dunning, Jr., *Gaussian basis sets for use in correlated molecular calculations*, J. Chem. Phys. **90** (1989), 1007–1023.

[41] E. B. Wilson and J. B. Howard, *The vibration-rotation energy levels of polyatomic molecules*, J. Chem. Phys. **4** (1936), 260–268.

[42] D. Papoušek and M. R. Aliev, *Molecular vibrational-rotational spectra*, Elsevier, 1982.

[43] K. G. Watson, *Simplification of the molecular vibration-rotation hamiltonian*, Mol. Phys. **15** (1968), 479–490.

[44] J. Antony, G. von Helden, G. Meijer, and B. Schmidt, *Anharmonic midinfrared vibrational spectra of benzoic acid monomer and dimer*, J. Chem. Phys. **123** (2005), 014305–1–014305–11.

[45] G. M. Chaban, J. O. Jung, and R. B. Gerber, *Ab initio calculation of anharmonic vibrational states of polyatomic systems: Electronic structure combined with vibrational self-consistent field*, J. Chem. Phys. **111** (1999), 1823–1829.

[46] K. M. Christoffel and J. M. Bowman, *Investigations of self-consistent field, SCF CI and virtual state configuration interaction vibrational energies for a model three-mode system*, Chem. Phys. Lett. **85** (1982), 220–224.

[47] J. Franck, *Elementary processes of photochemical reactions*, Trans. Faraday Society **21** (1926), 536–542.

[48] E. Condon, *A theory of intensity distribution in band systems*, Phys. Rev. **28** (1926), 1182–1201.

[49] G. Placzek, in *Handbuch der radiologie*, E. Marx (ed.), Academische Verlagsgesellschaft, Leipzig, 1934.

[50] I. M. Degtyarenko, K. J. Jalkanen, A. A. Gurtovenko, and R. M. Nieminen, *L-alanine in a droplet of water: A density-functional molecular dynamics study*, J. Phys. Chem. B **111** (2007), 4227–4234.

[51] A. Klamt and G. Schürmann, *COSMO: A new approach to dielectric screening in solvents with explicit expressions for the screening energy and its gradient*, J. Chem. Soc. Perkin Trans. **2** (1993), 799–805.

[52] P. Daněček, *Gvib: A package for vibrational analysis*, http://gvib.sf.net.

[53] M. Diem, *Introduction to modern vibrational spectroscopy*, John Wiley & Sons, 1993.

[54] M. M. Wohar and P. W. Jagodzinski, *Infrared spectra of H_2CO, $H_2{}^{13}CO$, D_2CO, and $D_2{}^{13}CO$ and anomalous values in vibrational force fields*, J. Mol. Spectrosc. **148** (1991), 13–19.

[55] S. Ataka, H. Takeuchi, and M. Tasuni, *Infrared studies of N-methylformamide and N-methylacetamide in low-temperature nitrogen matrices*, J. Mol. Struct. **113** (1984), 147–160.

[56] L. C. Mayne and B. Hudson, *Resonance Raman spectroscopy of N-Methylacetamide*, J. Phys. Chem. **95** (1991), 2962–2961.

[57] A. Mellouki, J. Liévin, and M. Herman, *The vibrational spectrum of pyrrole and furan in the gas phase*, Chem. Phys. **271** (2001), 239–266.

[58] P. Daněček, J. Kapitán, V. Baumruk, L. Bednárová, V. Kopecký, Jr., and P. Bouř, *Anharmonic effects in IR, Raman, and Raman optical activity spectra of alanine and proline zwitterions*, J. Chem. Phys. **126** (2007), 224513.

[59] J. Kapitán, V. Baumruk, V. Kopecký, Jr., and P. Bouř, *Conformational flexibility of L-alanine zwitterion determines shapes of Raman and ROA spectral bands*, J. Chem. Phys. A **110** (2006), 4689–4696.

[60] J. Kapitán, V. Baumruk, V. Kopecký, Jr., R. Pohl, and P. Bouř, *Proline zwitterion dynamics in solution, glass, and crystalline state*, J. Am. Chem. Soc. **128** (2006), 13451–13462.

[61] C. Altona and M. Sundaralingam, *Conformational analysis of the sugar ring in nucleosides and nucleotides. A new description using the concept of pseudorotation*, J. Am. Chem. Soc. **94** (1972), 8205–8212.

[62] P. Bouř, J. Sopková, L. Bednárová, P. Maloň, and T. A. Keiderling, *Transfer of molecular property tensors in cartesian coordinates: A new algorithm for simulation of vibrational spectra*, J. Comp. Chem. **18** (1997), 646–659.

[63] M. J. Frisch, G. W. Trucks, H. B. Schlegel, et al., *Gaussian 03, Revision C.02*, Gaussian, Inc., Wallingford, CT, 2004.

[64] E. Charney, *The molecular basis of optical activity*, John Wiley & Sons, 1979.

[65] V. Barone, *Vibrational spectra of large molecules by density functional computations beyond the harmonic approximation: the case of pyrrole and furan*, Chem. Phys. Lett. **383** (2004), 528–532.

[66] A. Szabo and N. S. Ostlund, *Modern quantum chemistry*, MacGraw-Hill, Inc., 1989.

[67] L. D. Barron, *Molecular light scattering and optical activity*, Cambridge University Press, 1982.

[68] D. A. Long, *The Raman effect*, John Wiley & Sons, 2002.

List of Figures

2.1 Comparison of Slater and contracted Gaussian functions 27
2.2 Linear harmonic oscillator 32
2.3 Comparison of exact and harmonic potential 33
2.4 The symmetric stretching vibration in formaldehyde 34
2.5 Semidiagonal quartic and harmonic potential 34
2.6 Comparison of real, VSCF and harmonic potential 36
2.7 Probability amplitude of absorption as a function of frequency 40
2.8 Raman diagram 43
2.9 VCD diagram 46
2.10 Magnetic dipole moment of enantiomers 47
2.11 ROA diagram 48

3.1 Water, formaldehyde and furan – average harmonic and PT2/Harm error 55
3.2 (+)-α-Pinene 61
3.3 Raman spectra of α-Pinene 62
3.4 ROA spectra of (-)-α-Pinene 63
3.5 Alanine and proline 65
3.6 Gly-Pro, Pro-Gly, Ala-Pro and Pro-Ala 66
3.7 Calculated and experimental Raman spectra of Gly-Pro. 67
3.8 Calculated and experimental Raman spectra of Pro-Gly. 67
3.9 Poly-proline II. 68

4.1 Numerical differentiation and CPCM 75

List of Tables

3.1 Henon-Heiles potential 53
3.2 Christoffel potential 53
3.3 Calculated and experimental frequencies of water I 54
3.4 Calculated and experimental frequencies of water II 56
3.5 Calculated and experimental frequencies of formaldehyde I 57
3.6 Calculated and measured frequencies of formaldehyde II 58
3.7 Calculated and experimental frequencies of NMA 59
3.8 Calculated and measured frequencies of furan 60
3.9 Energies of Gly-Pro and Ala-Pro conformers. 66

Acronyms

AAT	Atomic axial tensor	46
APT	Atomic polar tensor	43
BOA	Born-Oppenheimer approximation	12
CC	Coupled cluster	22
CI	Configuration interaction	21
CIS	Singly excited CI	22
CISD	Singly and doubly excited CI	22
CPCM	Conductor-like PCM	50
COSMO	Conductor-like screening model	??
DFT	Density functional theory	23
eVSCF	Excited-state VSCF with self-consistent excited states	36
FWHM	Full width at half maximum	50
GGA	Generalized gradient approximation	25
gVSCF	Ground-state VSCF with orthogonal excited states	36
HF	Hartree-Fock theory	19
ICP	Incident circular polarization	47
IR	Infrared absorption spectroscopy	7
LDA	Local density approximation	25
LHO	Linear harmonic oscillator	9
LSDA	Local spin density approximation	25
MP2	Møller-Plesset perturbation theory	23
PCM	Polarizable continuum model	50
PES	Potential energy surface	8
PT2/Harm	Perturbation theory applied to harmonic approximation	37
PT2/VSCF	Perturbation theory applied to VSCF	37
ROA	Raman optical activity	7
VCD	Vibrational circular dichroism	7
VCI	Vibrational configuration interactions	9
VOA	Vibrational optical activity - VCD and ROA	7
VPT	Vibrational perturbation theory	9
VSCF	Vibrational self consistent field	9

Index

anharmonic potential, 34
anti-Stokes scattering, *see* scattering
approximation
    adiabatic, 12
    Born-Oppenheimer, 12, 23
    dipole, 41
    harmonic, 30, 32, 36, 37
    local density, 25
    Placzek, 44, 48
atomic axial tensor, 46
atomic polar tensor, 43

B3LYP, 25, 53, 55, 57
back-scattering, 45, 48
Boltzmann's law, 43
BPW91, 25, 53, 55, 57

cc-pVTZ, 28, 32–34, 36, 53–56
CC-VSCF, 37
CCSD, 22, 32–34, 36, 53, 55, 56
CI, 21, 22
CIS, 22
CISD, 22
configuration interaction, 21, 37
    vibrational, *see* VCI
contracted Gaussian functions, 26
correlation energy, 21
coupled cluster, 22
CPCM, 50, 75, 76
cubic constants, 33

degenerate states, 16, 71
density functional theory, 23
DFT, 23
dipole strength, 41, 42, 46

eigenvalue problem, 14, 16, 20
electric dipole moment, 41–43, 45–47
electric quadrupole moment, 47
electromagnetic radiation, 39
electronic density, 23
energy
    exchange-correlation, 24
equation
    Schrödinger
        time-dependent, 11
equations
    Hartree-Fock, *see* HF
    Kohn-Sham, 24
equilibrium geometry, 29
eVSCF, 36

functional
    energy, 24

gVSCF, 36

Hartree-Fock equations, *see* HF
Hermite polynomials, 31
Hessian, 29
HF, 20, 25, 26, 35, 55

ICP, 47

Kohn-Sham equations, 24

Lambert-Beer law, 42
linear harmonic oscillator, 31, 37, 42, 45

magnetic dipole moment, 46, 47
matrix
    force field, 29
    Hermitian, 11
molar extinction coefficient, 42
MP2, 23, 53, 55

normal modes, 29, 35, 42, 45

operator
    Coulomb, 20
    exchange, 20
    Hamiltonian, 11
    perturbation, 15, 37
orbital
    atomic, 20
    Gaussian type, 26
    molecular, 20

PCM, 50
perturbation theory
    time-dependent, 17, 40, 44, 47
    time-independent, 15, 36
    vibrational, 36
PM3, 26, 55
polarizability, 48
    electric dipole-electric dipole, 44, 48
    electric dipole-electric quadrupole, 48
    electric dipole-magnetic dipole, 48
polarization, 39
    circular, 39, 46
    linear, 39, 47
potential energy surface, 13

quartic constants, 33

Raman scattering, *see* scattering
Rayleigh scattering, *see* scattering
ROA, 46
Roothaan equations, 20
rotational strength, 46

scalar potential, 39
scattering
    anti-Stokes, 43, 44
    Raman, 43, 44, 47
    Rayleigh, 43, 44
    Stokes, 43, 44
selection rules, 42, 45
semidiagonal quartic constants, 33
size consistent, 22
Slater determinant, 19
spin, 19
spin orbital, 19
Stokes scattering, *see* scatterings

transition dipole moment, 42

variational principle, 14, 20, 24, 35, 37
VCD, 47
VCI, 37
vector potential, 39
vibrational circular dichroism, 46
VSCF, 35–37

Watson Hamiltonian, 30
wave function, 11

zwitterion, 64

Appendix B: Publications

Comparison of the Numerical Stability of Methods for Anharmonic Calculations of Vibrational Molecular Energies

PETR DANĚČEK,[1,2] PETR BOUŘ[1]

[1]*Institute of Organic Chemistry and Biochemistry, Academy of Sciences of the Czech Republic, Flemingovo nám. 2, 16610 Prague, Czech Republic*

[2]*Institute of Physics, Charles University, Ke Karlovu 5, 12116 Prague, Czech Republic*

Received 17 March 2006; Accepted 15 May 2006
DOI 10.1002/jcc.20654
Published online 5 March 2007 in Wiley InterScience (www.interscience.wiley.com).

Abstract: On model examples, we compare the performance of the vibrational self-consistent field, variational, and four perturbational schemes used for computations of vibrational energies of semi-rigid molecules, with emphasis on the numerical stability. Although the accuracy of the energies is primarily dependent on the quality of the potential energy surface, approximate approaches to the anharmonic vibrational problem often do not converge to the same results due to the approximations involved. For furan, the sensitivity to variations of the anharmonic potential was systematically investigated by adding random noise to the cubic and quartic constants. The self-consistent field methods proved to be the most resistant to the potential variations. The second order perturbational techniques are sensitive to random degeneracies and provided the least stable results. However, their stability could be significantly improved by a simple generalization of the perturbational formula. The variational configuration interaction is practically limited by the size of the matrix that can be diagonalized for larger molecules; however, relatively fewer states need to be involved than for smaller ones, in favor of the computing.

 J Comput Chem 28: 1617–1624, 2007

Key words: anharmonic vibrational energies; vibrational self-consistent field; second-order perturbation; numerical stability; vibrational spectroscopy

Introduction

Computations of the vibrational molecular energies beyond the harmonic limit appear necessary for many important systems including biologically relevant molecules,[1,2] solute-solvent complexes,[3] and industrially important compounds.[4] Particularly, the involvement of the anharmonic part is imperative for studies of spectral temperature dependencies and molecular stability.[5] For semi-rigid molecules many methods have been developed,[6] based primarily on perturbation calculus[7–9] or vibrational self-consistent field (VSCF).[10–12] Except of small systems, nuclear potentials (potential energy surfaces) used in these computations as input parameters are known only approximately as they usually depend on the ab initio approximation of the electronic problem. The errors in the potential frequently transfer differently into the errors of the vibrational energies if also approximate vibrational schemes are used. Therefore, in this study, we try to compare various approaches and concentrate on the stability of the vibrational energies obtained by various methods. It turns out that small and big molecules behave differently. The latter are notoriously affected by the random degeneracies of the vibrational energy levels, which inhibits application of the perturbation calculus. For such cases we propose a generalization of the second-order formula as outlined below. Our implementations of the VSCF, variational (vibrational configuration interaction, VCI), and second-order perturbation (PT) methods in one program package enabled us to make a consistent comparison.

In the next section working equations for the VCI, VSCF, and PT approaches are outlined. Then their performances are tested and discussed for two and three-dimensional analytical potentials used for calibration of the anharmonic calculus previously.[12] These tests are followed by applications to real molecules, furan, formaldehyde, and α-pinene. For furan, systematic noise was added in various ways to the ab initio potential so that the numerical stability of the vibrational algorithms could be analyzed. Finally, dependence of VCI energies on the basis set size is analyzed.

Correspondence to: P. Bouř; e-mail: bour@uochb.cas.cz

Contract/grant sponsor: Agency of the Czech Republic; contract/grant number: 203/06/0420

Methods

For semi-rigid molecules the nuclear potential V can be expanded in a Taylor series around the equilibrium geometry. For example, in the vibrational normal-mode coordinates (Q_i) and the atomic units,

$$V(Q_1,\ldots,Q_M) = \sum_{i=1}^{M}\frac{\omega_i^2}{2}Q_i^2 + \frac{1}{6}\sum_{i=1}^{M}\sum_{j=1}^{M}\sum_{k=1}^{M}c_{ijk}Q_iQ_jQ_k + \frac{1}{24}\sum_{i=1}^{M}\sum_{j=1}^{M}\sum_{k=1}^{M}\sum_{l=1}^{M}d_{ijkl}Q_iQ_jQ_kQ_l + \cdots, \quad (1)$$

where M is the number of the modes.[13] For simplicity we neglect other anharmonic and rotation-vibration interaction terms stemming from the kinetic energy operator. To approach the solution of the Schrödinger equation,

$$\left(-\tfrac{1}{2}\sum_{i=1\ldots M}\frac{\partial^2}{\partial Q_i^2} + V\right)\Psi = E\Psi,$$

we implemented the VSCF, PT, and VCI approximations as follows.

Vibrational Self-Consistent Field

Following the usual procedure[1,10] the wavefunction was expressed as a product of one-dimensional parts,

$$\Psi(Q_1,\ldots,Q_M) \approx \prod_{i=1}^{M}\psi_i(Q_i), \quad (2)$$

and the potential as a sum of effective potentials,

$$V(Q_1,\ldots,Q_M) \to \sum_{i=1}^{M}v_i(Q_i), \quad (3)$$

with

$$v_i(Q_i) = \left\langle \prod_{j=1,j\neq 1}^{M}\psi_j(Q_j)\middle| V(Q_1,\ldots,Q_M)\middle|\prod_{k=1,k\neq 1}^{M}\psi_k(Q_k)\right\rangle.$$

Note, that a general VSCF approach is not dependent on the Taylor expansion (1) of the potential; the Taylor form; however, was used here for the sake of comparison with the other methods. Under the assumption of the separability the Schrödinger equation divides into a sum of effective 1D equation,

$$\left(-\frac{1}{2}\frac{\partial^2}{\partial Q_i^2} + v_i(Q_i)\right)\psi_i(Q_i) = e_i\psi_i(Q_i), \quad (4)$$

where $i = 1\cdots M$, and can be easily solved in a harmonic oscillator basis. Because of the dependence of the effective potentials on the resultant wavefunction, the solving has to be repeated "self-consistently" until the energy values (e_i) stabilize. Also, a self-interaction correction term has to be subtracted from the energy sum, in order to obtain molecular energy of a physical relevance,

$$E = \sum_{i=1\ldots M}e_i - (M-1)\langle\Psi|V|\Psi\rangle. \quad (5)$$

As the excited states can be treated only approximately within the VSCF scheme two alternate approaches were implemented. First, only the lowest-energy (ground) states (ψ_i) were used for determining the potential in eq. (3) (which is referred to as **gVSCF**), while in the second approximation ("**eVSCF**") excited states were included in the averaging. Thus, in the **gVSCF** method, resultant set of excited states is orthogonal, but not self-consistent. On the contrary, in **eVSCF** the self-consistency holds at the expense of the orthogonality. The **gVSCF** computation requires only one set of the self-consistent iterations for the ground state, while this has to be repeated for each excited state in **eVSCF**.

Second-Order Perturbation

The cubic and quartic terms in eq. (1) are often small (in terms of their influence on the energies of interest) and, with respect to the harmonic solutions, can be treated as a perturbation potential directly. Also for the VSCF wave functions, the perturbation can be defined, in analogy to the electronic MP2 theory,[14] as a difference between the exact and the VSCF potential,

$$W = V - \sum_{i=1\ldots M}v_i. \quad (6)$$

Note, that for VSCF formula 5 is correct to the first order. A second-order correction can be obtained from a standard perturbation calculus as

$$E_n^{(2)} = \sum_{m\neq n}\frac{|W_{nm}|^2}{E_n - E_m}, \quad (7a)$$

with $W_{nm} = \langle n|W|m\rangle$. The division by the energy difference in eq. (7a) makes the second-order perturbation (**PT2**) numerically unstable because of random degeneracies. Simple treatment based on separation of the degenerate and non-degenerate states was proposed previously.[15] Here we explore a differently modified algorithm, replacing the **PT2** formula 7a for all states by

$$E_n^{(2)} = \frac{1}{2}\sum_{m\neq n}\left[E_m - E_n + W_{mm} - W_{nn} \pm \sqrt{(E_m - E_n + W_{mm} - W_{nn})^2 + 4|W_{nm}|^2}\right] \quad (7b)$$

where the + sign holds for $E_n > E_m$ and −sign for $E_n < E_m$. It can be easily verified that the formula 7b provides exact solu-

tions for two-state (n,m) system including the degenerate case, while for small perturbations ($W \rightarrow 0$) its polynomial expansion is equal to 7a up to the second powers of W.

Vibrational Configuration Interaction

If the wavefunction is expressed as a sum of harmonic oscillator functions, we obtain a solution of the Schrödinger equation directly by the Hamiltonian diagonalization. As this method is limited by the size of the matrix that must be diagonalized, number of the harmonic states (j) must be restricted. They can be selected, for example, based on of the ratio $\eta = |W_{fj}/E_f - E_j|$, bigger than given limit for at least some ground or fundamental state f. Although indirect iterative diagonalization methods[16] (not used in the present study) enable to increase the number of the states significantly, for larger molecules some selection is always necessary. In addition, the speed of the diagonalization, mostly scaled as M^3, becomes the limiting factor for such cases. For our tests we systematically increased the number the states varying the perturbation parameter η. Because the force field (1) was expanded up to the quartic terms, states with a maximum of five excitations were considered in VCI, similarly as for the methods described above. For example, a non-zero force constant d_{123} in a three mode system can make the matrix element $\langle 001|V|212\rangle$ non-zero, mediating thus an interaction of $1\times$ excited normal mode number 3 ($|001\rangle$) and the state with 2, 1, and 2 excitations on modes 1, 2, and 3 ($|212\rangle$). By similar arguments we could deduce that a six-time excited state (e.g. $|213\rangle$) would have probably a negligible effect on the $|000\rangle \rightarrow |001\rangle$ fundamental transition, etc.

Computations

For equilibrium geometries of the model molecules analytical second derivatives were calculated by the Gaussian program,[17] while the third and fourth derivatives were obtained by a numerical differentiation, using a step of 0.025 Å (0.07 Å for α-pinene). The normal mode derivatives were calculated from the Cartesian constants. The geometries were obtained as local energy minima for each approximation used, that is for the Becke3LYP(B3L)[18,19]/6-311++G**, B3L/6-31G*, and MP2/6-311++G* methods. Only semi-diagonal quartic constants with two and more identical indices (e.g. d_{ijkk}) were considered. Anharmonic interactions of some lowest strongly anharmonic modes were neglected in the computations (one for furan, ring torsion calculated at 610 cm^{-1}, five for α-pinene, CH_3 rotation, and wagging modes[20] within 0–229 cm^{-1}).

Results and Discussion

Model Potentials

To test our programs as well as to investigate the behavior of the different anharmonic approaches for small systems, we selected model two- and three-dimensional potentials introduced previously.[10–12] In Table1, state energies computed using the harmonic, gVSCF, eVSCF, and perturbational [eq. (7a)] methods are compared with (exact) VCI results. We see that any method involving the anharmonic part of the potential reduces the error. The VSCF methods are slightly inferior to the simple (harmonic) perturbation theory. However, as found also in previous studies,[12] application of the PT2 theory within the VSCF reduces the overall error significantly. For the ground states (|00>, |000>) the gVSCF and eVSCF approaches obviously provide the same numbers. For the excited states the plain eVSCF approach gives consistently smaller errors by ~3–50% than gVSCF. The difference is even emphasized when the self-consistent methods are coupled with the perturbational approach, as the eVSCF/PT2 errors of excited energies are several times smaller than for gVSCF/PT2. This may reflect the fact that the gVSCF/PT2 approach bases the perturbation expansion on unperturbed ground state wave functions, not variationally optimal for the excited states. However, even the gVSCF/PT2 calculus seems to be significantly better than the direct application of the perturbation theory to harmonic solutions.

Table 1. State Energies Obtained for Two Model Potentials by Various Methods.

	State[a]				
Method	$\|00\rangle$	$\|20\rangle$	$\|000\rangle$	$\|010\rangle$	$\|101\rangle$
E-E(VCI)					
Harmonic part	0.00837	0.05313	0.00625	0.02814	0.02328
gVSCF	0.00084	0.00564	0.00128	0.01259	0.00793
eVSCF	0.00084	0.00546	0.00128	0.00618	0.00478
Harmonic/PT2[b]	0.00031	0.00469	0.00013	0.00103	0.00116
gVSCF/PT2[b]	0.00001	0.00045	0.00002	0.00036	0.00053
eVSCF/PT2[b]	0.00001	0.00008	0.00002	0.00012	0.00009
E(VCI)					
VCI	0.99163	2.03085	1.49375	2.77186	3.17672

[a]Quantum numbers are specified for the Henon–Heiles two- and Christoffel three-dimensional dimensionless potentials, as implemented in Refs. 11 and 12 (there is a misprint in the definition of the 3D potential in the latter reference, for this case the original work[11] was followed).
[b]Formula 7a.

Ab Initio Potential Variation

To investigate possible effects of usual ab initio potential variations on the vibrational energies, we calculated three different vibrational potentials of furan: in vacuum and with the COSMO[21,22] solvent models, using the B3L approximation, and in vacuum at the MP2 level, all with the 6-311++G** basis. No significant differences in the equilibrium geometries were observed, bond lengths varied less than by 0.01 Å, which contrasts with the force field changes. An inspection of the cubic and quartic field, for example, revealed that for larger constants the variations caused by the solvent inclusion are typically smaller than about 5%. For small constants (smaller than about 10% of the maximal cubic or quartic term), however, no correlation between the vacuum and COSMO values was observed. Supposedly these differences are largely numerical artifacts of the calculation and do not reflect physical changes that occur in the potential when the molecule is submerged into water. In any case, for computation of the vibrational energies beyond the har-

Table 2. Average Differences of Vibrational Energies of the Fundamental Transitions in Furan Obtained with the B3L, MP2, and B3L/COSMO (H_2O) Force Fields, as Calculated by Various Vibrational Methods.

	E(B3L/COSMO)-E(B3L)			E(B3L)-E(MP2)		
Method	δ_{AVE}	$\lvert\delta\rvert_{AVE}$	$\lvert\delta\rvert_{MAX}$	δ_{AVE}	$\lvert\delta\rvert_{AVE}$	$\lvert\delta\rvert_{MAX}$
Harmonic	−3	12	25	3	31	127
gVSCF	−6	15	29	−18	23	59
eVSCF	−6	15	29	−18	22	57
Harmonic/PT2[a]	−5 (−7)	25 (15)	101 (27)	4 (−13)	46 (31)	179 (76)
gVSCF/PT2[a]	−8 (−7)	14 (15)	26 (26)	−14 (−16)	20 (22)	61 (61)
eVSCF/PT2[a]	−14 (−2)	21 (20)	105 (79)	−11 (−21)	25 (26)	94 (88)
VCI[b]	−9	14	30	−25	32	115

δ_{AVE}, $\lvert\delta\rvert_{AVE}$, and $\lvert\delta\rvert_{MAX}$: average plain, absolute, and maximal deviations in cm^{-1}.
[a]Formula 7b was used for the values in parentheses.
[b]1000 states ($\eta > \sim 0.001$).

monic limit we obviously desire a method that does not unrealistically magnify such a noise. The calculated average frequency differences are summarized in Table 2. Apparently, both the **gVSCF** and **eVSCF** methods provide rather conservative estimates of energy changes under the force field variations (B3L → B3L/COSMO or B3L → MP2). The changes are close to those obtained by the VCI method, in terms of systematic and absolute deviations. Interestingly, while the VCI maximal deviation (30 cm^{-1}) is comparable with that obtained by VSCF (29 cm^{-1}) for the B3L → B3L/COSMO force field change, the VCI method leads to a notably larger maximal deviation of 115 cm^{-1} for the B3L → MP2 variations. Further increase of the number of the states involved in VCI (from 1000 to 4000) brought only minor energy changes of the order of 1 cm^{-1}.

More importantly, direct application of the perturbation formula 7a leads to rather unrealistic variations of the energies; this is apparent namely from the values of the absolute and maximal deviations (up to 179 cm^{-1} for harmonic/PT2). The gVSCF/PT2 combination seems to provide somewhat more stable results than harmonic/PT2. Because the average deviations remain reasonable we can conclude that the PT2 method even for such a simple molecule effectively generates random errors in calculated energies due to near degeneracies. The erratic behavior of the PT2 method; however, can be eliminated by using the generalized formula 7b. Indeed, in this case, the frequency changes given in parentheses in Table 2 are more realistic and also consistent with the VSCF and VCI values.

An example of the effect of the ab initio potential variation on the furan modes 2–7 is depicted in Figure 1. The B3L and MP2 vacuum force fields are compared. For modes 2 and 7, out and in plane deformations of the carbonyl five-member ring respectively, the two ab initio methods provide similar force fields. However, the harmonic approximation and the DFT (B3L) method are known to be inadequate for an exact description of the C—H out of plane bending in the neighborhood of a conjugated electronic π-system. For modes 3–6 involving this motion, similarly as for the N—H bending in the amide group,[23] rather complicated mixing of the σ and π electrons takes place and the MP2 computation may be more appropriate. Already the harmonic DFT and MP2 frequencies for the four bending modes differ significantly, up to 130 cm^{-1} for the mode number 6. This nature of the vibrations clearly transmits differently to the other vibrational differences given in Figure 1. The nearly harmonic modes 2 and 7, where additionally the DFT and MP2

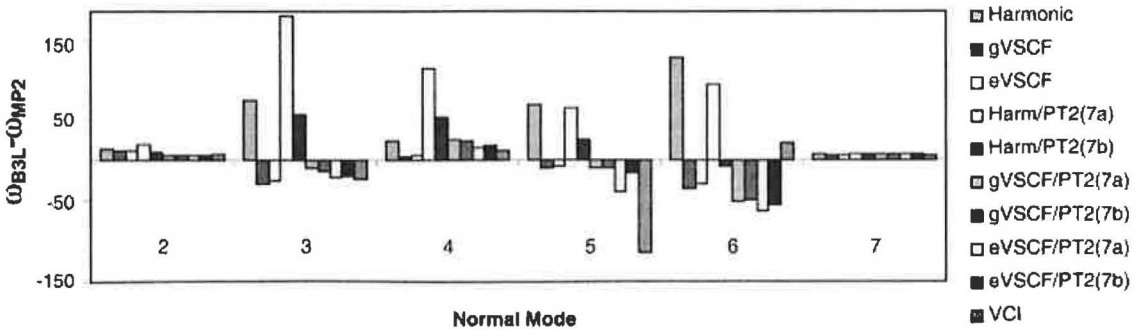

Figure 1. Differences between furan vibrational energies calculated with the B3L and MP2 force fields, for fundamental transitions 2–7, as obtained by the 10 various approaches to the vibrational problem indicated at the right hand side. [Color figure can be viewed in the online issue, which is available at www.interscience.wiley.com.]

Table 3. Frequency Differences (cm^{-1}) Caused by Random Noise in the Anharmonic Potential (B3L/6-311++G**) of Furan.

	Absolute noise "$c \pm \Delta$"		Relative noise "$c \times (1 \pm \Delta)$"	
Method	$\|\delta\|_{AVE}$	$\|\delta\|_{MAX}$	$\|\delta\|_{AVE}$	$\|\delta\|_{MAX}$
gVSCF	20	84	11	123
eVSCF	22	96	12	180
Harmonic/PT2[a]	136 (81)	1538 (185)	12 (12)	141 (125)
gVSCF/PT2[a]	295 (83)	16245 (235)	16 (13)	501 (208)
eVSCF/PT2[a]	273 (94)	42285 (310)	23 (15)	567 (199)
VCI[b]	38	187	14	200

Averages for sets of 20 computations.
[a]Formula 7b was used for the values in parentheses.

force fields are similar, are not affected by the treatment of the anharmonic problem, while the modes 3–6 are more sensitive. As an extreme case, the B3L frequency of mode number 3 is bigger by 180 cm^{-1} than the MP2 value if calculated with the harmonic/PT2 method (formula 7a). This is partially an artifact of the perturbational calculus, but can be improved by the simplified degeneracy treatment (formula 7b) only incompletely. A similar situation occurs for the mode number 6. From the point of the computational efficiency and reliability, it seems reasonable to prefer the VSCF methods over the plain PT2, as the former quickly provides energy corrections mostly consistent with the VCI results.

Random Potential Changes

To investigate the influence of the potential variations on vibrational energies more systematically, the B3L/6-311++G** furan force field was arbitrarily modified. Firstly, random increments were added to all anharmonic normal mode constants pertaining to the dimensionless normal-mode coordinates q_i, $q_i = \sqrt{\omega_i} Q_i$.[13] Increments within (−0.00031, 0.00031) hartree were used for both cubics and quartics. As an alternate option, relative sizes of the constants were modified up to 30% of their ab initio values. Supposedly, both modifications are relevant, because smaller anharmonic constants are usually produced with significantly larger relative errors than the bigger ones. For each modification type a series of 20 computations was performed, and the vibrational energies obtained by various anharmonic methods were compared with the unperturbed values.

The frequency changes caused by the two types of random perturbations are summarized in Table 3. Similarly as for the force field differences investigated in Table 2, the VSCF methods are least sensitive to the noise and tend to smooth the potential variations. Interestingly however, as can be seen in Table 3, the behavior of the absolute and relative noise perturbations differ. For the former, the simple perturbation formula (7a) produces clearly worst artifacts, which can be removed by the

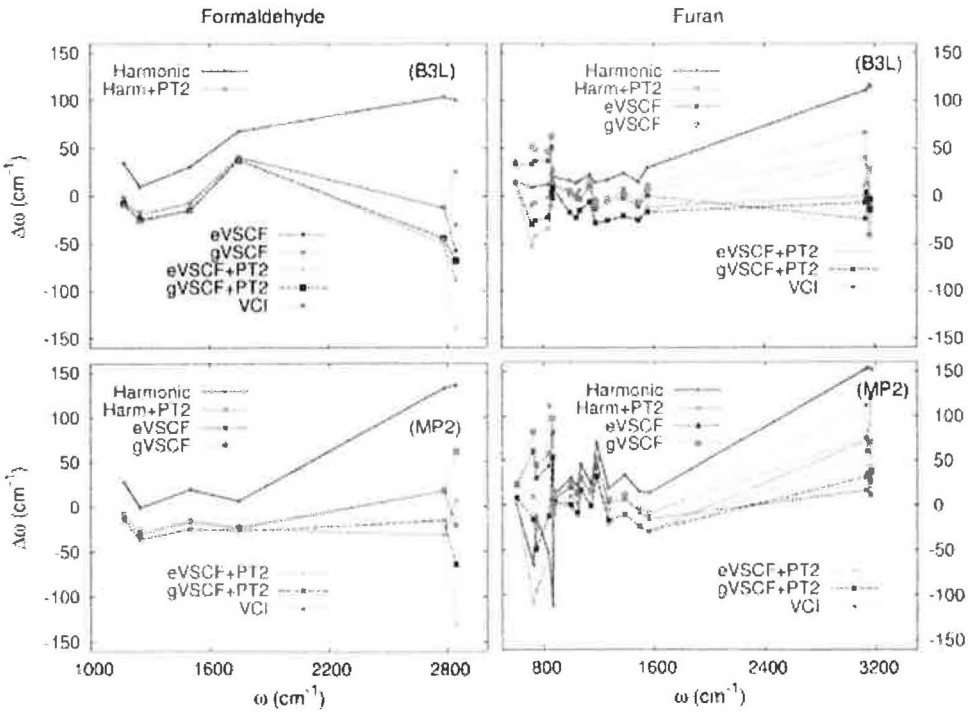

Figure 2. Comparison of the errors of vibrational frequencies computed by different methods for B3L (top) and MP2 (bottom) force field of formaldehyde (on the left) and furan (right hand side). Experimental formaldehyde[26] and furan[27] frequencies were used as a reference, the 6-311++G** basis used in the force field computations. [Color figure can be viewed in the online issue, which is available at www.interscience.wiley.com.]

degeneracy correction (7b); the pure VSCF and VCI methods remain the most stable. For the relative noise, the corrected perturbational calculus provides energy changes more in line with the (supposedly correct) VCI values. The advantage of the combined VSCF/PT2 over uncorrected harmonic/PT2 method observed for the various ab initio force fields in Table 2 does not seem to be conserved for the random noise perturbations where the harmonic/PT2 approach appears slightly but consistently more stable. The eVSCF/PT2 method is somewhat more prone to the random noise than gVSCF/PT2, probably because of bigger volatility of the excited states to the potential changes. A problematic convergence behavior of the perturbation methods with the VSCF was also observed previously;[24,25] however, the harmonic/PT2 computations may presumably exhibit similar difficulties as the degeneracies occur randomly.

Molecular Size

The numerical stability of the vibrational computations becomes crucial for larger molecules. This can be seen in Figure 2 where deviations of calculated (B3L/6-311++G**) frequencies from the experimental values[26,27] of formaldehyde and furan are plotted for individual fundamental transitions. The DFT (B3L) computations presented at the upper part of the figure were repeated with the MP2 force field and are plotted at the bottom. For formaldehyde, similarly as for the model potentials mentioned above, the anharmonic methods converge to common values, mostly better than those obtained by the harmonic approximation. An exception is the highest-frequency mode where the eVSCF method provides a frequency very close to the experiment and the PT2 correction (7b) destroys this agreement. For furan; however, various anharmonic methods provide very different results and often do not correct the harmonic values at all. Especially for the lowest-frequency modes the perturbational, but also pure VSCF methods, cause unrealistic frequency deviations and thus the benefit of correcting the anharmonicity is overshadowed by numerical artifacts. Obviously, the quality of the computed frequencies is also dependent on the quality of the ab initio force field, detailed analysis of which goes beyond the scope of this work. Nevertheless, it should be noted that the DFT methods are generally believed to be less sensitive to potential variations, providing reasonable harmonic frequencies, but are not able to capture the anharmonic effects to the same accuracy as the accurate wavefunction methods (MP2, CCSD(T)).[28] Because of the great many of available DFT functionals; however, it is difficult to generalize particular cases; for example, a very good performance of the DFT for the anharmonic force fields was observed for azabenzenes recently.[29] For the formaldehyde presented in Figure 2 the MP2 computations seems to be more appropriate, while for furan the B3L results are closer to experiment.

Unlike for the perturbational and VSCF methods, accuracy of the VCI energies can be systematically improved up to the Schrödinger limit by increasing the vibrational basis set size.

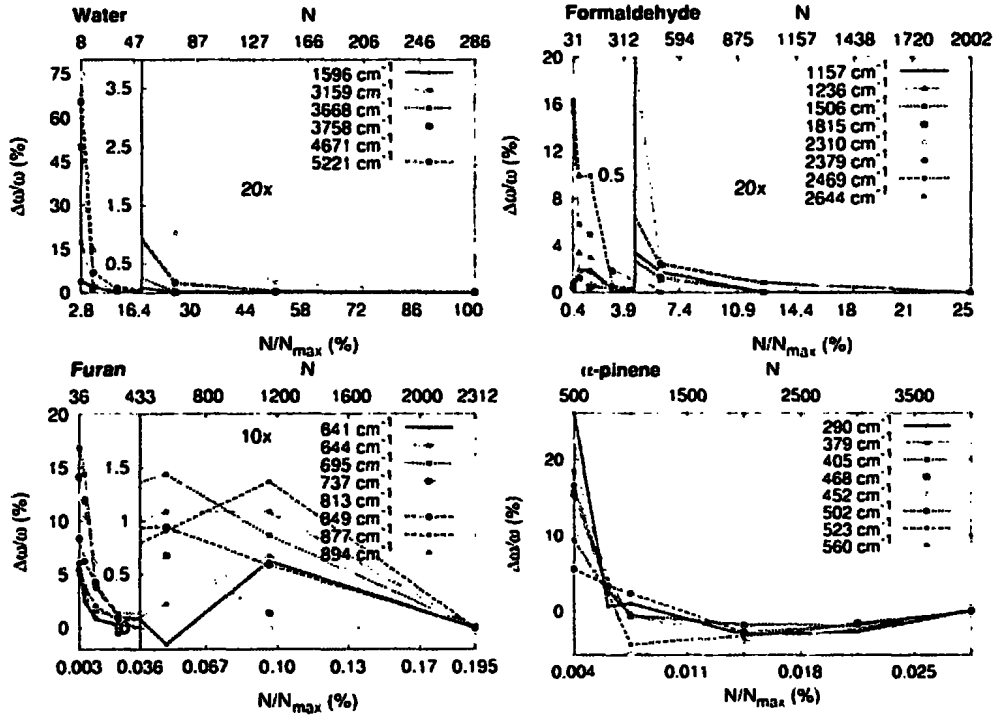

Figure 3. Convergence of the VCI energies. For selected vibrational levels in water, formaldehyde, furan and α-pinene the dependencies of the energy differences (cm^{-1}) from the best calculation on the number of the states involved are plotted. The B3L/6-31G** force fields and the maximum of 286, 2002, 2312, and 4000 vibrational functions (for H_2O, H_2CO, furan and α-pinene, respectively) were used. [Color figure can be viewed in the online issue, which is available at www.interscience.wiley.com.]

Table 4. Errors of Fundamental Frequencies (cm^{-1}) of α-pinene Obtained with the Becke3LYP/6-31G** Force Field.

	C—H stretching			Mid ir			Entire region		
Method	δ_{AVE}	$\lvert\delta\rvert_{AVE}$	$\lvert\delta\rvert_{MAX}$	δ_{AVE}	$\lvert\delta\rvert_{AVE}$	$\lvert\delta\rvert_{MAX}$	δ_{AVE}	$\lvert\delta\rvert_{AVE}$	$\lvert\delta\rvert_{MAX}$
Harmonic	153	153	174	29	30	76	55	55	174
gVSCF	15	98	89	23	21	60	21	27	89
eVSCF	−12	33	81	21	21	49	14	23	81
Harmonic/PT2[a]	10 (3)	34 (17)	116 (40)	−9 (−4)	16 (10)	220 (46)	−2 (−4)	37 (11)	605 (47)
gVSCF/PT2[a]	16 (−4)	37 (15)	140 (37)	−2 (−3)	11 (9)	47 (45)	2 (−3)	17 (10)	140 (45)
eVSCF/PT2[a]	43 (−8)	98 (18)	605 (47)	−14 (−3)	21 (9)	423 (44)	−5 (−2)	19 (12)	220 (46)
VCI[b]	127	128	213	83	83	113	92	92	213

Frequencies were compared to experiment in Refs. 30 (mid ir region) and 31 (matrix experiment, C—H stretching region).
[a]In parentheses, values obtained with the generalized formula 7b are given.
[b]4000 states included, with $\eta < 0.02$.

Additionally, VCI fundamental and combination states can be easily obtained at once. As aforementioned, however, only a small fraction of the states formally interacting with the fundamental transitions of interest can be included for big molecules. Therefore, in Figure 3, we look at the convergence of the VCI energies with respect to the fraction of the 5-times excited vibrational states needed for a balanced second-order correction to the fundamental transitions in water, formaldehyde, furan, and α-pinene. The energy differences (in %) are related to those obtained with the biggest vibrational basis used. Clearly, if a small fraction of the states is included, larger frequency deviations occur. Combination transitions also included in the graphs behave similarly as the fundamentals. Nevertheless the relative number of the states needed for reasonably precise results is smaller for larger molecules. For example, for water 16% of the states need to be included to achieve errors smaller than 2%, while for formaldehyde and furan it is about 7 and 4% of all states, respectively. It is obviously dangerous to approximate the dependence for α-pinene in Figure 3, when only such a tiny fraction of the states is considered. Nevertheless, relative frequency changes for strongly anharmonic modes (not included) are even smaller, and certainly the fraction of the states that must be considered in order to produce comparable effect is again much smaller than for the previous systems. Thus, from the point of practical computations, application of VCI with reasonably-chosen basis set may be meaningful even for larger molecules.

For α-pinene, as an example of a bigger molecule, we also compare the performance of the vibrational methods in Table 4, in terms of average deviations of calculated frequencies from the experiment.[30,31] The experimental values are preferred as a fully converged VCI computation appears unrealistic, even with the indirect diagonalization schemes.[16] It is important to note that $(M + 4)!/(5!(M - 1)!)$ states must be included to produce the balanced second-order correction for the fundamental transitions and the quartic potential (1), which makes the computational time of the diagonalization proportional to $\sim(M^5)^3 = M^{15}$. Thus we have to accept that the error of the VCI computation is caused by the basis set incompleteness. On the other hand, all the other schemes lead to improvement of the harmonic frequencies. Additionally, we can observe a different behavior in the high and low(mid)-frequency region; in the former even the VCI is partially beneficial. On the contrary, for the transitions in the mid ir, the convergence of the VSCF and PT2 is very convincing. The VSCF/PT2 (uncorrected) methods provide best performance and are followed by the harmonic/PT2 combination and the plain VSCF schemes. This corresponds to the behavior of the benchmark potentials in Table 1 only approximately; particularly the harmonic/PT2 method provided much bigger energy errors than the VSCF/PT2 computations for the benchmarks. For the α-pinene, the generalized PT2 formula leads to further improvement of the energies and provides virtually identical results for both harmonic and VSCF functions. For the high-frequency C-H stretching modes the behavior slightly differ as the combination of the VSCF and perturbational technologies is beneficial only with the degeneracy correction.

Conclusions

We have implemented and extended some of the computational methods suitable for calculating molecular vibrational energies of semi-rigid molecules beyond the harmonic approximation. On the model examples the performance was analyzed with emphasis on the numerical stability. The results indicated that the algorithms behave differently under different circumstances and should not be applied universally. For example, the VSCF procedure was found to be the most stable with respect to the minor potential variations and also provided the anharmonic part of the vibrational energies only with a relatively minor computational effort. However, the combination of the VSCF with the standard perturbational calculus was found beneficial only for nearly harmonic problems, such as the benchmark potential or mid ir vibrations of α-pinene. For small systems the eVSCF variant provided somewhat better frequencies for the excited states than the gVSCF. The usual second-order perturbational formula seems to be almost unusable for everyday use due to the random degeneracies. Thus, however, could be improved significantly by the modification based on the two-state degenerate model. The conventional VCI results are often hampered by incompleteness of the basis set for bigger molecules, yet a relatively tiny frac-

tion of the basis states subjected to VCI may be already beneficial and improves the agreement with the experiment.

References

1. Brauer, B.; Chaban, G. M.; Gerber, R. B. Phys Chem Chem Phys 2004, 6, 2543.
2. Brauer, B.; Gerber, R. B.; Kabeláč, M.; Hobza, P.; Bakker, J. M.; Riziq, A. G. A.; deVries, M. S. J Phys Chem A 2005, 109, 6974.
3. Chaban, G. M.; Gerber, R. B. J Chem Phys 2001, 115, 1340.
4. Katzer, G.; Sax, A. F. J Phys Chem A 2002, 106, 7204.
5. McGrane, S. D.; Barber, J.; Quenneville, J. J Phys Chem A 2005, 109, 9919.
6. Clabo, D. A.; Allen, W. D.; Remington, R. B.; Yamaguchi, Y.; Schaefer, H. F., III. Chem Phys 1988, 123, 187.
7. Bouř, P.; Bednárová, L. J Phys Chem 1994, 99, 5961.
8. Barone, V. J Phys Chem A 2004, 108, 4146.
9. Barone, V. J Chem Phys 2005, 122, 014108.
10. Bowman, J. M. J Chem Phys 1978, 68, 608.
11. Christoffel, K. M.; Bowman, J. M. Chem Phys Lett 1982, 85, 220.
12. Norris, L. S.; Ratner, M. A.; Roitberg, A. E.; Gerber, R. B. J Chem Phys 1996, 105, 11261.
13. Papoušek, D.; Aliev, M. R. Molecular Vibrational/Rotational Spectra; Academia: Prague, 1982.
14. Møller, C.; Plesset, M. S. Phys Rev 1934, 46, 618.
15. Matsunaga, N.; Chaban, G. M.; Gerber, R. B. J Chem Phys 2002, 117, 3541.
16. Carter, S.; Bowman, J. M.; Handy, N. C. Theor Chem Acc 1998, 100, 191.
17. Frisch, M. J.; Trucks, G. W.; Schlegel, H. B.; Scuseria, G. E.; Robb, M. A.; Cheeseman, J. R.; Montgomery, J. A.; Vreven, J. T.; Kudin, K. N.; Burant, J. C.; Millam, J. M.; Iyengar, S. S.; Tomasi, J.; Barone, V.; Mennucci, B.; Cossi, M.; Scalmani, G.; Rega, N.; Petersson, G. A.; Nakatsuji, H.; Hada, M.; Ehara, M.; Toyota, K.; Fukuda, R.; Hasegawa, J.; Ishida, M.; Nakajima, T.; Honda, Y.; Kitao, O.; Nakai, H.; Klene, M.; Li, X.; Knox, J. E.; Hratchian, H. P.; Cross, J. B.; Adamo, C.; Jaramillo, J.; Gomperts, R.; Stratmann, R. E.; Yazyev, O.; Austin, A. J.; Cammi, R.; Pomelli, C.; Ochterski, J. W.; Ayala, P. Y.; Morokuma, K.; Voth, G. A.; Salvador, P.; Dannenberg, J. J.; Zakrzewski, V. G.; Dapprich, S.; Daniels, A. D.; Strain, M. C.; Farkas, O.; Malick, D. K.; Rabuck, A. D.; Raghavachari, K.; Foresman, J. B.; Ortiz, J. V.; Cui, Q.; Baboul, A. G.; Clifford, S.; Cioslowski, J.; Stefanov, B. B.; Liu, G.; Liashenko, A.; Piskorz, P.; Komaromi, I.; Martin, R. L.; Fox, D. J.; Keith, T.; Al-Laham, M. A.; Peng, C. Y.; Nanayakkara, A.; Challacombe, M.; Gill, P. M. W.; Johnson, B.; Chen, W.; Wong, M. W.; Gonzalez, C.; Pople, J. A.; Gaussian: Pittsburgh, PA, 2003.
18. Becke, A. Phys Rev A 1988, 38, 3098.
19. Becke, A. D. In Modern electronic structure theory; Yarkony, D. R., Ed.; World Scientific: Singapore, 1995; pp. 1022–1046.
20. Bouř, P.; Baumruk, V.; Hanzliková, J. Collect Czech Chem Commun 1997, 62, 1384.
21. Klamt, A. In The Encyclopedia of Computational Chemistry; Schleyer, P. R.; Allinger, N. L.; Clark, T.; Gasteiger, J.; Kollman, P. A.; Schaefer, H. F., III; Schreiner, P. R., Eds.; Wiley: Chichester, 1998; pp. 604–615.
22. Klamt, A.; Schuurmann, G. J Chem Soc Perkin Trans 1993, 2, 799.
23. Bouř, P.; Bednárová, L. J Phys Chem 1995, 99, 5961.
24. Christiansen, O.; Luis, J. M. Int J Quantum Chem 2005, 104, 667.
25. Christiansen, O. J Chem Phys 2004, 120, 2140.
26. Reisner, D. E.; Field, R. W.; Kinsey, J. L.; Dai, H. L. J Chem Phys 1984, 80, 5968.
27. Mellouki, A.; Lievin, J.; Herman, M. Chem Phys 2001, 271, 239.
28. Rauhut, G. J Chem Phys 2004, 121, 9313.
29. Boese, A. D.; Martin, J. M. L. J Phys Chem A 2004, 108, 3085.
30. Bouř, P.; McCann, J.; Wieser, H. J Phys Chem A 1998, 102, 102.
31. Schlosser, D. W.; Devlin, F.; Jalkanen, K. J.; Stephens, P. J. Chem Phys Lett 1982, 88, 286.

THE JOURNAL OF CHEMICAL PHYSICS **126**, 224513 (2007)

Anharmonic effects in IR, Raman, and Raman optical activity spectra of alanine and proline zwitterions

Petr Daněček
Institute of Organic Chemistry and Biochemistry, Academy of Sciences, Flemingovo náměstí 2, 16610 Prague 6, Czech Republic and Institute of Physics, Faculty of Mathematics and Physics, Charles University, Ke Karlovu 5, 12116 Prague 2, Czech Republic

Josef Kapitán
Institute of Organic Chemistry and Biochemistry, Academy of Sciences, Flemingovo náměstí 2, 16610 Prague 6, Czech Republic

Vladimír Baumruk
Institute of Physics, Faculty of Mathematics and Physics, Charles University, Ke Karlovu 5, 12116 Prague 2, Czech Republic

Lucie Bednárová
Institute of Organic Chemistry and Biochemistry, Academy of Sciences, Flemingovo náměstí 2, 16610 Prague 6, Czech Republic

Vladimír Kopecký, Jr.
Institute of Physics, Faculty of Mathematics and Physics, Charles University, Ke Karlovu 5, 12116 Prague 2, Czech Republic

Petr Bouř[a)]
Institute of Organic Chemistry and Biochemistry, Academy of Sciences, Flemingovo náměstí 2, 16610 Prague 6, Czech Republic

(Received 23 February 2007; accepted 17 April 2007; published online 13 June 2007)

The difference spectroscopy of the Raman optical activity (ROA) provides extended information about molecular structure. However, interpretation of the spectra is based on complex and often inaccurate simulations. Previously, the authors attempted to make the calculations more robust by including the solvent and exploring the role of molecular flexibility for alanine and proline zwitterions. In the current study, they analyze the IR, Raman, and ROA spectra of these molecules with the emphasis on the force field modeling. Vibrational harmonic frequencies obtained with 25 *ab initio* methods are compared to experimental band positions. The role of anharmonic terms in the potential and intensity tensors is also systematically explored using the vibrational self-consistent field, vibrational configuration interaction (VCI), and degeneracy-corrected perturbation calculations. The harmonic approach appeared satisfactory for most of the lower-wavelength (200–1800 cm^{-1}) vibrations. Modern generalized gradient approximation and hybrid density functionals, such as the common B3LYP method, provided a very good statistical agreement with the experiment. Although the inclusion of the anharmonic corrections still did not lead to complete agreement between the simulations and the experiment, occasional enhancements were achieved across the entire region of wave numbers. Not only the transitional frequencies of the C–H stretching modes were significantly improved but also Raman and ROA spectral profiles including N–H and C–H lower-frequency bending modes were more realistic after application of the VCI correction. A limited Boltzmann averaging for the lowest-frequency modes that could not be included directly in the anharmonic calculus provided a realistic inhomogeneous band broadening. The anharmonic parts of the intensity tensors (second dipole and polarizability derivatives) were found less important for the entire spectral profiles than the force field anharmonicities (third and fourth energy derivatives), except for a few weak combination bands which were dominated by the anharmonic tensor contributions. © *2007 American Institute of Physics*. [DOI: 10.1063/1.2738065]

I. INTRODUCTION

The spectroscopy of the Raman optical activity (ROA) has significantly advanced for the past decade due to improvements of the instrumentation as well as development of the simulation techniques.[1,2] The ability of chiral molecules to scatter differently left- and right-circularly polarized light was first predicted by Barron and Buckingham[3] and it was soon confirmed experimentally.[4] Since then, the potential of ROA has been widely recognized and the technique successfully applied for a large number of small chiral molecules,[5] protein and nucleic acid biopolymers, and even for viruses.[5,6] Although useful information can already be obtained on an

[a)]Electronic mail: bour@uochb.cas.cz

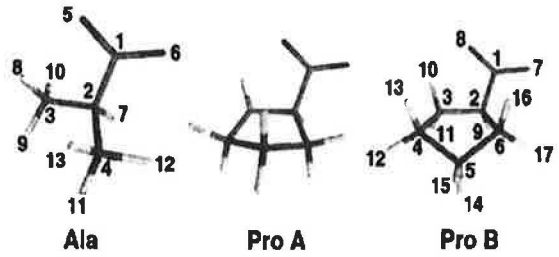

FIG. 1. L-alanine and L-proline zwitterions. The A and B proline conformers have approximately the same energy and equal populations in aqueous solutions at room temperature (Ref. 10). In the potential energy scans, the angles $\varphi=\angle(9,3,2,1)$ and $\psi=\angle(3,2,1,5)$ for alanine and the ring torsion angles of proline were varied. For the latter molecule, the angles were recalculated to the pseudorotation coordinates P, θ_m as defined in Ref. 10.

empirical basis comparing marker bands and characteristic features for similar structures,[7,8] it is generally accepted that only precise *ab initio* computations provide reliable basis for complete interpretation of the experiment.

The theoretical modeling often becomes quite complex and requires careful consideration of many contributions, such as conformational equilibria,[9] solvent-solute interactions, and molecular flexibility.[2,10] In the current study, in order to improve the accuracy of the simulations, we concentrate on the force field and limitations of the harmonic approximation. The analyzed spectra of proline and alanine zwitterions reported previously[2,10] serve as typical examples of molecules that are conveniently explored by ROA, particularly as good models of peptides, proteins, and other polar biopolymers. The anharmonic corrections represent relatively minor, but visible contribution. According to our knowledge, anharmonic effects in ROA spectra have not been systematically investigated yet.

Anharmonic effects in vibrational spectroscopy were often ignored or included in empirical corrections, such as the scaling constants for harmonic force fields.[11,12] Alternatively, simplified fields were proposed for this purpose.[13,14] Only for small molecules accurate potential energy surfaces can be obtained, for example, via single-point calculations at selected geometries around the equilibrium and an interpolation.[15] This approach is particularly useful when only a limited number of strongly anharmonic vibrational modes can be considered.[16] In this study we follow a more frequent method based on Taylor potential series near the equilibrium geometry.[17] The solution of the vibrational problem beyond the harmonic approximation becomes quite tedious as the motion of many degrees of freedom cannot be separated into independent coordinates.[18] Most general methods tackling this problem are based on the variational principle and involve plain vibrational configuration interaction (VCI),[19–21] vibrational coupled cluster (VCC),[22] or vibrational self-consistent field (VSCF).[19,20,23] More advanced approximations combine several approaches [e.g., VSCF and CI (Ref. 20)] or explore the perturbation theory.[24] As discussed previously, such approximate solvers of the anharmonic Schrödinger equation may not provide same solutions and are even differently sensitive to inaccuracies in the vibrational potential.[25] A particular problem in bigger molecules stems from an increased number of the harmonic vibrational states that have nearly same energies. This degeneracy, conventionally called "random" for low-symmetry systems, prevents to apply standard perturbational techniques directly to the harmonic Hamiltonian. Thus the second-order perturbation formula, for example, has to be adapted before it becomes usable for systems with the degeneracies.[25,26]

The theoretical basis of the calculations is briefly reviewed at Sec. II in the current work. In order to explore the limits of the harmonic approach the alanine and proline Raman and ROA spectra are simulated with 25 different density functional theory (DFT) potentials and compared to the experiment. Then we apply various VSCF, perturbational, and VCI anharmonic methods to the zwitterionic force fields and test their performance against experimental Raman frequencies. Finally, the anharmonic calculus is used for modeling of the vibrational frequencies and IR, Raman, and ROA spectral intensities; the significance of the anharmonic corrections is discussed in light of the approximation errors, band broadening stemming from the Boltzmann averaging, and molecular flexibility.

II. METHOD

A. Experiment

The backscattered Raman and incident circular polarization ROA spectra of both L and D enantiomers of proline and alanine were recorded on our spectrometer located at the Institute of Physics, as described in detail elsewhere.[2,10] The laser excitation wavelength was 514.5 nm, with a laser power of 440 mW, a spectral resolution of 6.5 cm^{-1}, and acquisition times of 6 and 9 h for the H_2O and D_2O measurements, respectively. Aqueous (H_2O) solutions with final concentrations of about 3 mol/l were prepared with deionized water; D_2O solutions (2 mol/l) were prepared from doubly lyophilized samples. The solution Raman spectra were remeasured over a broader wave number range including the hydrogen stretching regions on a LabRam HR800 Raman microspectrometer (Horiba Jobin Yvon). A continuous Kiefer scanning mode was used with a 600 grooves/mm grating, a liquid-nitrogen-cooled charge coupled device (CCD) detector (1024×256 pixels), a spectral resolution of about 4 cm^{-1} (varying within the spectral range of frequencies recorded simultaneously), and a 632.8 nm laser excitation wavelength. The IR spectra of both compounds (about 10% aqueous solutions) were recorded on a Vectra 33 Fourier transform infrared spectrometer (Bruker) using a single reflection diamond horizontal attentuated reflection (HATR) accessory (Pike Technologies).

B. Anharmonic corrections

A simplified potential expansion in the vibrational normal mode coordinates $\{Q_i\}$ was used,

TABLE I. Comparison of the harmonic vibrational frequencies of alanine and proline calculated at 25 approximation levels to experimental Raman and ROA data. The CPCM solvent model and 6-31++G** basis set were used in the modeling. Slopes (a), standard deviations [$\Delta(\omega_{calc}-\omega_{expt})$], and dispersions [$\delta(\omega_{calc}-a\omega_{expt})$] are given for a linear fit to experimental wave numbers within 200–1800 cm^{-1}. Methods giving best Raman and ROA intensity profiles (judged subjectively by visual comparison to experiment) are marked by the asterisk (*).

	Alanine in H_2O			Proline in H_2O			Proline in D_2O		
Method[a]	a	Δ	δ	a	Δ	δ	a	Δ	δ
HF	1.088	104	28	1.092	101	19	1.089	96	22
BHandHLYP*	1.042	53	23	1.046	51	14	1.043	48	18
MP2	1.018	32	24	1.021	27	16	1.018	27	20
MPW1PW91*	1.006	17	16	1.012	19	14	1.009	19	17
B1LYP	1.004	24	24	1.008	17	15	1.004	20	19
B3P86*	0.999	16	16	1.006	15	14	1.002	17	17
B3PW91*	0.999	17	17	1.005	15	14	1.001	17	17
*PBE1PBE**	1.004	15	15	1.002	19	19	1.004	22	22
B98*	0.998	21	20	1.002	16	16	0.998	19	19
B3LYP*	0.997	21	21	1.001	15	15	0.997	19	19
HCTH	0.983	27	18	0.989	19	15	0.994	19	18
HCTH147	0.978	32	20	0.984	24	15	0.979	29	19
VSXC	0.977	37	26	0.980	26	15	0.975	32	19
OLYP	0.974	36	21	0.980	28	17	0.976	32	20
LSDA	0.976	43	33	0.975	37	25	0.971	38	23
BPW91	0.965	45	20	0.971	35	15	0.967	40	19
BPW91[b]	...	...	...	0.966	40	14	0.962	44	18
BPW91[c]	...	...	...	0.971	34	13	0.967	39	18
SVWN5	0.972	45	31	0.971	40	24	0.968	40	22
PW91PW91	0.964	45	18	0.970	35	14	0.966	39	18
G96LYP	0.963	49	25	0.968	39	19	0.964	45	23
BLYP	0.960	52	26	0.965	42	19	0.960	48	23
BP86	0.961	49	19	0.964	45	22	0.962	43	18
PW91LYP	0.960	51	23	0.964	43	17	0.959	48	22
PBELYP	0.958	53	24	0.963	43	17	0.958	49	22

[a]GGA functionals are written *in italic*.
[b]AUG-cc-PVDZ basis.
[c]AUG-cc-PVTZ basis.

$$V(Q_1,\ldots,Q_M)=\sum_{i=1}^{M}\frac{\omega_i^2}{2}Q_i^2+\frac{1}{6}\sum_{i=1}^{M}\sum_{j=1}^{M}\sum_{k=1}^{M}c_{ijk}Q_iQ_jQ_k+\frac{1}{24}\sum_{i=1}^{M}\sum_{j=1}^{M}\sum_{k=1}^{M}\sum_{l=1}^{M}d_{ijkl}Q_iQ_jQ_kQ_l+\cdots, \quad (1)$$

while the rotation-vibration coupling was neglected. Only semidiagonal normal mode quartic constants with two and more identical indices (e.g., d_{ijkk}) were considered, obtained from semidiagonal Cartesian quartic constants; $\{\omega_i\}$ are the harmonic frequencies and $M=3\times$number of atoms-6. For the solution of the anharmonic problem the VCI, VSCF, and the second-order perturbation theory (PT2) were used as described in detail elsewhere and implemented in our program GVIB.[25] In the VCI calculations 1000–6000 harmonic oscillator basis functions were included, which contained at most five excitations. In the VSCF method[19] one-dimensional Schrödinger equations,

$$\left(-\frac{1}{2}\frac{\partial^2}{\partial Q_i^2}+v_i(Q_i)\right)\psi_i(Q_i)=e_i\psi_i(Q_i), \quad (2)$$

were solved iteratively until changes of the energies e_i were smaller than 10^{-6} cm^{-1}. The self-consistent averaged potentials are defined as $v_i(Q_i)=\langle\Pi_{j=1,j\neq i}^{M}\psi_j(Q_j)|V(Q_1,\ldots,Q_M)|\Pi_{k=1,k\neq i}^{M}\psi_k(Q_k)\rangle$. As described previously,[25] the potentials can be averaged either using the ground state only or with appropriate excited states. These two approaches are referred to as gVSCF and eVSCF, respectively.

A perturbational calculus was applied to the harmonic (referred to as PT2/Harm) as well as to the VSCF solutions (PT2/VSCF).[24] In both cases, a modified second-order perturbational formula was used, as it previously provided superior results to the conventional approach, especially for systems with nearly degenerate energy levels.[25] Specifically, the second-order correction to the energy of a state n was obtained as

$$E_n^{(2)}=\tfrac{1}{2}\sum_{m\neq n}[E_m-E_n+W_{mm}-W_{nn}\pm\sqrt{(E_m-E_n+W_{mm}-W_{nn})^2+4|W_{nm}|^2}], \quad (3)$$

where the + sign holds for $E_n>E_m$ and − sign for $E_n<E_m$. $\{E_n\}$ are the unperturbed energies and $W_{nm}=\langle n|W|m\rangle$ is the perturbation potential matrix element.

Incident circular polarized backscattering Raman and ROA intensities as well as the IR absorption were obtained for each method with corresponding vibrational wave func-

TABLE II. rms deviations (cm^{-1}) between the experimental and calculated alanine and proline frequencies within 200-1800 cm^{-1}; nine levels of the vibrational problem are compared. By default, three (five for BPW91) lowest-frequency states of alanine and six of proline were ignored.

	Alanine			Proline
Vibrational approximation	Electronic level B3LYP/6-31++G**	B3LYP/6-311++G**	BPW91/6-31++G**	B3LYP/6-31++G**
Harmonic	21	20	45	15
gVSCF	31	34	69	25
eVSCF	34	37	72	25
gVSCF+PT2	50	54	89	41
eVSCF+PT2	54	56	90	42
Harm+PT2	50	53	86	40
Harm+VCI[a]	18	17	34	24
Harm+VCI[b]	33	...	...	30[d]
Harm+VCI[c]	29	18	...	32

[a]1000 VCI states.
[b]1000 VCI states, one mode ignored.
[c]6000 VCI states.
[d]Four modes ignored.

tions using general formulas that can be found elsewhere.[27,28] For PT2 frequencies the harmonic intensities were used in spectral plots.

C. Computations

Alanine and proline equilibrium geometries (see Fig. 1 for the lowest-energy alanine and two proline conformers) and harmonic force fields were obtained with the aid of the GAUSSIAN program[29] using 25 different levels of electronic theory including the HF,[30] MP2,[31] BHandHLYP,[32] MPW1PW91,[33] B1LYP,[34] B3P86,[35,36] B3PW91,[35,37] PBE1PBE,[38] B98,[39] B3LYP,[35] HCTH,[40] HCTH147,[40] VSXC,[41] OLYP,[42] LSDA,[43] BPW91,[32,37] SVWN5,[44] PW91PW91,[45] G96LYP,[46,47] BLYP,[47] BP86,[36] PW91LYP,[47] and PBELYP[38] DFT functionals, mostly with the 6-31++G** basis set and the CPCM ("COSMO-PCM")[48] solvent model. Raman intensities were calculated at the same level. For computation of the anharmonic corrections (third and fourth energy derivatives, second tensor derivatives) the B3LYP/6-31++G** method was used by default, with occasional utilization of the BPW91 and PW91PW91 functionals and smaller 6-31+G** and 6-31G** basis sets. Basis sets of similar quality appeared satisfactory for ROA spectra previously.[49]

The anharmonic constants were calculated by numerical differentiation with a displacement of 0.025 Å. Control computations with steps within 0.005–0.075 Å provided similar results. Occasionally, individual anharmonic constants were calculated unrealistically high, which was attributed to an unstable CPCM model implementation. In control computations molecular CPCM cavities were both fixed at the optimized geometry and allowed to follow displaced nuclei during the differentiation. As both approaches gave very similar vibrational frequencies, the default Gaussian procedure (with the cavity displacement) was used further on. Raman and ROA spectra were simulated using the GVIB program and the theory described above, with Lorentzian bands $\Delta=6.5$ cm^{-1} wide (full width at half height). Contribution of each transition of frequency ω_i to the spectrum was thus

$$S(\omega) = I\left[1-\exp\left(-\frac{\omega_i}{kT}\right)\right]^{-1}\frac{1}{\omega_i}\left[4\left(\frac{\omega-\omega_i}{\Delta}\right)^2+1\right]^{-1},$$

where $I=6(7\alpha_{ij}\alpha_{ij}+\alpha_{ii}\alpha_{ii})$ for Raman and $I=(48/c)(3\alpha_{ij}G'_{ij}-\alpha_{ii}G'_{jj}+\omega_{exc}\varepsilon_{ijk}\alpha_{il}A_{jkl}/3)$ for ROA backscattered intensities, where ω_{exc} is the laser light frequency, T temperature (298 K), and k the Boltzmann constant; $\boldsymbol{\alpha}$, $\mathbf{G}'$, and $\mathbf{A}$ are the electric dipole–electric dipole, magnetic dipole–electric dipole, and electric quadrupole–electric dipole polarizability normal mode derivatives.[27] For absorption spectra the same Lorentzian shapes were used without any temperature correction. 0–5 lowest-energy modes were not included in the anharmonic corrections in order to avoid numerical instabilities. Supposedly, their coupling to the higher-frequency modes is small and their influence on the spectra can be partially accounted to by the Boltzmann averaging as discussed below.

III. RESULTS AND DISCUSSION

A. The harmonic limit

In the past the harmonic approximation has been established as an effective and surprisingly accurate approximation for interpreting vibrational spectra of most molecules.[18,50] This appears to be also the case for the proline and alanine zwitterions. The precision of the harmonic nuclear potential, however, depends strongly on the electronic approximation level and modeling of the environmental factors. Also, one has to realize that atoms may move in an effective harmonic well while other effects are averaged out. For example, the zwitterions would not exist in vacuum and the solvent needs to be added at the electronic computations. Fortunately, the CPCM continuum model used in this study provides reasonable frequencies for the two amino acids in aqueous solutions.[2,10]

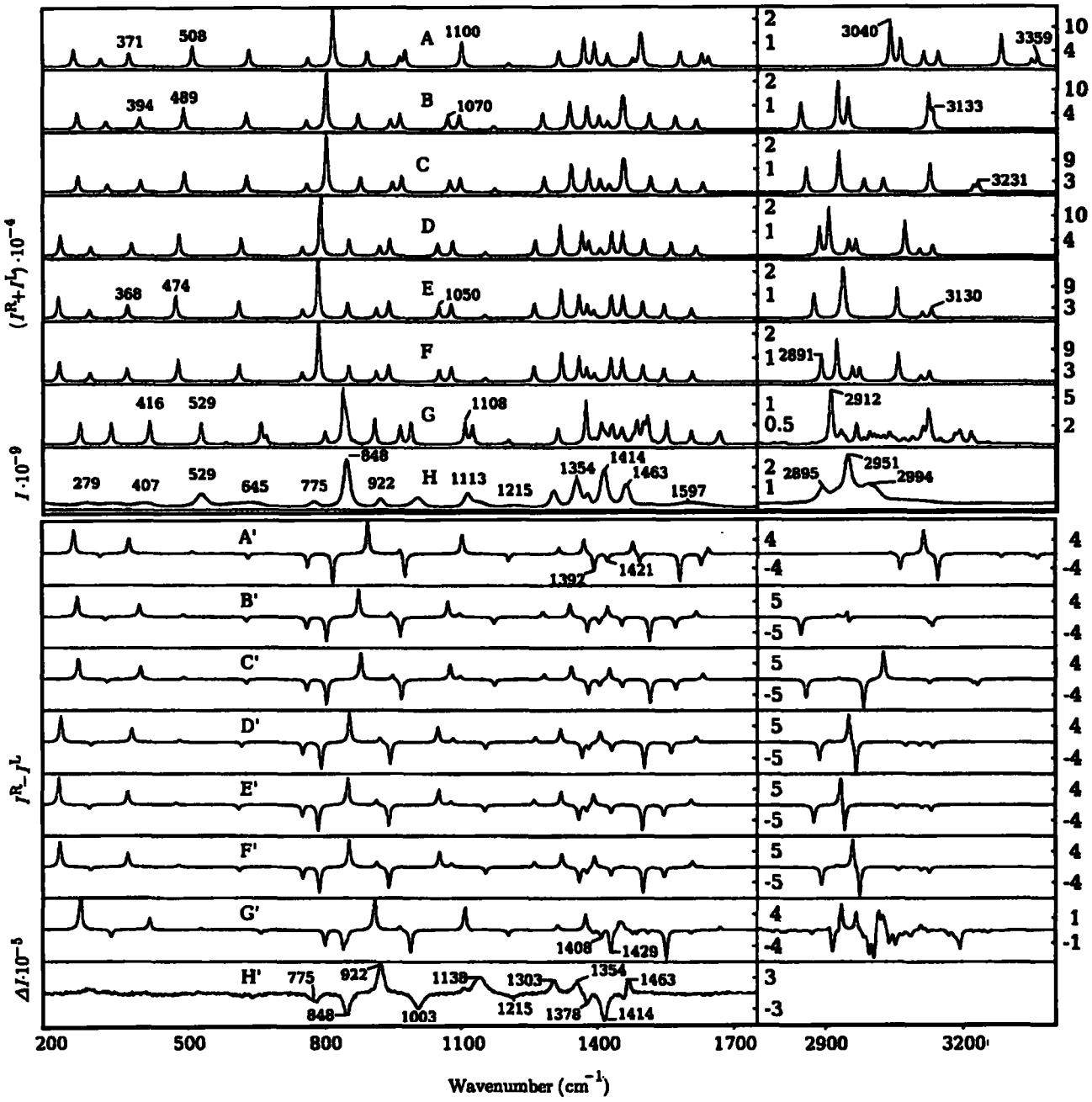

FIG. 2. Raman (A–H) and ROA (A′–H′) spectra of L alanine: comparison of the harmonic (A and A′), eVSCF (B and B′), gVSCF (C and C′), PT2 (D and D′), PT2/eVSCF (E and E′), PT2/gVSCF (F and F′), and VCI (G and G′, with 5000 harmonic oscillator basis functions) calculations with the experiment (H and H′). The B3LYP/CPCM/6-31++G^{**} force field and polarizability derivatives were used in all calculations, three low-frequency modes were ignored. The y scale is arbitrary for the simulations, while for experiment it corresponds to the number of counts on the CCD detector. The absolute scale does not apply to the high-frequency part of the Raman spectrum (>2500 cm^{-1}, trace H) which was measured separately on the microscope.

Systematic improvement of the DFT electronic methods is difficult. On the other hand, they are often the only computationally feasible alternatives for bigger systems. Under these circumstances, we find it important to test their performance at least statistically. Particularly, in Table I, we compare systematic and root mean square errors for alanine and proline vibrational frequencies within 200–1800 cm^{-1} as obtained by 25 approximation levels. In this comparison, we neglect the anharmonic effects and calibrate the computational methods against the experimental values directly. At the same time, the band assignments were verified by visual comparison of experimental and simulated spectral intensities.

Generally, the approximations to the electronic problem summarized in Table I provide similar errors as observed previously for other molecules in vacuum.[12,51] On average the present calculations are closer to the experiment, because of the solvent correction and the exclusion of the high-frequency vibrations from the statistics. The HF method still overestimates the frequencies most significantly, by about 9% for both amino acids (see the slope a of the fit). At the other extreme, most of the "pure" generalized gradient approximation (GGA) functionals underestimate the frequencies, up to by ~4% for the PW91LYP and PBELYP methods. Not surprisingly, the "mixed" functionals containing both the HF nonlocal and the GGA local (density-dependent)

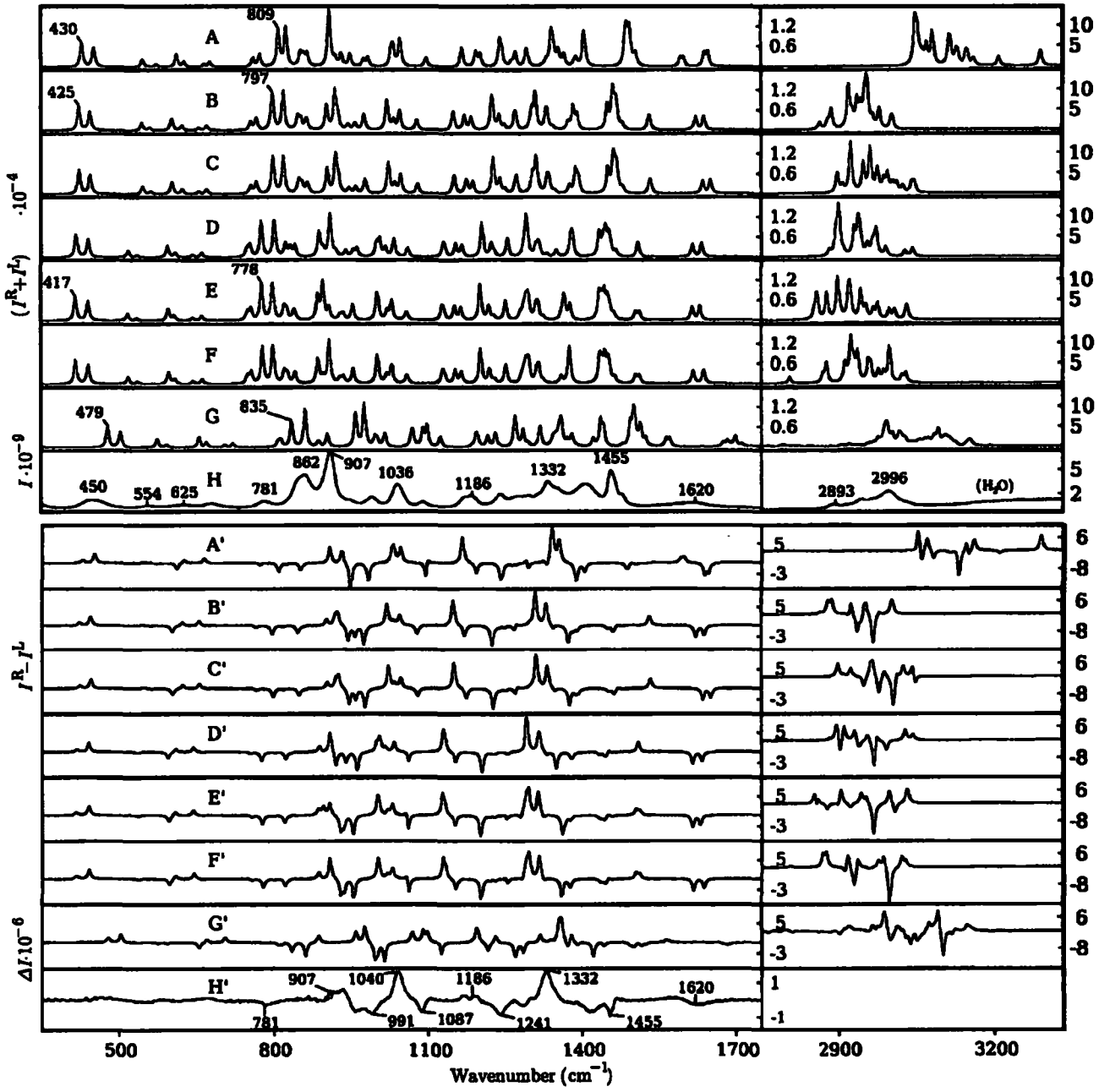

FIG. 3. Raman (A–H) and ROA (A′–H′) spectra of L proline: comparison of the harmonic (A and A′), eVSCF (B and B′), gVSCF (C and C′), PT2 (D and D′), PT2/eVSCF (E and E′), PT2/gVSCF (F and F′), and VCI (G and G′, with 5000 harmonic oscillator basis functions) calculations with the experiment H and H′). The B3LYP/CPCM/6-31++G^{**} force field and polarizability derivatives were used for all calculations, five lowest wave number modes were ignored.

energy term, such as B3LP or B3PW91, thus provide the best results. Note that the slope of the fit (a) often differs from one by ~0.1% only. Nevertheless, some pure GGA functionals missing the HF exchange terms, such as HCTH or PBE1PBE, perform very well, too, and may be favored in applied computations because of their lesser demands on computer CPU time and memory. Previously, we and others often used the BPW91 functional for simulation of the peptide and protein vibrational circular dichroism (VCD), as it provided better amide I frequencies (C=O stretch) with more modest computational demands than the more frequent B3LYP.[52] Although the BPW91 method also provides reasonable Raman and ROA spectral shapes (not shown) for the zwitterions, the vibrational frequencies are too low. Thus application of this functional to the Raman spectra comprising a wide range of transitions does not appear as advantageous as for VCD.

We can also see that it is the treatment of the correlation energy, not the exchange, that most significantly improves the HF results: the MP2 perturbation correlation treatment reduces the HF error significantly. However, for the DFT techniques, a more detailed discussion of the contribution of the exchange and correlation parts is not meaningful due to the empirical and often complicated mathematical form of the functionals. More importantly, previous experience suggests[2,10] that even the functionals providing the best fre-

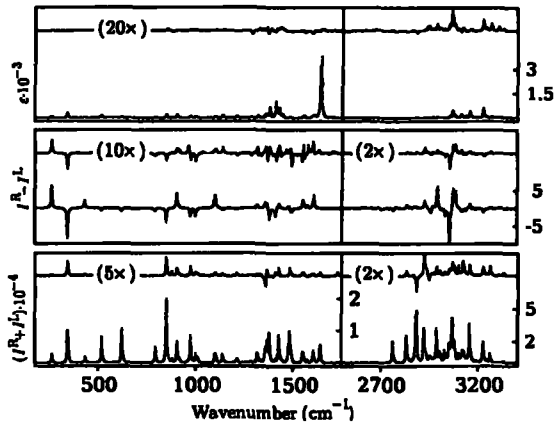

FIG. 4. Absorption (top), ROA (middle), and Raman (bottom) alanine spectral intensities with the second dipole and polarizability derivative contributions. The contributions are magnified and plotted separately above the spectra as simulated by the VCI method (1000 basis functions, three ignored modes).

quencies and Raman and ROA spectral profiles [e.g. those indicated by the asterisk (*) in Table I] could not completely explain all the experimental features. This situation may be even more problematic for bigger molecules or for regions with many overlapping bands. For such cases neither the best precision (15–20 cm^{-1}) achieved can lead to correct prediction of spectral band ordering and a proper assignment.

B. Anharmonic corrections below 1800 cm^{-1}

For the harmonic computations we restrict ourselves to the DFT potentials, mostly the B3LYP functional, because more advanced methods become prohibitively demanding in terms of computer power. Nevertheless, we rely on the previous experience[53] indicating that the main anharmonic effects can be described by DFT practically with the same precision as with the wave-function-based electronic calculus. Inclusion of the anharmonic potential does not make automatically the agreement with the experiment better. While this is true for abstract model systems,[24] many loopholes are hidden in practical applications. Limited precision of the electronic models, such as those in Table I, probably burdens the harmonic frequencies with an error comparable to the anharmonic corrections. Similar inaccuracies may be expected in estimation of the anharmonic constants. Also, as pointed out previously, approximate solvers of the anharmonic vibrational problem are very sensitive to random errors in the potential, even when the random degeneracy problem is avoided.[25] Particular problem represents the many inaccurate terms that are summed over in the VSCF and PT2 methods.

Due to these factors the VSCF, PT, and VCI anharmonic corrections summarized in Table II do not lead to a convincing statistical improvement. The VCI computation improves the harmonic results for alanine, but only when three lowest-energy modes are ignored. An incompleteness of the VCI state space does not seem to be a problem in the lower-frequency region (<1800 cm^{-1}) where the state density is low. The VSCF method provides rms deviations by about 50% bigger than the harmonic limit, while the perturbation methods give a 100% increase of the deviation. Calculated harmonic and anharmonic frequencies of proline are on average closer to the experiment than for alanine; otherwise relative performance of all the vibrational methods is about the same for both molecules. Based on our previous experience[25] we suspect that the anharmonic force field inaccuracies stemming from the discrete solvent CPCM model implementation are most responsible for the errors. Apparently, the modified second-order perturbational formula (3) could eliminate sensitivity to random degeneracies, but it still at least mildly amplifies the nuclear potential inaccuracies. Thus we have to conclude that the applied methods cannot statistically improve the harmonic frequencies in the lower wave number region.

C. Spectral intensities and the high-frequency region

However, the unconvincing improvement in the lower-frequency region does not mean that the estimation of the anharmonic part of the potential is meaningless. On the contrary, as can be seen in Figs. 2 and 3 for alanine and proline, respectively, the anharmonic computations can significantly improve not only the higher-frequency region dominated by the hydrogen stretching modes but also cause intensity redistributions in the lower-frequency region. In Figs. 2 and 3 seven approximations of the vibrational Hamiltonian (harmonic, eVSCF, gVSCF, PT2, PT2/eVSCF, PT2/gVSCF, and VCI) are compared to the solution (H_2O) Raman and ROA amino acid spectra. The nonvariational methods converge relatively smoothly for the transitions below 1800 cm^{-1}, mostly overcorrecting the harmonic results and provide frequencies too low. For example, for alanine, the harmonic CO_2 rocking band at 508 cm^{-1} (trace A, Fig. 2) is calculated at 474 cm^{-1} by the PT2 methods, while the experimental value is 529 cm^{-1}. The VCI computation brings the frequency back to the harmonic and experimental value, to 529 cm^{-1}. This is a typical behavior for both the proline and alanine spectral bands within 200–1000 cm^{-1} and can also be observed, for example, for the respective harmonic/(eVSCF)PT2/VCI/experimental frequencies of CH3 wagging and C–C stretch (1100/1050/1108/1113 cm^{-1}) and $NC_\alpha C$ deformation modes (371/368/416/407 cm^{-1}) of alanine, and CO_2 bending (430/417/479/450 cm^{-1}) and ring deformation (809/778/835/862 cm^{-1}) of proline.

Therefore only the VCI method seems to have the potential to improve the harmonic computations in this region. For VSCF and VCI, virtually same Raman and ROA intensities are obtained for most bands as at the harmonic limit (anharmonic intensity corrections were not implemented for the PT methods). The gVSCF and eVSCF spectra (traces B, C, B′, and C′ in Figs. 2 and 3) are very similar, as are all the PT2 simulations (D–F and D′–F′). Only for the highest-frequency (N–H stretching) vibration of alanine the eVSCF and gVSCF corrections differ substantially: the former shifts the harmonic band (3359 cm^{-1}, trace A in Fig. 2) to 3133 cm^{-1} (trace B), while the second provides a much smaller shift, to 3231 cm^{-1} (trace C). The application of the second-order perturbation theory significantly changes the VSCF results, often by tens of cm^{-1}. In the case of the ala-

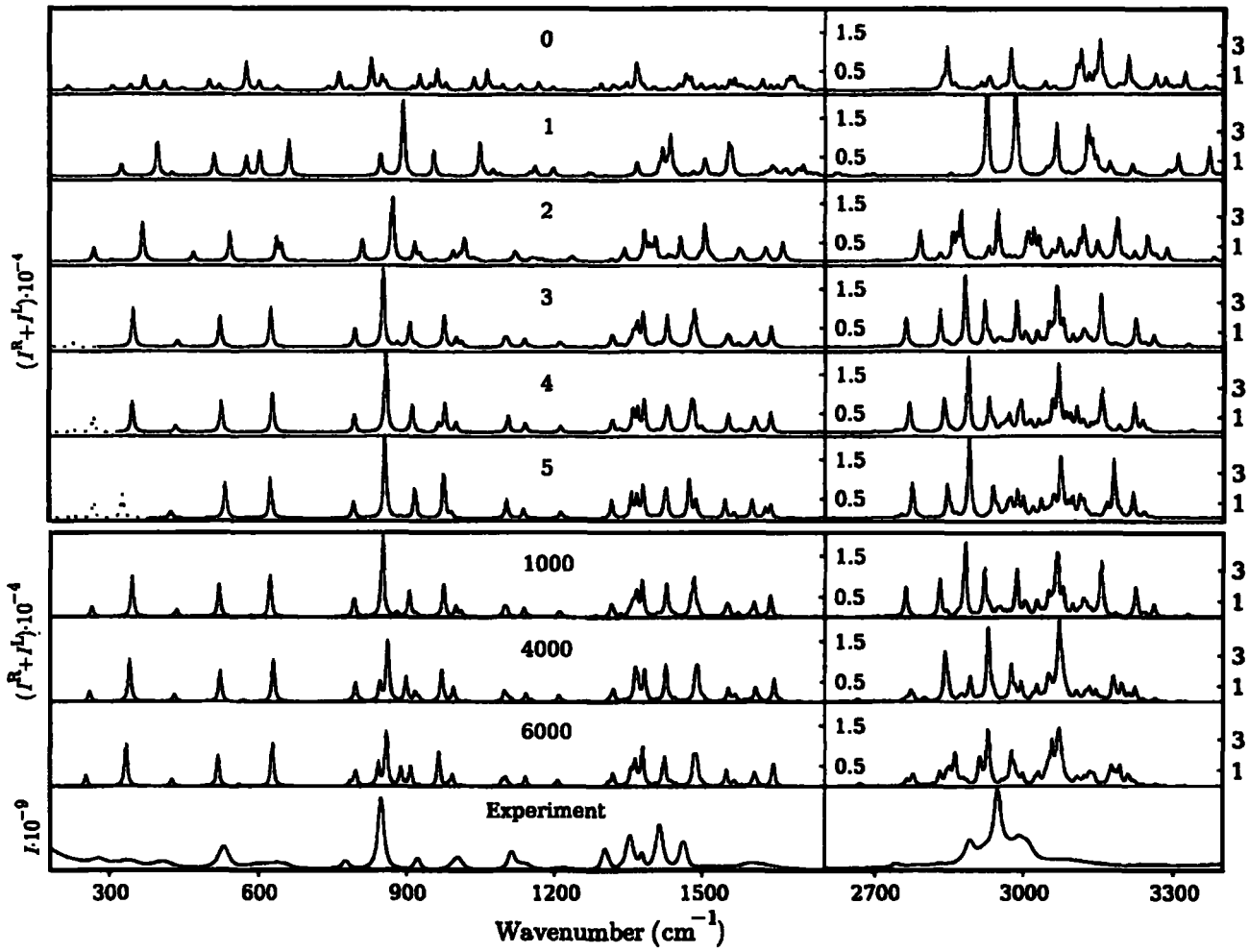

FIG. 5. Convergence of the alanine B3LYP/CPCM/6-31++G^{**} VCI calculation: At the top, dependence of the Raman spectra on the number of ignored modes (written in the figure, their harmonic contributions are plotted by the dashed line) for 1000 VCI states. For three ignored modes the dependence of the spectra on the number of VCI states is plotted in the lower panel.

nine N–H stretch, for example, the PT2 corrections smooth out the gVSCF and eVSCF differences, giving approximately the same frequency (~3130 cm^{-1}, traces E and F in Fig. 2) if applied to both methods.

Within ~200–1200 cm^{-1} the anharmonic corrections provided mostly plain frequency shifts. Within 1200–2000 cm^{-1}, however, even the VSCF and PT2 methods cause a visible redistribution of the Raman and ROA intensities. This region is dominated by C–H and N–H bending and C=O and C–N stretching modes, and the density of vibrational states becomes quite high. Resultant spectral shapes can thus be easily influenced by a small change of the numerical model. Again, only the VCI calculus provides a clear improvement of the harmonic spectra. For example, the relative intensities of the negative ROA alanine bands at 1392 and 1421 cm^{-1} (Fig. 2, A′) are switched in VCI (G′, smaller band at 1408, deeper at 1429 cm^{-1}), in favor of the experiment (H′, 1378 and 1414 cm^{-1}). Also for proline (Fig. 3) the overall Raman and ROA profile seems to be best reproduced by the VCI simulation; however, in this case the spectra are becoming too complex to be explicable on a basis of individual transitions. Clearly, the anharmonic calculus is important and can mostly improve the spectra in the entire wave number region, but it is very difficult to obtain a band-to-band agreement for our solvated and flexible molecules. An improvement of the solvent modeling may be desirable, namely, for a better reproduction of the force field of the polar groups. This task appears presently too complex and goes beyond the scope of this study. On the other hand, the flexibility aspect can be modeled more easily and will be discussed below.

In the C–H and N–H stretching regions all the anharmonic methods improve the harmonic frequencies. For example, the lowest C–H stretching band of alanine is obtained at 3040 cm^{-1} at the harmonic limit, while the 2891 and 2912 cm^{-1} PT2/gVSCF and VCI peaks are much closer to the experimental value of 2895 cm^{-1}. The VCI method provides best Raman C–H stretching profiles, although the agreement with the experiment is far from being perfect. Unfortunately, the N–H stretching vibrations are influenced by the hydrogen bonding, very poorly reproduced by the continuum solvent model; additionally, this region is obscured by the O–H water stretching and unusable for even a qualitative analysis. Reliable experimental ROA spectra could not be obtained in this region so far.

As follows from the basic properties of the harmonic oscillator,[18] higher dipole and polarizability derivatives do not contribute to spectral intensities in harmonic systems.

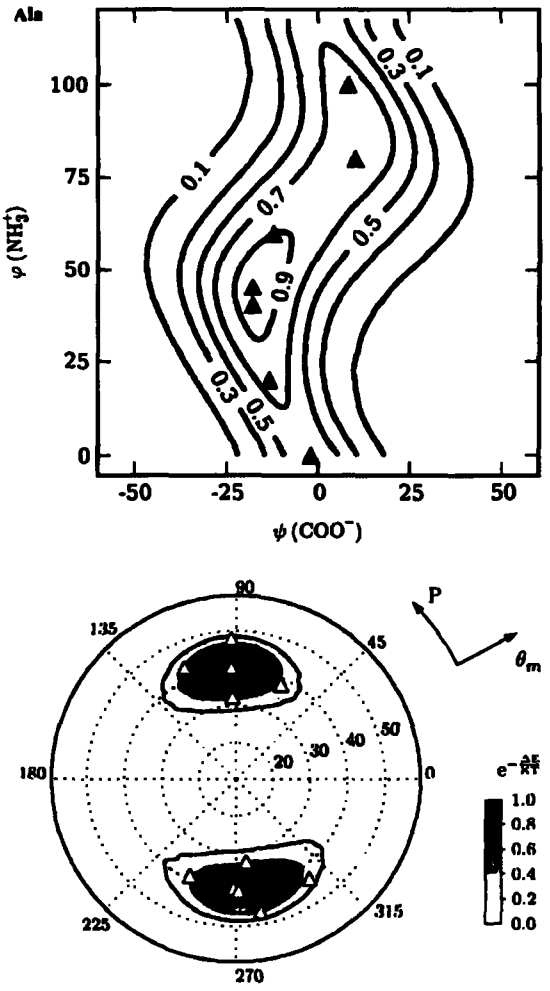

FIG. 6. Relative probability distributions of alanine (top) and proline (bottom) conformers at 300 K. For conformers marked by the triangles anharmonic IR, Raman, and ROA spectra were calculated and averaged in Figs. 7–9. (Note that the polar proline plot starts with $\theta_m = 10°$ in the center.)

Leaving this method known also as the "double-harmonic" approximation we can investigate separately anharmonic spectral corrections stemming from the force field (in the present model third and fourth energy derivatives) and the intensity tensors (second derivative of the electric dipole-electric dipole, electric dipole–magnetic dipole, and electric dipole–electric quadrupole polarizabilities[27]). As shown in Fig. 4 where the absorption, ROA, and Raman L-alanine spectra are simulated with the VCI method, the second intensity tensor derivatives constitute relatively minor contributions to total intensities. However, this term seems to be more important for Raman and ROA spectra than for the absorption. This may imply a generally increased sensitivity of the Raman spectroscopy to small geometry variations. As expected, the higher-frequency strongly anharmonic vibrations are more affected by the "intensity tensor anharmonicity" than the lower-frequency transitions. In practical terms, the inclusion of the second polarizability derivatives may be most important for improving the Raman intensities, relative ratios of which can be measured with a high precision. It is probably too small to be detectable in ROA due to the experimental noise. Similar magnitude of the tensor second derivative corrections was also observed for the proline zwitterion and is not shown in the manuscript.

D. Error estimation and stability analyses

The limited fourth-order Taylor expansion is not suitable for representing the potential energy surface along the low-frequency normal modes, such as the rotations of methyl or carbonyl groups. The anharmonic (VSCF and VCI) methods appeared to be very sensitive to such potentials and we noticed repeatedly convergence problems, unless the lowest lying modes were ignored ("frozen"). For example, typically about three to five modes had to be frozen for alanine and six for proline before the eVSCF calculations fully converged. This freezing is partially justifiable by a limited coupling of these modes to the higher-frequency vibrations. However, the coupling cannot be *a priori* excluded. Therefore, an extension of the anharmonic treatment, at least for some low-frequency vibrations, via a Boltzmann temperature averaging will be shown below.

Nevertheless, in Fig. 5, we can see that the freezing does not affect the calculated frequencies dramatically. The influence of the anharmonic coupling of the low-frequency modes can be seen in the upper part of the figure, where the alanine Raman spectra are simulated with 0–5 ignored modes. When all modes are included, the VCI spectrum is unrealistic. Additionally, the lowest-energy state obtained by the Hamiltonian diagonalization does not correspond to the real ground state. From two ignored modes (approximately corresponding to NH_3^+ and CO_2^- group rotations), however, the VCI spectra start to converge and inclusion/omission of the mode number 3–5 does not seem to be crucial for reproduction of the middle and high frequencies.

The ignoring of the lowest-energy modes in the anharmonic calculus also enables us to limit the number of VCI states taken in the diagonalization. Alanine Raman spectra simulated with 1000, 4000, and 6000 states (lower part of Fig. 5) appear reasonably converged within 300–3300 cm^{-1}. In this region of fundamental vibrations the density of vibrational states is relatively low. The amount of 6000 states (representing only 1.4% of all five-times excited states contributing to the second-order fundamental corrections), for example, thus seems to be sufficient to cover most of the coupling and diagonal anharmonic interactions. However, small intensity changes are still visible, even for the bands around 900 cm^{-1}. As discussed before,[25] application of the VCI method to bigger molecules will be always limited. Even when the number of the states can be somewhat increased using indirect diagonalization methods[21] (not implemented here) it is questionable if a fully converged mathematical solution exists and should be sought. Clearly, for proline and alanine the plain VCI method is not usable for the Taylor-style potential unless the lowest-energy modes are treated separately. Additionally, an involvement of all-mode coupling in VCI appears rather luxurious with respect to the physical reality, where 3–4 mode interactions usually determine the frequencies with a sufficient accuracy.[14,16,54] Therefore, for the incomplete anharmonic potentials, it appears reasonable to use the limited VCI, which comprises most of the intermode coupling and provides a first-order correction to the spectra.

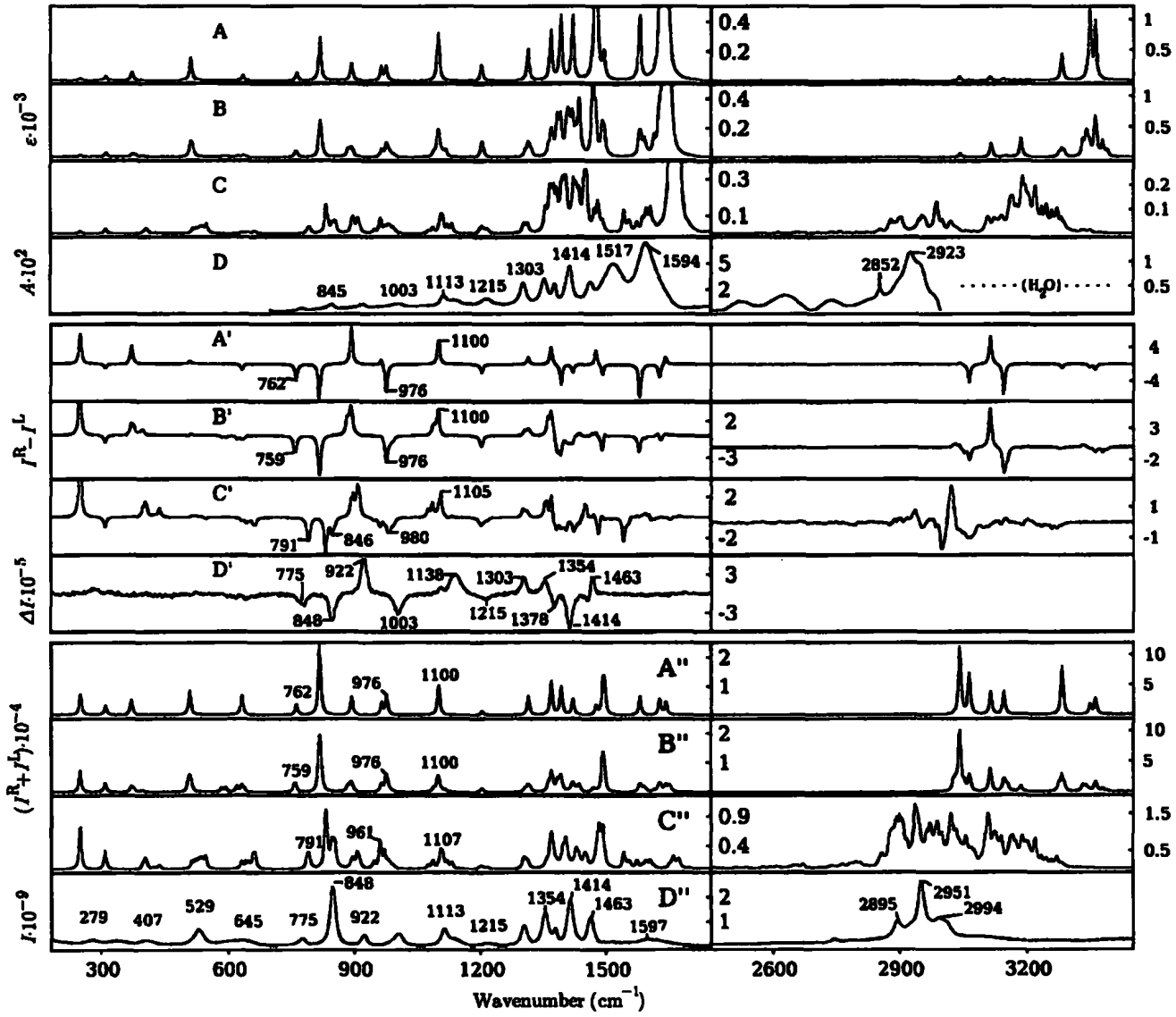

FIG. 7. The effect of the Boltzmann conformer averaging on absorption (A–D), ROA (A′–D′), and Raman (A″–D″) alanine spectra: harmonic approximation for the equilibrium geometry (A, A′, and A″), conformer averaging of harmonic (B, B′, and B″), and anharmonic (C, C′, and C″) spectra for the structures defined in Fig. 6. The experimental IR absorbance (D) was measured by the ATR technique. The experimental ROA (D′) and Raman (D″) spectra are taken from Ref. 2. The simulations were done for the temperature of 300 K at the B3LYP/CPCM/6-31++G^{**} level, using 5000 VCI states with three low-frequency modes frozen.

E. Spectra averaging

In order to judge the effect of the anharmonic corrections, it is important to estimate all other factors that may contribute to the spectra with the same magnitude, including molecular flexibility and temperature averaging. For proline and alanine, at least two lowest-energy modes have to be averaged in room temperature.[2,10] In Fig. 6 we reproduce relative probability distributions obtained with the B3LYP/CPCM/6-31++G^{**} energy surfaces. 7 (for alanine) and 11 (for proline) conformations visible as the triangles in Fig. 6 were taken in the averaging. A more complete sampling of the conformer space, as could be done at the harmonic limit,[2,10] was prohibited by the time needed to calculate the anharmonic terms. However, with a balanced selection of the conformers the extent of the averaging changes could also be estimated for the anharmonic case. Particularly, Figs. 7 and 8 compare absorption (traces A–D), ROA (A′–D′), and Raman (A″–D″) alanine and proline spectra simulated at the harmonic level for rigid molecules (A, A′, and A″) with the harmonic (B, B′, and B″) and anharmonic (C, C′, and C″) averages, together with the experiments (D, D′, and D″).

The harmonic and anharmonic averages in the absorption spectra (B and C in Figs. 7 and 8) are quite similar below 800 cm^{-1}; this region, however, is not accessible experimentally. A maximum absorption intensity within 800–1800 cm^{-1} is mostly associated with the movement of the polar groups (NH_3^+, NH_2^+, and CO_2^-). This is not a favorable situation for the modeling, because such harmonic frequencies are calculated with the biggest error due to the interaction with the solvent. The experimental C—O stretching signal is strongly mixed with the water absorption and the base line subtraction may have somewhat affected the apparent frequencies and intensities of the corresponding

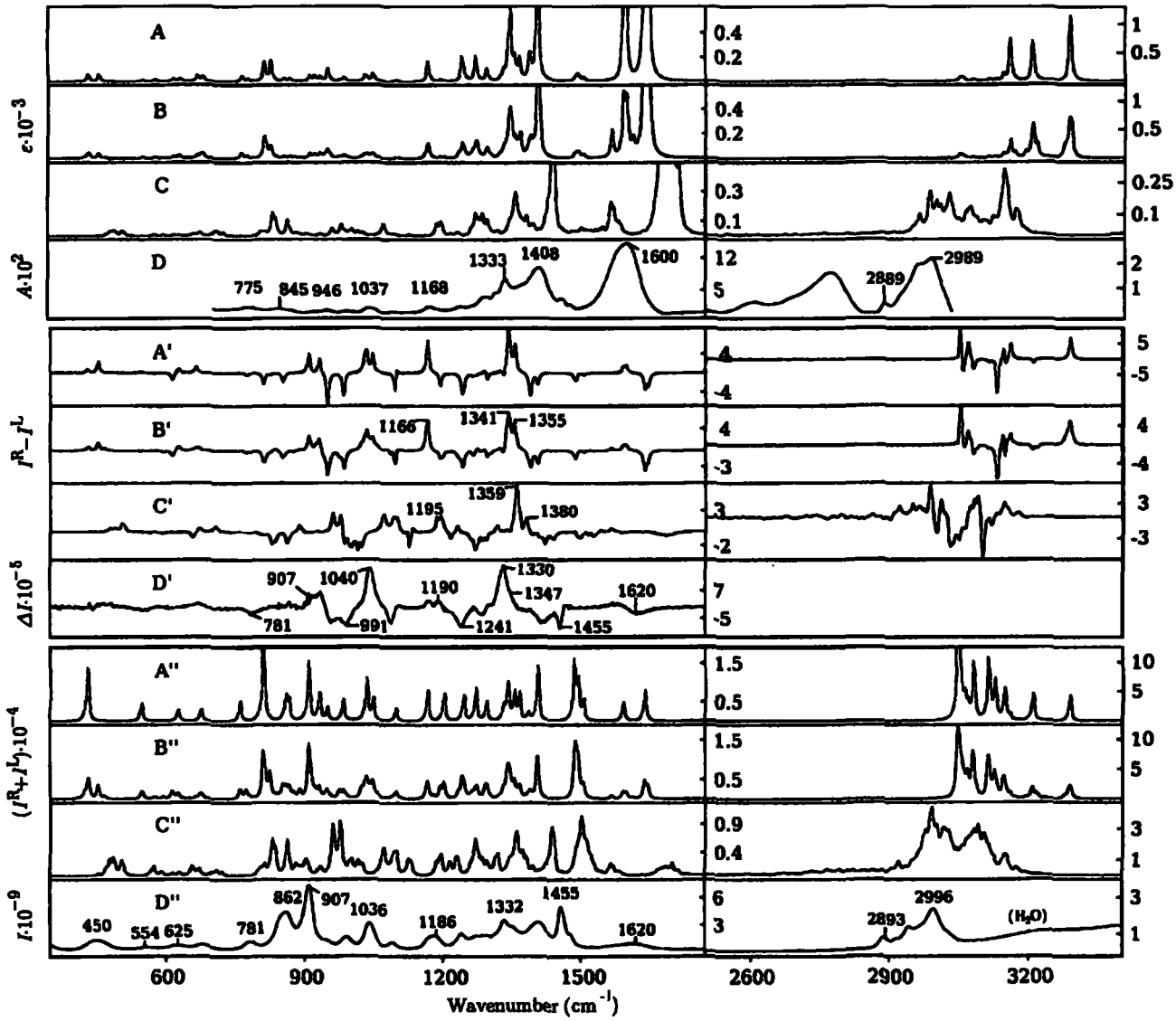

FIG. 8. The effect of Boltzmann conformer averaging on absorption (A–D), ROA (A′–D′), and Raman (A″–D″) proline spectra. The layout of the figure is analogous to Fig. 7: harmonic approximation (A, A′, and A″, average of the A+B conformers in Fig. 1), Boltzmann-weighted conformer averaging (Fig. 6) of the harmonic (B, B′, and B″), and anharmonic (C, C′, and C″) spectra (300 K, B3LYP/CPCM/6-31++G^{**}, 5000 VCI states, five modes frozen). The experimental absorption spectrum (D) was measured by the ATR technique; the experimental ROA (D′) and Raman (D″) spectra are taken from Ref. 10.

IR bands at 1594 and 1599 cm^{-1} for alanine and proline, respectively. Similarly, the water absorption and the broad N–H stretching signal may obscure the region above 2500 cm^{-1} with the very weak C–H stretching signal. Nevertheless, the averaged anharmonic C–H stretching frequencies (2900–3100 cm^{-1}) are clearly superior to the harmonic simulations, although detailed absorption profile cannot be compared. Within 2500–2850 cm^{-1} we can see a relatively strong signal, particularly in the proline absorption spectrum, which we currently cannot explain. Same spectral features were also observed in an optical cell; only the attentuated total reflection (ATR) measurements, however, are shown because of the extended available frequency range. The N–H stretching signal($\sim>3000$ cm^{-1}) (Ref. 55) is most affected by the hydrogen bonding and cannot be identified in the IR experiment at all. In Raman scattering, the NH stretching contribution is identifiable, but very weak and broad.

For the Raman and ROA intensities most of the positive effects of the anharmonic corrections discussed above for the rigid geometries also persist after the averaging. In the lower wave number region, for example, we can see improved alanine frequency of the 759/791/775 cm^{-1} band (harmonic average/anharmonic average/experiment, traces B″/C″/D″ in Fig. 7), new peak at 846 cm^{-1} (trace C′, experimentally detectable as a weak negative ROA shoulder at 861 cm^{-1}, trace D′), improved frequency and relative intensity of the 976/980/1003 cm^{-1} band, and more realistic relative intensities of the 1087–1100 (harm) /1085–1105 (anharm) /1104–1140 cm^{-1} ROA and Raman bands. As pointed out above, the region of 1300–1550 cm^{-1} is difficult to simulate. We can only conclude that the anharmonic forces play a substantial role at the coupling of involved vibrations and the anharmonic corrections improve a general ROA and Raman intensity profile, if compared with the harmonic case, but a band-to-band comparison is not possible. The same is also true for the C–H stretching Raman signal at 2900–3100 cm^{-1}. Simi-

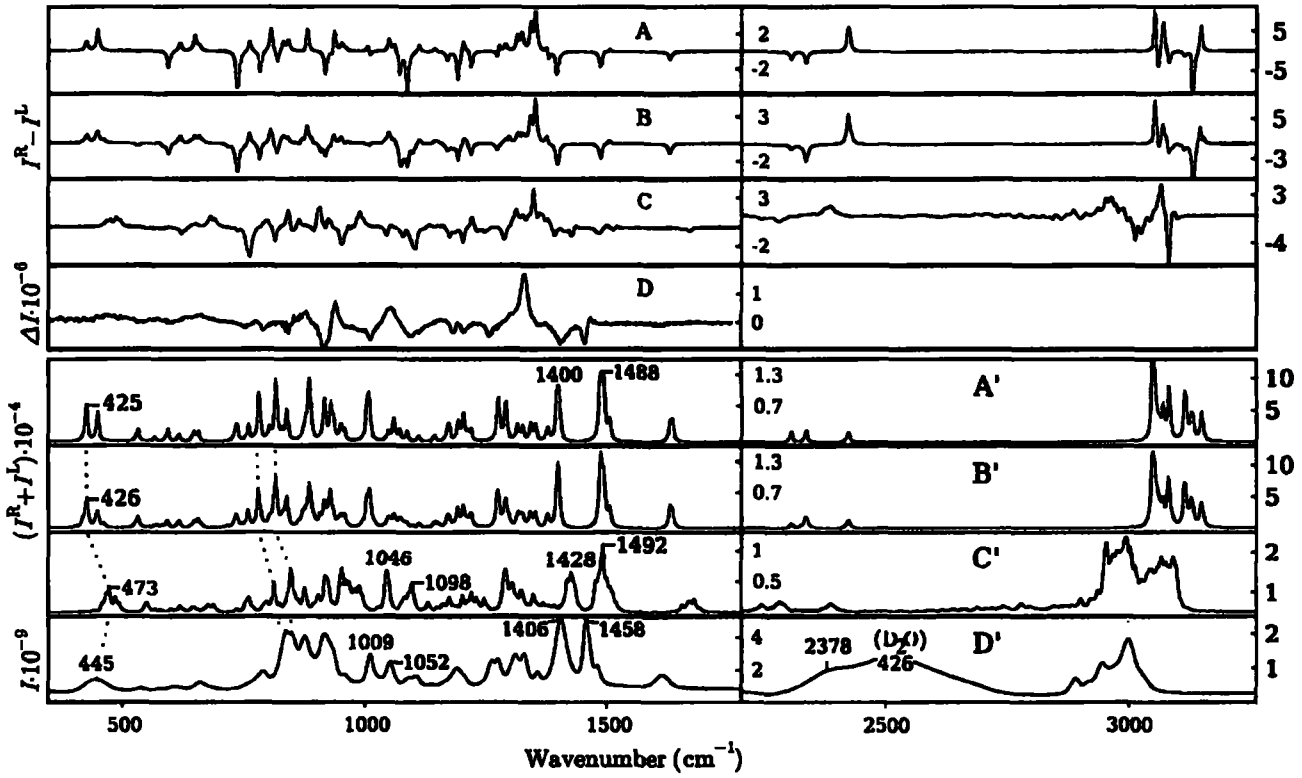

FIG. 9. Harmonic (A and A'), Boltzmann-averaged harmonic (B and B'), and VCI (C and C', for 300 K, B3LYP/CPCM/6-31++G^{**}, 5000 VCI states, five modes frozen) Raman (A–D) and ROA (A'–D') spectra for deuterated (ND_3^+) proline, A+B conformer average. The experimental spectrum in D_2O (D and D') was taken from Ref. 10.

lar situation appears for the proline spectra (Fig. 8). Here, the anharmonic averaged simulation provides a reasonable agreement with the experiment even in the ~1205–1550 cm^{-1} region, which was found difficult for alanine: the shapes, frequencies, and intensities of the ROA bands (trace C') become more realistic. For example, the harmonic positive ROA band pair (1166 cm^{-1}, trace B') splits and the intensity decreases in C' (1186–1195 cm^{-1}), in favor of experimental values of 1167–1190 cm^{-1}, the positive harmonic doublet (trace B', 1341–1355 cm^{-1}) changes to the dominant single band at 1359 cm^{-1} with a shoulder at 1380 cm^{-1} in C', similarly as seen in the experimental spectrum D' (1330, shoulder 1347 cm^{-1}).

Similar extent of the anharmonic forces can be observed in the Raman and ROA spectra of deuterated (ND_2^+) proline plotted in Fig. 9. One might expect that the deuterated species would behave "more harmonic" as heavy atoms move less from their equilibrium positions ($\langle x^2 \rangle \propto 1/\sqrt{m}$) and sample less of the potential landscape. This is difficult to prove here because all simulations still significantly deviate from the experimental spectra. However, individual positive effects of the anharmonic forces in the spectra can be found, similarly as for the nondeuterated species. Most notably, the splitting of the harmonic bands at 1400 and 1488 cm^{-1} decreases (shifting them to 1428 and 1492 cm^{-1} in trace C', Fig. 9) and better corresponds to the observed values of 1406 and 1458 cm^{-1}. Consequently, the overall anharmonic ROA pattern within ~1300–1500 cm^{-1} (trace C) seems to be slightly better in comparison with the harmonic simulation B. Moreover, the relative intensity of the Raman bands observed experimentally (D') at 1009 and 1052 cm^{-1} improves due to the anharmonicities (at 1046 and 1098 cm^{-1} in C') as the higher-frequency band becomes stronger. All simulations provide reasonable frequencies of the N–D stretching bands, visible probably as a shoulder at ~2378 cm^{-1} on the heavy water (incompletely subtracted) O–D stretching signal[55] in D'.

IV. CONCLUSIONS

For the alanine and proline zwitterions we have applied the VSCF, PT2, and VCI anharmonic corrections in simulations of the Raman, ROA, and absorption spectra and analyzed their agreement with the experiment. The VSCF and PT2 methods did not provide convincing improvement of spectral shapes and frequencies except for the C–H stretching region. On the other hand, the VCI correction clearly improved the Raman and ROA spectral intensities, including the vibrations of 200–1800 cm^{-1}. Within 1205–1550 cm^{-1} the improvement still did not enable to assign all experimental features due to the high density of vibrational states (mostly C–H bending) and coupling to the motion of the polar groups strongly interacting with the environment. In spite of the limitations, we consider inclusion of the anharmonic effects to be an important step in the continuous effort to make interpretation of the vibrational spectra more accurate, which will lead to better understanding of molecular structure, dynamics, and interactions.

ACKNOWLEDGMENTS

The work was supported by the Grant Agency of the Czech Republic (Grant Nos. 203/06/0420 and 202/07/0732), Grant Agency of the Academy of Sciences (A400550702), Grand Agency of the Charles University (19707), and by the Ministry of Education, Youth and Sports of the Czech Republic (MSM 0021620835).

[1] L. D. Barron, L. Hecht, and A. D. Bell, in *Circular Dichroism and the Conformational Analysis of Biomolecules*, edited by G. D. Fasman (Plenum, New York, 1996), p. 653; L. A. Nafie, in *Modern Nonlinear Optics*, edited by M. Evans and S. Kielich (Wiley, New York, 1994), Vol. 85, pt. 3, p. 105; L. D. Barron, S. J. Ford, A. D. Bell, G. Wilson, L. Hecht, and A. Cooper, Faraday Discuss. **99**, 217 (1994); K. J. Jalkanen, R. M. Nieminen, M. Knapp-Mohammady, and S. Suhai, Int. J. Quantum Chem. **92**, 239 (2003); J. Kapitán, V. Baumruk, V. Kopecký, Jr., and P. Bouř, J. Am. Chem. Soc. **128**, 2438 (2006); K. Ruud, T. Helgaker, and P. Bouř, J. Phys. Chem. A **106**, 7448 (2002).
[2] J. Kapitán, V. Baumruk, V. Kopecký, Jr., and P. Bouř, J. Phys. Chem. A **110**, 4689 (2006).
[3] L. D. Barron and A. D. Buckingham, Mol. Phys. **20**, 1111 (1971).
[4] L. D. Barron, M. P. Bogaard, and A. D. Buckingham, J. Am. Chem. Soc. **95**, 603 (1973); W. Hug, S. Kint, G. F. Bailey, and J. R. Schere, *ibid.* **97**, 5589 (1975).
[5] P. L. Polavarapu, Angew. Chem., Int. Ed. **41**, 4544 (2002).
[6] L. D. Barron, L. Hecht, I. H. McColl, and E. W. Blanch, Mol. Phys. **102**, 731 (2004); F. Zhu, N. W. Isaacs, L. Hecht, and L. D. Barron, J. Am. Chem. Soc. **127**, 6142 (2005); E. W. Blanch, I. H. McColl, L. Hecht, K. Nielsen, and L. D. Barron, Vib. Spectrosc. **35**, 87 (2004); L. A. Nafie, G. S. Yu, and T. B. Freedman, *ibid.* **8**, 231 (1995); J. Kapitán, V. Baumruk, V. Gut, J. Hlaváček, H. Dlouhá, M. Urbanová, E. Wunsch, and P. Maloň, Collect. Czech. Chem. Commun. **70**, 403 (2005); P. Bouř, M. Buděšínský, V. Špirko, J. Kapitán, J. Šebestík, and V. Sychrovský, J. Am. Chem. Soc. **127**, 17079 (2005).
[7] C. N. Tam, P. Bouř, and T. A. Keiderling, J. Am. Chem. Soc. **118**, 10285 (1996).
[8] C. Toniolo, F. Formaggio, S. Tognon *et al.*, Biopolymers **75**, 32 (2004); E. W. Blanch, A. C. Gill, A. G. O. Rhie, J. Hope, L. Hecht, K. Nielsen, and L. D. Barron, J. Mol. Biol. **343**, 467 (2004).
[9] P. Bouř, V. Sychrovský, P. Maloň, J. Hanzlíková, V. Baumruk, J. Pospíšek, and M. Buděšínský, J. Phys. Chem. A **106**, 7321 (2002).
[10] J. Kapitán, V. Baumruk, V. Kopecký, Jr., R. Pohl, and P. Bouř, J. Am. Chem. Soc. **128**, 13451 (2006).
[11] C. E. Blom and C. Altona, Mol. Phys. **31**, 1377 (1976).
[12] P. Pulay, J. Phys. Chem. **99**, 3093 (1995).
[13] H. Romanowski, J. M. Bowman, and L. B. Harding, J. Chem. Phys. **82**, 4155 (1985); A. E. Roitberg and R. B. Gerber, J. Phys. Chem. B **101**, 1700 (1997).
[14] J. O. Jung and R. B. Gerber, J. Chem. Phys. **105**, 10332 (1996).
[15] G. Rauhut, J. Chem. Phys. **121**, 9313 (2004).
[16] S. Carter, J. M. Bowman, and N. C. Handy, Theor. Chem. Acc. **53**, 1179 (1997).
[17] W. Schneider and W. Thiel, Chem. Phys. Lett. **157**, 367 (1989); P. Bouř and L. Bednárová, J. Phys. Chem. **99**, 5961 (1994); V. Barone, J. Chem. Phys. **122**, 014108 (2005).
[18] D. Papoušek and M. R. Aliev, *Molecular Vibrational/Rotational Spectra* (Academia, Prague, 1982).
[19] J. M. Bowman, J. Chem. Phys. **68**, 608 (1978).
[20] K. M. Christoffel and J. M. Bowman, Chem. Phys. Lett. **85**, 220 (1982).
[21] S. Carter, J. M. Bowman, and N. C. Handy, Theor. Chem. Acc. **100**, 191 (1998).
[22] O. Christiansen, J. Chem. Phys. **120**, 2149 (2004).
[23] R. B. Gerber and M. A. Ratner, Chem. Phys. Lett. **68**, 195 (1979).
[24] L. S. Norris, M. A. Ratner, A. E. Roitberg, and R. B. Gerber, J. Chem. Phys. **105**, 11261 (1996).
[25] P. Daněček and P. Bouř, J. Comput. Chem. **28**, 1617 (2007).
[26] N. Matsunaga, G. M. Chaban, and R. B. Gerber, J. Chem. Phys. **117**, 3541 (2002).
[27] L. D. Barron, *Molecular Light Scattering and Optical Activity* (Cambridge University Press, Cambridge, 2004).
[28] P. L. Polavarapu, *Vibrational Spectra: Principles and Applications with Emphasis on Optical Activity* (Elsevier, Amsterdam, 1998); L. A. Nafie and C. G. Zimba, in *Biological Applications of Raman Spectroscopy*, edited by T. G. Spiro (Wiley, New York, 1987), Vol. 1, p. 307; L. A. Nafie and T. B. Freedman, in *Circular Dichroism: Principles and Applications*, 2nd ed., edited by N. Berova, K. Nakanishi, and R. W. Woody (Wiley-VCH, New York, 2000).
[29] M. J. Frisch, G. W. Trucks, H. B. Schlegel *et al.*, GAUSSIAN 03, Revision C.02, Gaussian, Inc., Wallingford, CT, 2004.
[30] C. C. J. Roothan, Rev. Mod. Phys. **23**, 69 (1951).
[31] C. Møller and M. S. Plesset, Phys. Rev. **46**, 618 (1934).
[32] A. Becke, Phys. Rev. A **38**, 3098 (1988).
[33] C. Adamo and V. Barone, J. Chem. Phys. **108**, 664 (1998).
[34] A. D. Becke, J. Chem. Phys. **104**, 1040 (1996).
[35] A. D. Becke, J. Chem. Phys. **98**, 5648 (1993).
[36] J. P. Perdew, Phys. Rev. B **33**, 8822 (1986).
[37] J. P. Perdew, K. Burke, and Y. Wang, Phys. Rev. B **54**, 16533 (1996).
[38] J. P. Perdew, K. Burke, and M. Ernzerhof, Phys. Rev. Lett. **77**, 3865 (1996).
[39] H. L. Schmider and A. D. Becke, J. Chem. Phys. **108**, 9624 (1998).
[40] F. A. Hamprecht, A. J. Cohen, D. J. Tozer, and N. C. Handy, J. Chem. Phys. **109**, 6264 (1998).
[41] T. van Voorhis and G. E. Scuseria, J. Chem. Phys. **109**, 400 (1998).
[42] N. C. Handy and A. J. Cohen, Mol. Phys. **99**, 403 (2001).
[43] R. G. Parr and W. Yang, *Density-Functional Theory of Atoms and Molecules* (Oxford University Press, New York, 1994).
[44] J. C. Slater, *The Self-Consistent Field for Molecular and Solids* (McGraw-Hill, New York, 1974).
[45] K. Burke, J. P. Perdew, and Y. Wang, *Electronic Density Functional Theory: Recent Progress and New Directions* (Plenum, New York, 1998).
[46] P. M. W. Gill, Mol. Phys. **89**, 433 (1996).
[47] C. Lee, W. Yang, and R. G. Parr, Phys. Rev. B **37**, 785 (1988).
[48] A. Klamt, in *The Encyclopedia of Computational Chemistry*, edited by P. R. Schleyer, N. L. Allinger, T. Clark, J. Gasteiger, P. A. Kollman, H. F. Schaefer III, and P. R. Schreiner (Wiley, Chichester, 1998), Vol. 1, p. 604.
[49] M. Reiher, V. Liegeois, and K. Ruud, J. Phys. Chem. A **109**, 7567 (2005).
[50] E. B. Wilson, J. C. Decius, and P. C. Cross, *Molecular Vibrations* (Dover, New York, 1980).
[51] P. Bouř, J. McCann, and H. Wieser, J. Phys. Chem. A **102**, 102 (1998); A. P. Scott and L. Radom, J. Phys. Chem. **100**, 16502 (1996).
[52] P. Bouř and T. A. Keiderling, J. Phys. Chem. B **109**, 23687 (2005); J. Kubelka, R. Huang, and T. A. Keiderling, *ibid.* **109**, 8231 (2005); P. Bouř, J. Kubelka, and T. A. Keiderling, Biopolymers **65**, 45 (2002).
[53] D. Begue, A. Benidar, and C. Pouchan, Chem. Phys. Lett. **430**, 215 (2006).
[54] O. Christiansen and J. M. Luis, Int. J. Quantum Chem. **104**, 667 (2005).
[55] M. Horák and D. Papoušek, *Infračervená Spektra a Struktura Molekul* (Academia, Prague, 1976).